

Air Force Institute of Technology

**AFIT Scholar**

---

Theses and Dissertations

Student Graduate Works

---

12-1998

## Three-Dimensional Calculation of Contaminant Transport in Groundwater at a Dover AFB Site

Tariq O. Hashim

Follow this and additional works at: <https://scholar.afit.edu/etd>



Part of the [Applied Mathematics Commons](#), [Computational Engineering Commons](#), and the [Water Resource Management Commons](#)

---

### Recommended Citation

Hashim, Tariq O., "Three-Dimensional Calculation of Contaminant Transport in Groundwater at a Dover AFB Site" (1998). *Theses and Dissertations*. 5136.

<https://scholar.afit.edu/etd/5136>

This Thesis is brought to you for free and open access by the Student Graduate Works at AFIT Scholar. It has been accepted for inclusion in Theses and Dissertations by an authorized administrator of AFIT Scholar. For more information, please contact [AFIT.ENWL.Repository@us.af.mil](mailto:AFIT.ENWL.Repository@us.af.mil).

AFIT/GAM/ENC/98D-01

**THREE-DIMENSIONAL CALCULATION  
OF CONTAMINANT TRANSPORT IN  
GROUNDWATER AT A DOVER AFB SITE**

**THESIS**

**Tariq O. Hashim B.S., M.S.  
Captain, USAF**

**AFIT/GAM/ENC/98D-01**

19990127 065

Approved for public release; distribution unlimited

## **REPRODUCTION QUALITY NOTICE**

**This document is the best quality available. The copy furnished to DTIC contained pages that may have the following quality problems:**

- **Pages smaller or larger than normal.**
- **Pages with background color or light colored printing.**
- **Pages with small type or poor printing; and or**
- **Pages with continuous tone material or color photographs.**

**Due to various output media available these conditions may or may not cause poor legibility in the microfiche or hardcopy output you receive.**



**If this block is checked, the copy furnished to DTIC contained pages with color printing, that when reproduced in Black and White, may change detail of the original copy.**

The views expressed in this thesis are those of the author and do not necessarily reflect the views of the School of Engineering, the Air University, the United States Air Force, the Department of Defense, or any agency mentioned in the document.

AFIT/GAM/ENC/98D-01

***THREE-DIMENSIONAL CALCULATION OF  
CONTAMINANT TRANSPORT IN GROUNDWATER  
AT A DOVER AFB SITE***

**THESIS**

Presented to the Faculty of the Graduate School of Engineering of the Air Force Institute of  
Technology Air University In Partial Fulfillment for the Degree of  
**Master of Science in Applied Mathematics**

Specialization in:

**BY**

**Tariq O. Hashim B.S., M.S.**  
**Captain, USAF**

Air Force Institute of Technology

Wright-Patterson AFB, Ohio

December 1998

Sponsored in part by:  
The Air Force Office of Scientific Research/AFIT M.O.A. Project Task PO-950007

Approved for public release; distribution unlimited

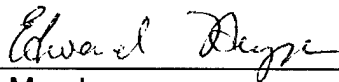
AFIT/GAM/ENC/98D-01

THREE-DIMENSIONAL CALCULATION  
OF CONTAMINANT TRANSPORT  
IN GROUNDWATER AT A DOVER AFB SITE

THESIS

Tariq O. Hashim B.S., M.S.  
Captain, USAF

Presented to the Faculty of the Graduate School of Engineering  
of the Air Force Institute of Technology  
In Partial Fulfillment of the  
Requirements for the Degree of  
Master of Science in Applied Mathematics



Member



Member



Chairman

## *Acknowledgments*

All praise be to the Almighty whom it pleases that I should attend AFIT, become an applied mathematician, and hopefully make a contribution to the environmental science through this research. I owe much gratitude to my friend, mentor, and faculty advisor Lieutenant Colonel Coulliette who made this difficult experience so educational and enjoyable. His unflagging encouragement, technical insight, and good nature are everything a student and junior officer could hope for in a leader. I also express my deepest appreciation to Dr. Dennis Quinn who went out of his way to facilitate my entry into the mathematics master's program at AFIT, then contributed his awesome knowledge of PDEs to my work. Much appreciated too is Dr. Alan Lair's welcoming me into his department. I credit Major Edward Heyse with opening my aeronautical eyes to the immense field of environmental science and thank him for his patience and willing assistance.

A special word of thanks to Dr. Jerry Lin of the Waterways Experiment Station who helped me get airborne initially with the FEMWATER code then repeatedly took hours of his time to check my calculations and help me debug. His altruistic spirit is in the highest tradition of science and scholarship. Likewise for Dr. Mansour Zakikhani of the same outfit who was a constant FEMWATER consultant and who dedicated an entire day to helping me interpret some of my results.

Not to be forgotten are two very reliable and competent computer resource managers, Kris Larsen at AFIT and MSgt John Luker at the Air Force Logistics Management Agency.

Finally, a heartfelt thanks to my patient and supportive wife Ruba and our children Imran and Farah who sacrificed so much family time towards this thesis. I owe them.

# *Table Of Contents*

Acknowledgments .....	ii
Table Of Contents .....	iii
List Of Figures .....	vi
List Of Tables .....	ix
Abstract .....	x
1. INTRODUCTION .....	1
1.1 BACKGROUND .....	1
1.1.a THE ENVIRONMENT .....	1
1.1.b PUMP-AND-TREAT .....	2
1.1.c MODELING CONCERNS .....	3
1.1.d BRIEF OVERVIEW OF PREVIOUS ANALYSES .....	4
1.1.e MOTIVATION FOR CURRENT RESEARCH .....	6
1.1.e.1 MACROSCALE APPROACH TO RATE-LIMITED SORPTION .....	7
1.1.e.2 THREE-DIMENSIONAL MODELING .....	7
1.1.e.3 DOVER AFB FIELD EXPERIMENT .....	8
1.2 SPECIFIC PROBLEM .....	8
1.3 RESEARCH OBJECTIVES .....	8
2. THE GMS/FEMWATER PACKAGE – AN OVERVIEW .....	9



2.1	FEATURES OF THE GROUND-WATER MODELING SYSTEM (GMS) . . . . .	9
2.1.a	OPERATIONAL MODULES . . . . .	9
2.1.b	DATA SETS . . . . .	11
2.1.c	VISUALIZATION . . . . .	11
2.1.d	GRID GENERATION . . . . .	12
2.2	MATHEMATICAL FORMULATION BEHIND FEMWATER . . . . .	12
2.2.a	GOVERNING EQUATIONS FOR FLOW . . . . .	13
2.2.b	GOVERNING EQUATIONS FOR TRANSPORT . . . . .	17
2.2.c	NUMERICAL FORMULATION . . . . .	20
3.	CHARACTERISTICS OF THE DOVER AFB SITE . . . . .	21
3.1	SITE DESCRIPTION . . . . .	21
3.2	DEFINING THE MODEL FOR FEMWATER . . . . .	24
3.2.a	CONCEPTUAL CELL . . . . .	24
3.2.b	FINITE ELEMENT MESH . . . . .	27
3.2.c	BOUNDARY CONDITIONS . . . . .	30
3.2.d	DISCRETIZATION OF WELLS . . . . .	30
3.2.e	CURVES OF SOIL HYDRAULIC PROPERTIES . . . . .	34
4.	NUMERICAL SIMULATIONS . . . . .	39
4.1	COMPUTATION OF FLOW SOLUTION . . . . .	40
4.2	MOMENT ANALYSIS CROSS-CHECK . . . . .	46

4.3	EFFECT OF RETARDATION FACTOR .....	57
4.4	REMEDICATION BY CONTINUOUS PUMPING .....	60
4.5	REBOUND .....	74
4.6	COMPARISON WITH FIELD EXPERIMENTAL DATA .....	79
4.7	COMPARISON WITH PREVIOUS NUMERICAL DATA .....	83
4.8	GENERAL OBSERVATIONS ON FEMWATER PERFORMANCE .....	86
5.	CONCLUSIONS & RECOMMENDATIONS FOR FURTHER STUDY .....	87
5.1	CONCLUSIONS .....	87
5.2	RECOMMENDATIONS .....	87
Appendix A.	UNIQUENESS IN THE ONE-DIMENSIONAL DIFFUSION EQUATION .....	88
Appendix B.	SAMPLE FEMWATER INPUT FILES .....	89
B.1	INPUT FILE FOR FLOW SOLUTION .....	89
B.2	INPUT FILE FOR TRANSPORT SOLUTION .....	98
Bibliography	.....	107
Vita	.....	110

## *List Of Figures*

Figure 1	The GMS Screen . . . . .	10
Figure 2	Schematic of Dover AFB Field Site (not to scale) . . . . .	23
Figure 3	Soil Layers and 4 Monitoring Points . . . . .	25
Figure 4	Finite-Element Mesh (33184 Nodes) . . . . .	28
Figure 5	Plan View of 3D mesh . . . . .	29
Figure 6	Mesh Detail in the Vicinity of Well . . . . .	29
Figure 7	Well Discretization by Point Sources and Sinks . . . . .	32
Figure 8	Source Placement and Streamsurface Geometry . . . . .	33
Figure 9	Moisture Content vs. Pressure Head (Sand) . . . . .	36
Figure 10	Water Capacity vs. Pressure Head (Sand) . . . . .	37
Figure 11	Relative Conductivity vs. Pressure Head (Sand) . . . . .	38
Figure 12	Velocity Vector Field . . . . .	41
Figure 13	Velocity Vectors in the Region of Detail . . . . .	42
Figure 14	Velocity Vectors Near a Sink Node . . . . .	43
Figure 15	Vertical Distribution of Longitudinal Velocity (m / hr) . . . . .	44
Figure 16	Schematic of Injection Pulse and Mass Recovery Curves . . . . .	48
Figure 17	Mass Recovery Rate vs. Time for 200 hr Injection Pulse . . . . .	50
Figure 18	Injection Pulse and Extrapolated Extraction Breakthrough . . . . .	51

Figure 19	Contaminant Plumes After 200 hour Injection Pulse (Aqueous Concentration) .....	53
Figure 20	Contaminant Plumes at T=500 hrs, After 300 Hours of Clean Water Flushing .....	54
Figure 21	Contaminant Plumes at T=1000 hrs, After 800 Hours of Clean Water Flushing .....	55
Figure 22	Contaminant Plumes at T=1500 hrs, After 1300 Hours of Clean Water Flushing .....	56
Figure 23	Breakthrough Curves Showing the Effect of Retardation Factor .....	58
Figure 24	Breakthrough Curves Showing the Effect of Retardation Factor .....	59
Figure 25	Initial Contaminant Profile T = 0 hrs .....	61
Figure 26	Initial Contaminant Profile and 4 Monitoring Points .....	62
Figure 27	Contaminant Concentration vs Time (Hours) at the Four Monitoring Points .....	63
Figure 28	Time and Depth Variation of Contaminant Concentration at Center of Cell .....	64
Figure 29	Contaminant Profile after 200 Hours of Clean-Water Flushing .....	66
Figure 30	Contaminant Profile after 400 Hours of Clean-Water Flushing .....	67
Figure 31	Contaminant Profile after 600 Hours of Clean-Water Flushing .....	68
Figure 32	Contaminant Profile after 800 Hours of Clean-Water Flushing .....	69
Figure 33	Contaminant Profile after 1000 Hours of Clean-Water Flushing .....	70
Figure 34	Contaminant Profile after 1200 Hours of Clean-Water Flushing .....	71
Figure 35	Contaminant Profile after 1400 Hours of Clean-Water Flushing .....	72
Figure 36	Contaminant Profile after 3600 Hours of Clean-Water Flushing .....	73
Figure 37	Contaminant Concentration at Monitor Point #2 Showing Rebound .....	76

Figure 38	Contaminant Concentration at Monitor Points 1 and 2 Showing Resumption of Pumping After Rebound .....	77
Figure 39	Contaminant Concentration in the Vicinity of the 4 Monitoring Points at T=3600 Hours .....	78
Figure 40	Elution Data for PCE (Fig G1 in [27]) .....	80
Figure 41	Pump Strength Schedule from Field Experiment .....	81
Figure 42	Breakthrough Curves for FEMWATER and Field Experiment .....	82
Figure 43	Initial Concentration Profile from Herman .....	84
Figure 44	Comparison of Spatial Concentration Traces .....	85

## *List Of Tables*

Table 1	Material Properties for Sand Layers . . . . .	26
Table 2	Material Properties for Clay Layers . . . . .	26
Table 3	Vertical Positioning of Central Monitoring Points . . . . .	26
Table 4	Van Genuchten Parameters for Soil Hydraulic Properties . . . . .	35
Table 5	Effects of Tightening Convergence Tolerance on Flow Solution . . . . .	86

## *Abstract*

Macroscale rate-limited sorption modeling was tested using a production transport code, the GMS/FEMWATER ground-water modeling package. The code (Version 1.1 of FEMWATER, dated 1 August 1995) was applied to a 3D conceptual model developed from a field site at Dover AFB, DL. A simulation was performed of a 200 hour contaminant injection pulse followed by clean water flushing. A moment analysis performed on the resulting breakthrough curve validated code self-consistency. Another injection pulse simulation showed that retardation temporally delays the breakthrough peak. Transport simulations of pulsed clean water pumping of the test cell with a prescribed initial contaminant distribution demonstrated both tailing and rebound without any additional microscale modeling. In comparison with both previous numerical solutions and the actual field data from the Dover AFB test site, FEMWATER has demonstrated high numerical dispersivity. For an initial contaminant distribution corresponding to the field data, the FEMWATER breakthrough curve was much flatter than the experimental result, failing to capture the plug-like elution of the field site.

# ***THREE-DIMENSIONAL CALCULATION OF CONTAMINANT TRANSPORT IN GROUNDWATER AT A DOVER AFB SITE***

## **1. INTRODUCTION**

### **1.1 BACKGROUND**

#### **1.1.a THE ENVIRONMENT**

We live in an era of ever-increasing efforts to right the environmental abuses of yesteryear. A major area of concern is the condition of our ground water – the entity that suffers when offensive substances are dumped "below decks"[30, pg 463] . According to the 1989 Toxic Release Inventory by the Environmental Protection Agency (EPA), 14% of toxic chemical releases were underground [10, pg 173] . Almost all rural households (95%) and 50% of the general population depend upon ground water as their primary drinking water source [23, pg 250] . Groundwater contamination exists at more than 85% of the 1208 sites included on the National Priority List (NPL). Further, over 33,000 other sites have been identified and included in the Comprehensive Environmental Response, Compensation, and Liability Information System for ranking and potential inclusion on the NPL. The EPA has identified or suspected contaminant release to ground water at more than 1700 Resource Conservation and Recovery Act facilities. Against this backdrop comes the disturbing realization that the Air Force has been a prime polluting culprit in many cases. Typical scenarios include leaky underground fuel storage tanks and careless disposal of toxic industrial chemicals like solvents and paint strippers. The Air Force is engaged in a program to identify, assess, and remediate hazardous waste sites at Air Force installations throughout the United States[12, pg 24] . These efforts are driven partially by the reality of



impending base closures and the subsequent turn-over of potentially contaminated lands to the civilian sector.

### **1.1.b PUMP-AND-TREAT**

"Pump-and-Treat" (PAT) is the collective term used to describe contaminated site remediation schemes in which water is extracted from the aquifer by wells or drains followed by treatment of the extracted water [25, pg 630] , [12, pg 25] , [18, pg 119] , [19, pg 216] . PAT remediation is the most frequently used remediation method used in practice [33, pg 1464] .

Field experience with PAT has demonstrated several trends in the effectiveness of the process [25, pg 630] , [18, pg 119] , [29, pg 44] :

1. Containment of ground-water plumes was usually achieved;
2. Contaminant concentrations dropped significantly, initially, followed by a leveling out and;
3. After the period of initial decline, the continued decreases in concentration were usually slower than anticipated (sometimes by decades). This effect is known as "tailing".
4. After the cessation of pumping, there were local increases in contaminant concentration. An effect known as "rebound".

Tailing and rebound are both attributed to "rate-limited sorption", also called "nonequilibrium sorption". The term sorption describes processes that exchange solutes between the fluid and solid phases of a medium. It is the generic term used to encompass the phenomena of adsorption, desorption, and other processes. Equilibrium assumes that the time scale of the chemical binding and release of solute onto porous and solid particles within the soil matrix is much faster than the time scale of bulk flow advection. So equilibrium sorption means that solute moves to or from the solid matrix as quickly as it advects downstream. Non-equilibrium sorption arises when physical or chemical processes at the single pore level are slow relative to advection in the bulk media [32, pg 1] . The rate of sorption is controlled by one of three possible rate-limiting steps [32, pg 9] :

1. chemical binding and release,
2. diffusion through immobile fluid, and,
3. diffusion through organic matter

According to several recent studies [35, pg 1699] , non-equilibrium solute transport is a key limitation to contaminant removal from ground water by "pump and treat" methods. Slow sorption (with attendant tailing and rebound effects) of organic substances within the soil has resulted in long periods of treatment, almost always in excess of those predicted by conventional equilibrium modeling, with attendant costs. Additionally, such scenarios lead to potentially difficult pumping strategy determinations. As a result, continuous pumping did not prove to be practical in many situations [25, pg 630] , [18, pg 119] , [29, pg 44] . "Pulse pumping" refers to intermittent pumping processes designed to improve the plume capture and reduce quantities of water extracted, to reach the goal of "clean water" more efficiently. Field experiments and modeling studies have demonstrated that this optimization of the process may achieve favorable results [3, pg 165] , [18, pg 122] , [12, pg 25] , [17, pg 37] , [1, pg 53] . Hence the importance of accurate numerical modeling of the ground-water contaminant transport process: remediation engineers can rely on these models to help optimize their pumping schedules – saving money in the long run.

### **1.1.c MODELING CONCERNS**

As in any computational effort, the emphasis is on gleaning as much physical insight from the model of a process or system, while using the least computer resources possible, thus minimizing cost. Often, one cannot obtain precise quantitative data but can nevertheless surmise important trends in the way the system responds to variations in any inherent parameters. Moreover, the ability to run numerical simulations then gives the researcher the platform to test his or her notions about the system and thus systematically arrive at a far narrower set of optimum

solutions than would otherwise be possible through mere contemplation or observation of the physical system.

Having stated the benefits as well as limits of numerical models, we can now state a key requirement concerning the credibility of the model: the need for validation. Validation is the process by which a researcher establishes a numerical code's credibility through a systematic procedure of comparing results produced by the code to those from other sources. There are at least two types of validation the researcher should perform:

1. Some sort of cross-check to determine whether the model is behaving in a self-consistent manner
2. Some type of comparison to actual physical data. Here, governing parameters should match one-to-one between the physical case being simulated and the numerical model's inputs.

#### **1.1.d BRIEF OVERVIEW OF PREVIOUS ANALYSES**

In coarse-grained, homogeneous aquifers, advective transport dominates the transport process. For this reason as well as for the simplification of the mathematical model in the design of capture and containment systems, it has been common to treat advection as the sole mechanism for contaminant transport [15, pg 42]. The vast majority of ground-water contaminant transport models are based on the assumption of instantaneous sorption and desorption between the liquid and the solid phases. This assumption is commonly called the local equilibrium assumption (LEA). Its validity and applicability have been documented in the literature [34], [40], [13], [35], [24], [32, pg 9], [6, pg 33-99], [4], [12, pg 24-25], [39, pg 499-528], [5, pg 353-368]. It is important to realize that when discussing the LEA versus rate-limited sorption, one must identify two distinct sources of non-equilibrium, namely: 1) Physical non-equilibrium, in which the overall sorption rate is controlled by the rate at which the solute is transported to and from the reacting soil surfaces and 2) Chemical non-equilibrium, in which the overall sorption rate is equal to the rate of reaction at the soil-solution interfaces. Clearly, the slowest process sets the

rate-limiting standard. In the present study, we consider only physical non-equilibrium. Examples of chemical non-equilibrium modeling can be found in [35, pg 1696] , [16, pg 602-604] . In the realm of physical models, considerable work has been done recently to develop models which accurately describe rate-limited sorption effects [22] , [4] , [1] , [7] , [31, pg 1457-1470] . Most of these models utilize a two-zone description of a porous medium. They implement non-equilibrium sorption in various ways, but all have considered non-equilibrium effects occurring throughout the porous medium on the microscopic scale. Huso [22] , using finite elements, and Adams and Virmontes [1, pg 1-2] using an analytical approach, modeled physical, non-equilibrium in radial, pulsed pumping tests. A notable recent work is that of Caspers [7] . who modified the widely used USGS SUTRA code [37] to incorporate rate-limited as well as equilibrium sorption effects. In his work, he describes rate-limitation by either a first-order law, or by Fickian diffusion of contaminant through a spherical immobile region. Casper's equilibrium methods under-predicted rebound, while his first-order diffusion simulations both under and over-predicted rebound within the matrix for certain regions and were somewhat equivalent to Fickian diffusion in equilibrium regimes for cleanup time prediction. Herman's work [21] investigated non-equilibrium sorption effects from only specific zones, not throughout the porous medium on the microscopic scale like Casper's simulations. In Herman's study, the USGS SUTRA code was coupled with a two dimensional diffusion code to model non-equilibrium effects from specific layers only. This allowed the study of non-equilibrium sorption from a macroscopic view of specific zones. Herman simulated PAT remediation at a field site at Dover AFB, Delaware and studied the effects of pulsed and continuous pumping within the time frame of the actual field experiment. Since both Casper's and Herman's works were based on SUTRA, they were both hamstrung by a fundamental limitation of that code, namely, the inability to vary retardation coefficient per heterogeneities in the soil strata under consideration. As Herman re-

ports, the SUTRA code did not allow specification of retardation coefficients in his loam layers. Accordingly, in his model, the distribution constant was one-third what it should have been in orange silty clay loam and two orders of magnitude less than what it should have been for black silty loam. This inflexibility resulted in an unrealistically high rate of mass mobilization from the clay layers of his contaminated strata. Even though the hydraulic conductivity was low in the clay layers, mass was still mobilized out of the loam layers because the significant retardation in the loam layers was not accounted for in the SUTRA model.

Both Caspers and Herman used the so-called "Split Operator Approach" to make the numerical problem more tractable. This approach, detailed by Miller and Rabideau [28] separates the governing equations into transport (for the mobile zone) and reaction operators (diffusion equations for the immobile zone) and solves them sequentially. This splitting allows the separation of the short time-scale process (mobile zone) from the long time-scale process (immobile). Operator splitting leads to smaller systems of equations, which can be solved faster than the original coupled equation.

#### **1.1.e MOTIVATION FOR CURRENT RESEARCH**

The three motivations for conducting the present research will be detailed in the following sections. They are:

1. Macroscale approach to rate-limited sorption
2. Three-dimensional vs two-dimensional modeling
3. The simulation of an actual field experiment being conducted at Dover AFB with particular attention paid to:
  - A. Pump and Treat
  - B. Tailing
  - C. Rebound

### ***1.1.e.1 MACROSCALE APPROACH TO RATE-LIMITED SORPTION***

Numerical modelers want to know if they can conduct preliminary investigations of actual field conditions without having to resort to complex microscale models which require detailed knowledge of characteristics like pore geometries, particle size distribution, or the split-operator approach in which a diffusive sub-model must be specially prepared. If the bulk of retardation occurs in macroscale soil structures (like layers or lenses), then a numerical formulation that assumes local chemical equilibrium and models diffusion as well as advection, while providing the capability to vary retardation coefficient throughout the modeled configuration should be able to simulate processes like rate-limited sorption that are diffusion dominated. This is the so-called macroscale approach. The fundamental question then is whether, devoid of any additional diffusive model, the current methodology is capable of reproducing the diffusion-dominated phenomena of tailing and rebound?

### ***1.1.e.2 THREE-DIMENSIONAL MODELING***

It is always true that efficiency dictates the need for the cheapest and fastest simulation possible, hence the need for 2D models of 3D configurations. However, it is also true that some geometries are strongly three-dimensional and can only be properly represented by a "full-up" 3D model. In light of this, the analyst must have a clear knowledge of when a 2D model is sufficient, when a 3D model is necessary, and what types of characteristic parameters or physical phenomena are the determining factors. Unfortunately, the only way to build this knowledge is by developing a mosaic of 2D and 3D simulations of sufficient breadth that unmistakable trends can be discerned, recorded and exploited by researchers. Obviously, the greater the number of simulations, the greater the "corporate knowledge" of when one can expect to get useful results from a 2D model, and when one must resort to a full 3D model.

### ***1.1.e.3 DOVER AFB FIELD EXPERIMENT***

One of the objectives of this work was to support a pump-and-treat field experiment being conducted at Dover AFB. This site was specifically prepared to test pulse-pumping efficiency with particular attention paid to tailing and rebound. Its soil has sections with significant rate-limiting properties and it is well-instrumented for comparison with computational results. The previous attempt to model the Dover site was a two dimensional one [21] ; in this research a 3D model of the same site will be implemented.

## **1.2 SPECIFIC PROBLEM**

The objective of this work is to mathematically model, in three dimensions, aquifer remediation by continuous and pulsed pumping when contaminant transport is affected by macroscale sorption and diffusion. This research will extend the work of Herman [21]

## **1.3 RESEARCH OBJECTIVES**

The specific objectives of this research are to:

1. Install and test the Ground-water modeling System/FEMWATER package as furnished by the Army Corps of Engineers' Waterways Experiment Station on AFIT computational facilities.
2. In a three step process, apply GMS/FEMWATER to a conceptual site developed from an actual field site at Dover AFB, Delaware:
  - i Conduct a moment analysis validation of the numerical formulation.
  - ii Determine, through numerical simulation, qualitative aspects of remediation by continuous pumping of this conceptual site with special attention to tailing and the effect of retardation factor.
  - iii Determine qualitative aspects of rebound due to pulse pumping.

## **2. THE GMS/FEMWATER PACKAGE – AN OVERVIEW**

This section will explain the strengths of the GMS graphical user interface and the FEMWATER FORTRAN program. This information will probably be dated upon publication since the software in question is constantly being revised and improved.

### **2.1 FEATURES OF THE GROUND-WATER MODELING SYSTEM (GMS)**

The Department of Defense Ground-Water Modeling System (GMS) is a comprehensive graphical user environment for numerical modeling. It was developed by Brigham Young University's Engineering Computer Graphics Laboratory in cooperation with the U.S. Army Corps of Engineers Waterways Experiment Station. GMS was originally intended for ground-water modeling applications and currently includes specialized interfaces to some of the more popular ground-water modeling programs such as MODFLOW, MT3D, and FEMWATER. However, GMS is written in a general fashion so that it can be used as a platform for any type of two or three-dimensional numerical modeling.

#### **2.1.a OPERATIONAL MODULES**

The GMS screen is shown in figure 1. The large central space is the Graphics Window. On the far left is the Tool Palette— a collection of pushbutton icons. The pull-down Menu Bar runs across the top. Finally, the Edit Window is under the Graphics Window (to the right of the Tool Palette).

The interface for GMS is divided into nine separate modules. GMS provides a module for each of the basic data types it supports such as Triangulated Irregular Network, Borehole, Solid, 2D and 3D mesh, or 3D Scatter Point. As the user switches from one module to another, the Tool Palette and the menus change. This allows the user to focus only on the tools and commands relevant to the data type the user will manipulate in the modeling process. The user can switch



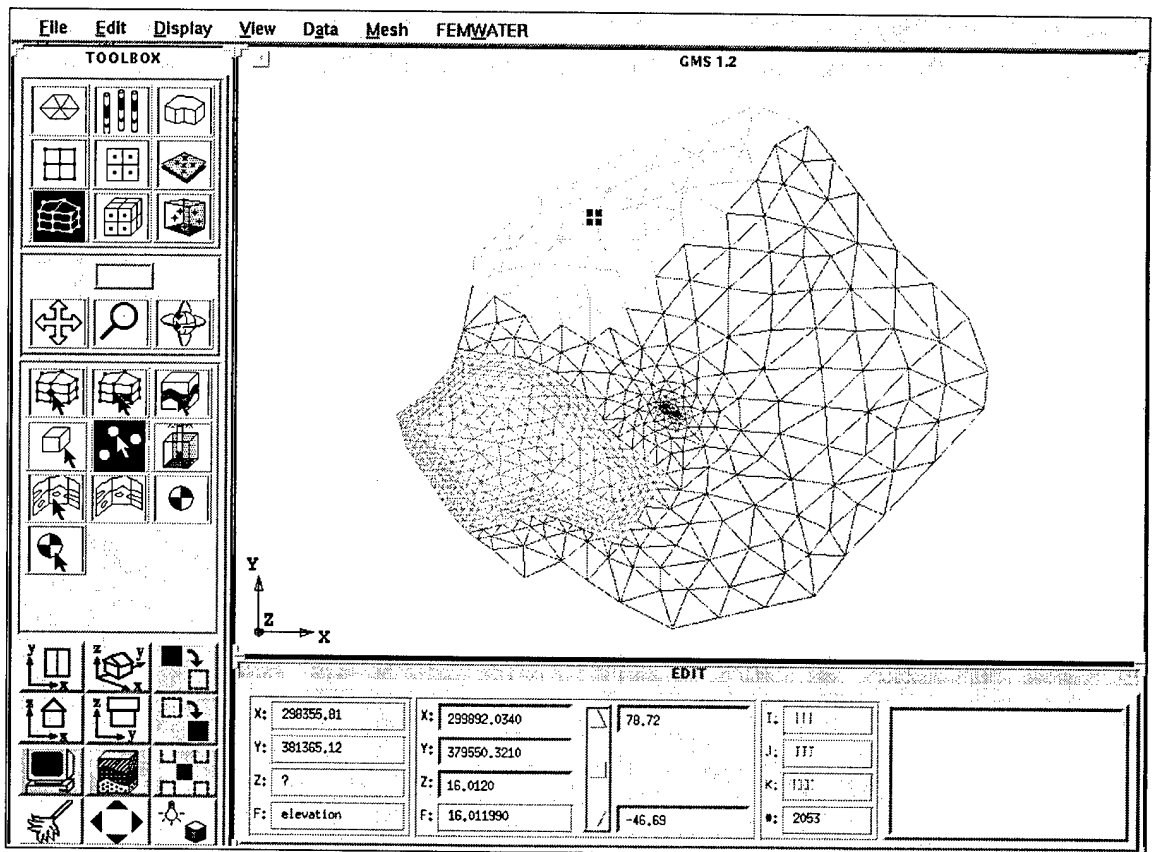


Figure 1. The GMS Screen

instantaneously from one module to another to facilitate the simultaneous use of several data types when necessary.

### **2.1.b DATA SETS**

The interface to each of the separate modules is designed in a consistent fashion. Once the user becomes familiar with the interface to one of the modules, the other modules can be used immediately with little further training. To help provide a consistent interface, GMS uses the concept of generic data sets. A data set is a set of scalar or vector values associated with an object. Each data set can be either steady state or transient (multiple values representing the data values at different points in time). All the different types of data groups have associated lists of scalar data sets and vector data sets. Each set has a single vector or scalar value for each node, cell, or data point.

Data sets can be used to represent a variety of different types of information. They can be imported from a file or they can be created by interpolating from a group of scattered data points. In some cases it is necessary to perform mathematical operations on data sets. The user can accomplish this in GMS using a "data set calculator". For example, to compare the difference in the solutions from two separate simulations on a finite difference grid, the two solutions can be input as data and the data calculator used to compute the absolute value of the difference between the two data sets. The resulting data set can be contoured or used to display iso-surfaces just like any other data set.

### **2.1.c VISUALIZATION**

GMS provides a large number of visualization tools. The user can display all objects in a 3D oblique view and rotate them interactively. He or she can also use hidden surface removal and color shading with a light source to generate highly realistic images. In addition,

the modeler can use contours and color fringes to display the variation of input data or computed data. Starting with 3D meshes and grids, he or she can generate cross sections and iso-surfaces. Given an object with an associated transient data set, the user can generate animation sequences showing data evolution.

The interface to the visualization tools in GMS is consistent for each of the supported data types. The dialogs and commands used for visualization are identical in each module.

The GMS Reference Manual [9] provides complete information on all of GMS's features.

#### **2.1.d GRID GENERATION**

Two very useful grid-generation features in GMS are the adaptive tessellation 2D mesh construction tool and the 3D borehole-to-mesh tool. The former allows the user to generate 2D meshes which are then projected onto the plan geometry of the site in question to give a 3D mesh. Adaptive tessellation is advantageous when there are interior regions around which finite elements must be wrapped. When a boundary polygon encloses these interior regions, and adaptive tessellation is used, the node spacing on the boundary of the input polygon is used to determine the element sizes on the interior. On the other hand, the borehole-to-mesh technique is particularly useful when the site stratification character is provided in the form of borehole data. The user is provided the means to connect between partitions in the boreholes and directly fill these with finite elements, making for rapid visually-intuitive mesh generation.

### **2.2 MATHEMATICAL FORMULATION BEHIND FEMWATER**

Before proceeding, the reader should note that the essential unknowns in the unsteady equations for fluid flow and contaminant transport are hydraulic head  $h$  and contaminant concentration  $C$ . Transport velocity is a function of  $h$ . As will be detailed below, the equation governing fluid flow and that governing contaminant transport are coupled through an unsteady

term  $\frac{\partial h}{\partial t}$  and through the dependence of water density and dynamic viscosity on contaminant concentration. If the density and dynamic viscosity of the water are independent of contaminant concentration, and if the problem under consideration is steady ( $\frac{\partial h}{\partial t} = 0$ ), the equations become uncoupled. Then, the velocity field can be computed independently of the concentration distribution. Once this velocity field is determined, it enters the transport equation as a spatially-variable coefficient. The transport equation can then be solved based on this pre-computed velocity field. The following two sections describe the governing equations in FEMWATER for flow and transport.

### 2.2.a GOVERNING EQUATIONS FOR FLOW

The governing equations for flow through aquifer material are based on continuity of fluid, continuity of solid, consolidation of the media, and the equation of state [38, pg 2] . As used in FEMWATER, these governing equations for flow are:

$$\frac{\rho}{\rho_0} F \frac{\partial h}{\partial t} = \nabla \cdot \left[ \mathbf{K} \cdot \left( \nabla h + \frac{\rho}{\rho_0} \nabla z \right) \right] + \frac{\rho^*}{\rho_0} q \quad 1$$

where  $\rho$  is the fluid density,  $\rho_0$  is the reference water density,  $F$  is the storage coefficient,  $h$  is the reference pressure head, and  $t$  is time. Here the hydraulic conductivity tensor  $\mathbf{K} = \frac{\rho g \mathbf{k}}{\mu}$  with  $\mu$  being the dynamic viscosity of the fluid,  $g$  the acceleration due to gravity and  $\mathbf{k}$  the intrinsic permeability tensor.  $z$  is the elevation head,  $\rho^*$  the density of the injected fluid, and  $q$  the internal source/sink.

Once the flow equation is solved for the h-field, the Darcy velocity vector for density-dependent flow is:

$$\mathbf{V} = -\mathbf{K} \cdot \left( \frac{\rho}{\rho_0} \nabla h + \nabla z \right)$$

The density and dynamic viscosity are functions of contaminant concentration and are assumed to take the following form:

$$\frac{\rho}{\rho_0} = a_1 + a_2C + a_3C^2 + a_4C^3$$

$$\frac{\mu}{\mu_0} = a_5 + a_6C + a_7C^2 + a_8C^3$$

where  $\mu_0$  is the reference water dynamic viscosity,  $C$  is the contaminant concentration ( $M/L^3$ ) and  $a_1, a_2, \dots, a_7, a_8$  ( $L^3/M$ ) are the parameters that are used to describe the concentration dependence of water density and dynamic viscosity. Clearly, if  $a_2 = a_3 = a_4 = a_6 = a_7 = a_8 = 0$  then the flow equation will be independent of contaminant concentration and therefore uncoupled from the transport equation (8).

The initial conditions for the flow equations are stated as:

$$h = h_i(x, z) \text{ in } R$$

where  $R$  is the region of interest and  $h_i$  is the prescribed initial condition for hydraulic head.

In order to describe boundary conditions, we must first define some nomenclature:

$n$  is the outward unit vector normal to the boundary;  $(x_b, y_b, z_b)$  is the spatial coordinate on the boundary;  $h_d, q_n, q_c$  are the Dirichlet functional value for hydraulic head, Neumann flux, and Cauchy flux, respectively;  $B_d, B_n, B_c, B_v$  are the Dirichlet, Neumann, Cauchy, and variable boundaries, respectively. Then the boundary is the union of  $B_d, B_n, B_c,$  and  $B_v$ . Next,  $h_p$  and  $q_p$  are the allowed ponding depth and the throughfall of precipitation, respectively, on the variable boundary;  $h_m$  is the allowed minimum pressure on the variable boundary; and  $q_e$  is the allowed maximum evaporation rate (= potential evaporation) on the variable boundary; for a boundary on a river (a common boundary for flow problems),  $K_R$  is the hydraulic conductivity on the river bottom sediment layer,  $b_R$  is the thickness of the river bottom sediment layer, and  $h_R$  is the depth of the river bottom measured from the river surface.

Five types of boundary conditions can be specified for the flow equations depending on the physical location of the boundaries. These boundary conditions are stated as:

Dirichlet Boundary Conditions:

$$h = h_d(x_b, y_b, z_b, t)$$

on  $B_d$

Neumann Boundary Conditions:

$$-\mathbf{n} \cdot \mathbf{K} \left( \frac{\rho_0}{\rho} \nabla h \right) = q_n(x_b, y_b, z_b, t)$$

on  $B_n$

Cauchy Boundary Conditions:

$$-\mathbf{n} \cdot \mathbf{K} \left( \frac{\rho_0}{\rho} \nabla h + \nabla z \right) = q_c(x_b, y_b, z_b, t)$$

on  $B_c$

Variable Boundary Conditions – During Precipitation Period:

$$h = h_p(x_b, y_b, z_b, t) \quad 2$$

on  $B_v$

or

$$-\mathbf{n} \cdot \mathbf{K} \left( \frac{\rho_0}{\rho} \nabla h + \nabla z \right) = q_p(x_b, y_b, z_b, t) \quad 3$$

on  $B_v$

Variable Boundary Conditions – During Non-Precipitation Period:

$$h = h_p(x_b, y_b, z_b, t) \quad 4$$

on  $B_v$

or

$$h = h_m(x_b, y_b, z_b, t) \quad 5$$

on  $B_v$

or

$$-\mathbf{n} \cdot \mathbf{K} \left( \frac{\rho_0}{\rho} \nabla h + \nabla z \right) = q_e(x_b, y_b, z_b, t) \quad 6$$

on  $B_v$

River Boundary Conditions:

$$-\mathbf{n} \cdot \mathbf{K} \left( \frac{\rho_0}{\rho} \nabla h + \nabla z \right) = \frac{K_R}{b_R} (h_R - h) \quad 7$$

on  $B_r$

Note that only one of Eqs. (2) through (6) is utilized at any point on the variable boundary at any time.

## 2.2.b GOVERNING EQUATIONS FOR TRANSPORT

The governing equations for material transport through ground-water systems are derived based on the laws of continuity of mass and flux. The major processes that are included are advection, dispersion/diffusion, decay, adsorption, biodegradation through both liquid and solid phases, the compressibility of media, as well as sources and sinks. Letting  $C$  be the dissolved concentration and  $S$  be the adsorbed concentration, the governing equation of the spatial-temporal distribution of dissolved concentrations can be stated as follows:

$$\begin{aligned} & \theta \frac{\partial C}{\partial t} + \rho_b \frac{\partial S}{\partial t} + \mathbf{V} \cdot \nabla C - \nabla \cdot (\theta \mathbf{D} \cdot \nabla C) = \\ & - \left( \alpha' \frac{\partial h}{\partial t} + \lambda \right) (\theta C + \rho_b S) - (\theta K_w C + \rho_b K_s S) + m \\ & - \frac{\rho^*}{\rho} q C + \left( F \frac{\partial h}{\partial t} + \frac{\rho_0}{\rho} \mathbf{V} \cdot \nabla \left( \frac{\rho}{\rho_0} \right) - \frac{\partial \theta}{\partial t} \right) C \end{aligned} \quad 8$$

where  $\theta$  is the dimensionless moisture content,  $\rho_b$  is the bulk density of the medium,  $\mathbf{V}$  is the darcy velocity,  $\mathbf{D}$  is the matrix of dispersion coefficients,  $\lambda$  is the decay constant (1/T),  $K_w$  is the first order biodegradation constant through dissolved phase (1/T),  $K_s$  is the first order biodegradation constant through adsorbed phase (1/T),  $q$  is the internal source/sink, and  $m$  is external source/sink rate per medium volume ((M/L<sup>3</sup>)/T). Equation (8) above involves two unknowns  $C$  and  $S$ , so for closure, constitutive relationships must be posed. In FEMWATER, the following empirical relationships are used:

For the linear isotherm:

$$S = K_d C$$

For the Langmuir isotherm:

$$S = \frac{s_{\max} K C}{1 + K C}$$

For the Freundlich isotherm:



$$S = KC^n$$

where  $K_d$  is the distribution coefficient ( $L^3/M$ ),  $s_{\max}$  is the maximum concentration permitted in the medium in the Langmuir nonlinear isotherm,  $K$  is the coefficient in the Langmuir or Freundlich nonlinear isotherm, and  $n$  is the power index in the Freundlich nonlinear isotherm. Note that all three of these models relate dissolved concentration to adsorbed concentration by using the local equilibrium assumption.

Assuming that initially the dissolved concentrations are known throughout the region of interest:

$$C = C_i(x, z) \text{ in } R$$

where  $C_i$  is the initial concentration and  $R$  is the region of interest. Initial concentrations for the dissolved concentrations may be obtained from field measurements.

The specification of boundary conditions is a difficult and intricate task in transport modeling. From the dynamic point of view, a boundary segment may be classified as either flow-through or impervious. From a physical point of view, it is a soil-air interface, or soil-soil interface, or soil-water interface. From the mathematical point of view, it may be treated as a Dirichlet boundary on which the total analytical concentration is prescribed, a Neumann boundary on which the flux due to the gradient of total analytical concentration is known, or a Cauchy boundary on which the total flux is given.

An even more difficult mathematical boundary is the variable boundary conditions on which the boundary conditions are not known *a priori* but are themselves the solution to be sought. In other words, on the mathematically variable boundary, either Neumann or Cauchy conditions may prevail and change with time. Which condition prevails at a particular time can be determined only in the cyclic processes of solving the governing equations, iterating time-step by time-step between solution fields and boundary conditions[38, pg 95] .

Whatever point of view is chosen, all boundary conditions eventually must be transformed into mathematical equations for quantitative solutions. Thus, we will specify the boundary conditions from the mathematical point of view in concert with dynamic and physical considerations. The boundary conditions imposed on any segment of the boundary are taken to be either Dirichlet, Neumann, Cauchy, or variable. Thus, the global boundary may be split into four parts,  $B_d$ ,  $B_n$ ,  $B_c$ , and  $B_v$  denoting Dirichlet, Neumann, Cauchy, and variable boundaries, respectively. The conditions imposed on the first three types of boundaries are given as:

Prescribed Concentration (Dirichlet) Boundary Conditions:

$$C = C_d(x_b, y_b, z_b, t) \text{ on } B_d$$

Neumann Boundary Conditions:

$$\mathbf{n} \cdot (-\theta \mathbf{D} \cdot \nabla C) = q_n(x_b, y_b, z_b, t) \text{ on } B_n$$

Cauchy Boundary Conditions:

$$\mathbf{n} \cdot (\mathbf{V}C - \theta \mathbf{D} \cdot \nabla C) = q_c(x_b, y_b, z_b, t) \text{ on } B_c$$

where  $C_d$  is the prescribed concentration on the Dirichlet boundary  $B_d$ .  $(x_b, y_b, z_b)$  is the spatial coordinate on the boundary,  $\mathbf{n}$  is an outward unit vector normal to the boundary,  $\theta$  is the moisture content,  $q_n$  is the prescribed gradient flux through the Neumann boundary  $B_n$ , and  $q_c$  is the prescribed total flux through the Cauchy boundary  $B_c$ .

The conditions imposed on the variable-type boundary, which is normally the soil-air interface or soil-water interface, are either the Neumann with zero gradient flux or the Cauchy with given total flux. The former is specified when the water flow is directed out of the region from the far away boundary, whereas the latter is specified when the water flow is directed into the region. This type of variable condition would normally occur at flow-through boundaries.

Written mathematically, the variable boundary condition is given by

$$\mathbf{n} \cdot (\mathbf{V}C - \theta \mathbf{D} \cdot \nabla C) = \mathbf{n} \cdot \mathbf{V}C_v(x_b, y_b, z_b, t) \text{ on } B_v \text{ if } \mathbf{n} \cdot \mathbf{V} \leq 0$$

$$\mathbf{n} \cdot (-\theta \mathbf{D} \cdot \nabla C) = 0 \text{ on } B_v \text{ if } \mathbf{n} \cdot \mathbf{V} > 0$$

where  $\mathbf{V}$  is the Darcy velocity,  $C_v$  is the specified concentration of water through the variable boundary and  $B_v$  is the variable boundary.

An issue to be aware of is the possibility of ill-posing the transport problem which may result in a non-unique solution. For a simplified mathematical explanation see appendix A.

### 2.2.c NUMERICAL FORMULATION

The interested reader may see [38, pg 97-123] for details on the numerical formulation of FEMWATER. However, some of the notable numerical features of the code are:

1. Spatial discretization is of the finite element variety. Time discretization is by finite differences.
2. The flow module in FEMWATER has the following features:
  - A. Galerkin finite element method for spatial discretization
  - B. To linearize the matrix equation, the Picard method is used instead of the Newton-Raphson which would result in an asymmetric matrix.
  - C. In solving the linearized matrix equations, direct methods aren't practical in dealing with large 3-dimensional problems. Instead, three iteration modules are available to the user:
    - \* Successive point iteration
    - \* Polynomial preconditioned conjugate gradient
    - \* Incomplete Cholesky preconditioned conjugate gradient
  - D. To handle the mass matrix resulting from the storage term, 2 options are available (lumping & consistent)
  - E. In approximating the time derivatives, 2 options are available (time-weighted difference and mid-difference).
3. The transport module in FEMWATER provides the equation-solving options of the flow model plus three finite element options:
  - Galerkin
  - Upstream weighting
  - Hybrid Lagrangian-Eulerian

### **3. CHARACTERISTICS OF THE DOVER AFB SITE**

This numerical study parallels an experimental effort conducted by Ball et al [27] of the Johns Hopkins University in collaboration with the University of Waterloo and the Air Force Research Laboratory (Tyndall AFB, Florida). The primary objective of the experiment was to determine whether there are discernible advantages to a pulsed-pumping strategy compared to continuous pumping at a "real-world" site where the ground water and subsurface solids had long been contaminated by volatile organic contaminants (VOCs). The underlying scientific goal was to identify the most significant sources of mass transfer rate limitation at the field site and to develop appropriate conceptual and computational models to describe and predict the resulting effects on aquifer decontamination. The experimentalists chose the specific site for its following attributes:

1. Well-studied, mildly heterogeneous, moderately sorbing sand/gravel aquifer impacted for at least a decade with chlorinated volatile organic contaminants (VOCs) at concentrations several orders of magnitude above typical practical quantification levels.
2. The water table is within 20 feet of ground surface (to allow sampling by pumps at the surface).
3. A competent (confining) clay aquitard within 50 feet of ground surface to form the bottom of the isolated portions of the aquifer.
4. Available power and other utilities, ease of access, and security

#### **3.1 SITE DESCRIPTION**

Figure 2 is a schematic top view of the experimental site. Two cells, of roughly identical physical dimension, lie beside each other. By design, the experimentalists had two practically identical cells in which to compare the remediative performances of continuous versus pulsed pumping – each technique exclusively applied to a single cell.

The cells were sealed by driving sheet piling from the ground surface through the aquifer layers into the underlying clay aquitard. Each cell was then cored (borehole sampled) and instru-

mented with various types of wells. Three injection and three extraction wells were installed at the opposing ends of both cells. These were fully screened and penetrated to just above the clay layer. For complete details on the experimental procedure, see [27, pg. 37-42]

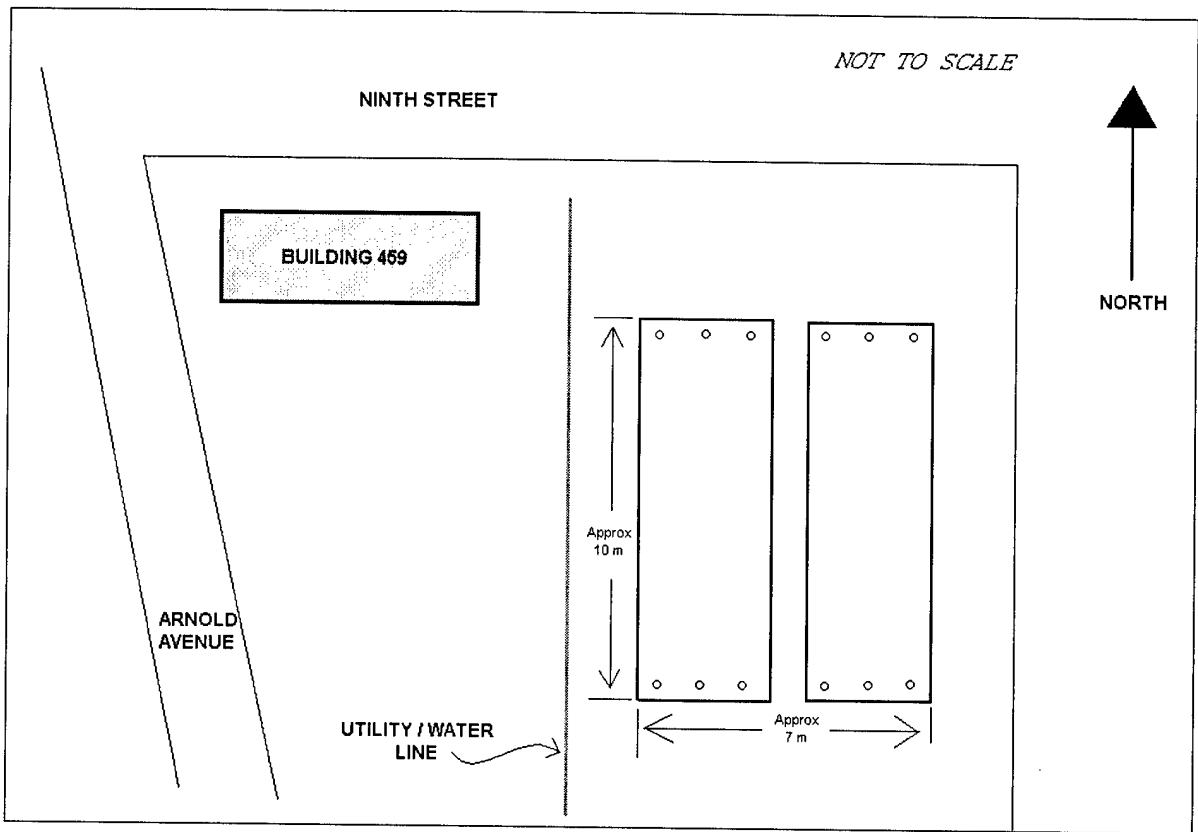


Figure 2. Schematic of Dover AFB Field Site (not to scale)

## 3.2 DEFINING THE MODEL FOR FEMWATER

### 3.2.a CONCEPTUAL CELL

Since the two actual cells are nearly identical, it suffices, for modeling purposes, to define a single "nominal" cell from a simple average of the two cells' dimensions. This conceptual cell [21, pg 9] is 3.8 meters wide by 10 meters long by 13 meters deep. The cell, like its parents, is heterogeneous but well stratified vertically. A simplified conceptual model assuming perfect stratification was developed from early field data. Figure 3, based on experimental borehole data, is a vertical cross section schematic of the soil layers.

Note that for numerical stability reasons, a thin layer (0.15 m thick) of fictitious material, called "Sandy Loam" was inserted between the Orange Coarse Sand layer and the Orange Silty Clay layer. This material's hydraulic conductivity was halfway between those of the two adjacent materials. This addition is in accordance with guideline 2 provided in section 3.2.b below. Tables 1 and 2 show each material's physical properties as used in the numerical simulation.

The four Rhombus-shaped symbols below the rightmost tip of the concentration profile in figure 3 represent the vertical positions of the four monitoring points in the geometric center ( $x = 5$  m and  $y = 1.9$  m) of the test cell. The placement of these monitoring points was in accordance with the following:

1. MP1 was at the edge of the clay layer
2. MP2 corresponds to Herman's [21] "central monitoring point", 6 inches above the clay layer
3. MP4 was at the peak of preliminary profiles (supplied by [27] ) of contaminant concentration versus depth
4. MP3 was approximately half-way between MP2 and MP4

The exact positions of these monitoring points, MP1 through MP4, are shown in Table 3 below:

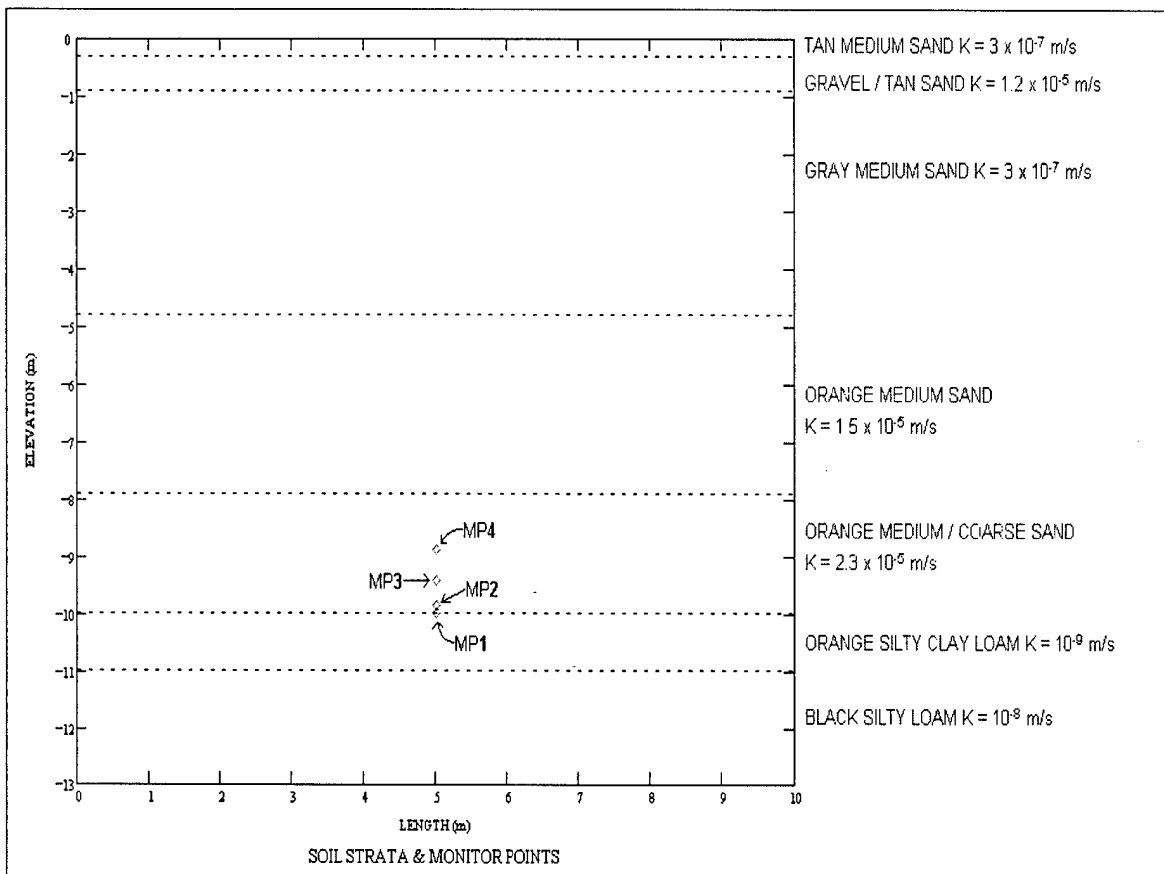


Figure 3. Soil Layers and 4 Monitoring Points



Table 1. Material Properties for Sand Layers

	Tan Medium Sand	Gravel Tan Sand	Gray Medium Sand	Orange Medium Sand	Orange Coarse Sand
Distribution Coefficient ( $\frac{m^3}{Kg}$ )	$10^{-4}$	$10^{-4}$	$10^{-4}$	$10^{-4}$	$10^{-4}$
Bulk Density ( $\frac{Kg}{m^3}$ )	1700	1700	1700	1700	1700
Longitudinal Dispersivity ( $m$ )	0.23	0.23	0.23	0.23	0.23
Lateral Dispersivity ( $m$ )	0.023	0.023	0.023	0.023	0.023
Molecular Diffusivity ( $\frac{m^2}{hr}$ )	$2.98 \cdot 10^{-6}$	$2.98 \cdot 10^{-6}$	$2.98 \cdot 10^{-6}$	$2.98 \cdot 10^{-6}$	$2.98 \cdot 10^{-6}$
Tortuosity	0.6	0.6	0.6	0.6	0.6
Decay Coefficient ( $\frac{m^3}{Kg}$ )	0	0	0	0	0
Freundlich N	1	1	1	1	1
Conductivity ( $\frac{m}{hr}$ )	$1.08 \cdot 10^{-3}$	$4.32 \cdot 10^{-2}$	$1.08 \cdot 10^{-3}$	$5.4 \cdot 10^{-2}$	$8.28 \cdot 10^{-2}$
Moisture Content	.36	.36	.36	.36	.36
Relative Conductivity ( $\frac{m}{hr}$ )	1	1	1	1	1
Water Capacity ( $\frac{1}{m}$ )	0	0	0	0	0

Table 2. Material Properties for Clay Layers

	Orange Silty Clay Loam	Black Silty Loam	Sandy Loam (Fictitious)
Distribution Coefficient ( $\frac{m^3}{Kg}$ )	$3.6 \cdot 10^{-4}$	$1.94 \cdot 10^{-2}$	$2.3 \cdot 10^{-4}$
Bulk Density ( $\frac{Kg}{m^3}$ )	1300	1300	1500
Longitudinal Dispersivity ( $m$ )	0.23	0.23	0.23
Lateral Dispersivity ( $m$ )	0.023	0.023	0.023
Molecular Diffusivity ( $\frac{m^2}{hr}$ )	$2.98 \cdot 10^{-6}$	$2.98 \cdot 10^{-6}$	$2.98 \cdot 10^{-6}$
Tortuosity	0.6	0.6	0.6
Decay Coefficient ( $\frac{m^3}{Kg}$ )	0	0	0
Freundlich N	1	1	1
Conductivity ( $\frac{m}{hr}$ )	$3.6 \cdot 10^{-6}$	$3.6 \cdot 10^{-5}$	$10^{-4}$
Moisture Content	.36	.36	.36
Relative Conductivity ( $\frac{m}{hr}$ )	1	1	1
Water Capacity ( $\frac{1}{m}$ )	0	0	0

Table 3. Vertical Positioning of Central Monitoring Points

Monitoring Point	MP1	MP2	MP3	MP4
Mesh Node Number	1	9334	12445	14519
Vertical Position	-10m	-9.8476m	-9.4327m	-8.8788m

### 3.2.b FINITE ELEMENT MESH

Figure 4 shows the three-dimensional finite element mesh used for this simulation. It consists of 33184 nodes. The corresponding finite elements are right prisms of triangular cross-section (figure 5).

Salient features of the mesh are:

1. Fine lateral clustering of nodes in the vicinities of the three injection and three extraction wells (figure 6).
2. Vertical clustering in accordance with the two FEMWATER guidelines [38, pg 16] calling for:
  - A. No more than 50% increase or decrease in widths of adjacent elements.
  - B. A minimum of three layers of elements vertically for each distinct stratigraphic unit, particularly if large variations of hydraulic conductivity occur in adjacent layers.
  - C. No more than three orders of magnitude difference in hydraulic conductivity between adjacent mesh layers.

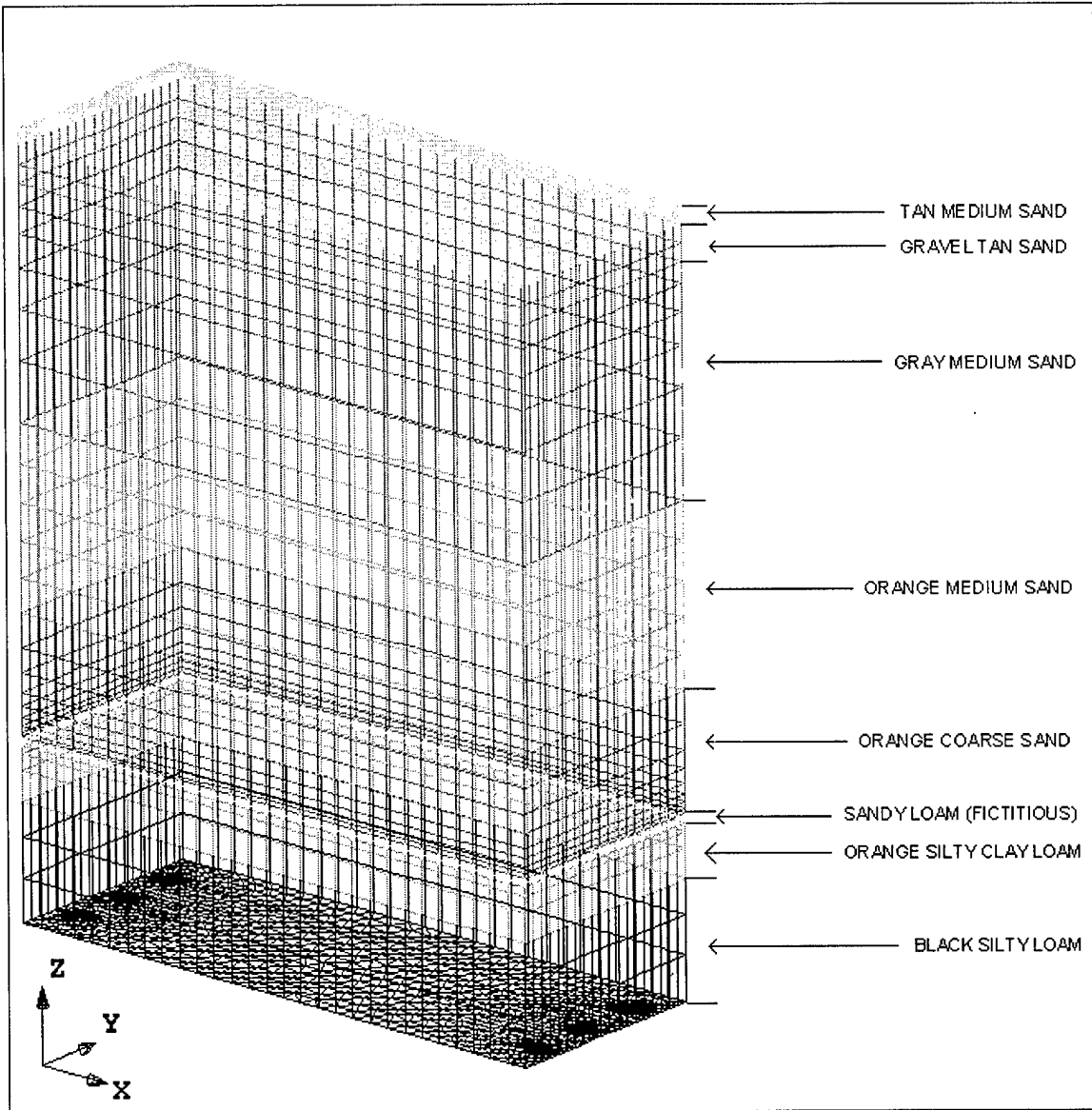


Figure 4. Finite-Element Mesh (33184 Nodes)

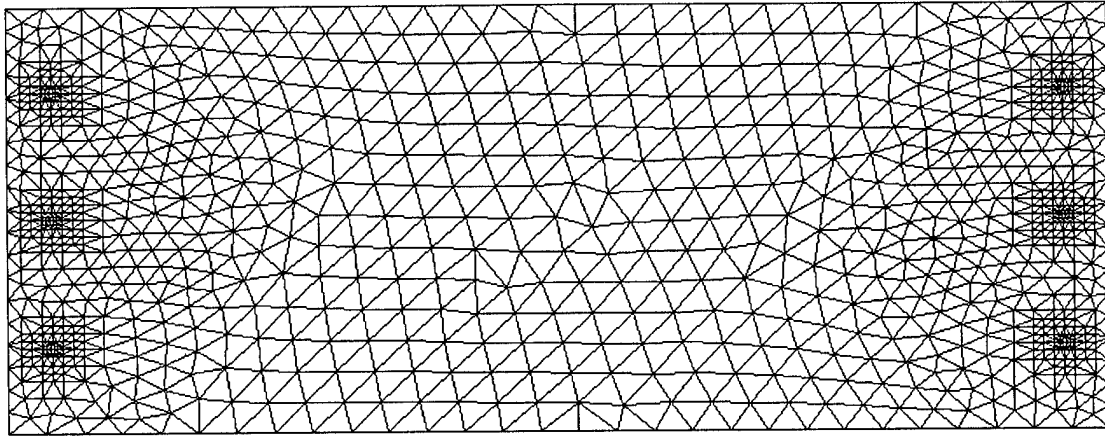


Figure 5. Plan View of 3D mesh

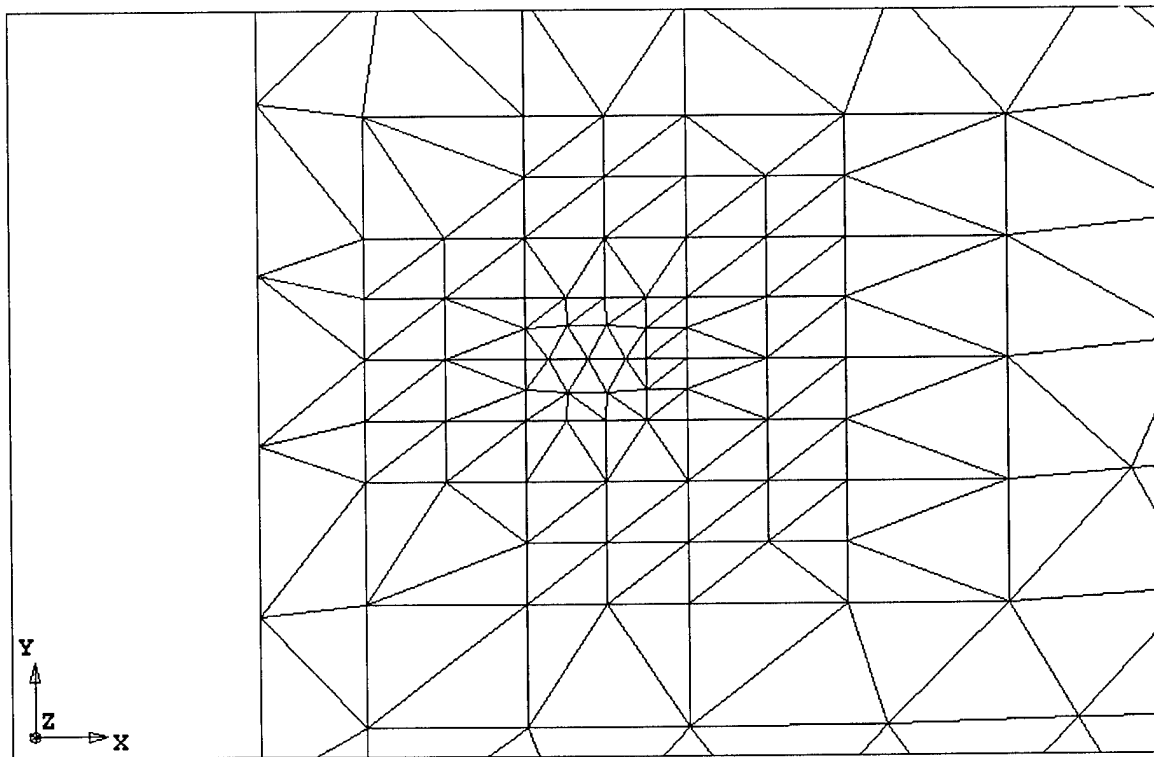


Figure 6. Mesh Detail in the Vicinity of Well

### 3.2.c BOUNDARY CONDITIONS

In imposing boundary conditions, two assumptions were made: First, that the lower bounding surface of the cell was in fact a confining, impermeable one. Second, that there was no ponding and that the water table coincident with the upper surface of the cell. Then, the boundary conditions were simply zero flux of flow or contaminant on all six sides of the test cell. The total volumetric pump rate for three injection wells was  $Q_T = 0.192 \frac{m^3}{hr}$ .

### 3.2.d DISCRETIZATION OF WELLS

Here, the challenge was to model an injection or extraction well – essentially a cylindrical sieve – in a discrete manner consistent with our finite element mesh. As shown in figure 7, Each injection and extraction well was modeled by a series of sources (or sinks, as appropriate). It would have been an over-simplification to simply divide the total injection (or extraction) flow rate  $Q_T$  by the total number of well nodes at the injection (or extraction) end to determine the individual source (or sink) strength. Had this been done, the result would have been that each source or sink would have had identical strength and this would have been inconsistent with the fact that each source's strength must be proportional to the hydraulic conductivity of its confining material. Since each source was sandwiched between materials of different conductivities, its respective strength had in turn to be different. Referring to figure 8, there were several underlying assumptions that had to be made. First, that the water acting under the pressure gradient  $\frac{dh}{dx}$  induced by the pumping process, moved from the injection wells to the extraction wells in parallel horizontal planes albeit at different velocities. Second, that this pressure gradient  $\frac{dh}{dx}$  was then constant across stream layers. These assumptions were consistent with observations made in seminal works such as [2]. Then, the Darcy equation [11, pg 16]  $Q_T = K \cdot W \cdot H \cdot \frac{dh}{dx}$  held not only for the whole cell (of width  $W$  and height  $H$ ), but also for each individual stream layer (of width  $w$  and height  $\delta s_j$ ). The stream layer width  $w$ , depended

on the relative strengths of adjacent wells. Referring to figure 7, The lateral hydraulic zone of influence of each well was in direct proportion to that well's volumetric flow strength. For simplicity, each well was assigned equal volumetric flow strength. Then  $Q_j = K_j \cdot w \cdot \delta s_j \cdot \frac{dh}{dx}$  could be written for each layer, where  $\delta s_j$  was the thickness of the stream layer in question and  $k_j$  a weighted hydraulic conductivity relevant to  $\delta s_j$  since  $\delta s_j$  spanned adjacent finite element mesh layers, of differing hydraulic conductivity. If the total volumetric flow rate of an injection well was  $Q_T$ , then the volumetric flow rate through stream layer  $\delta s_j$  was simply  $Q_j$  where  $Q_T = \sum Q_j = \sum (K_j \cdot w \cdot \delta s_j \cdot \frac{dh}{dx}) = w \cdot \frac{dh}{dx} \sum (K_j \cdot \delta s_j) = w \cdot \frac{dh}{dx} \cdot K \cdot \Delta z$ , the summation being over all stream layers  $j$ . Note that in what follows,  $i$  indexes mesh layer and  $j$  indexes stream layer. As shown in figure 8, the stream layers overlapped mesh layers. A vertical series of point flow sources of volumetric strengths  $Q_j$  was placed along the axis of the well in question, the sum of strengths  $Q_T$  producing the overall volumetric flow rate of the well. It then remained to determine the relative weighting of each of these point sources, consistent with the local hydraulic conductivities  $K_j$ . Well,  $Q_j = K_j \cdot w \cdot \delta s_j \cdot \frac{dh}{dx}$  but  $w \cdot \frac{dh}{dx} = \frac{Q_T}{K \cdot \Delta z} = \frac{Q_T}{\sum K_j \cdot \delta s_j} = \frac{Q_T}{\sum K_i \cdot \delta z_i}$  so  $Q_j = \left( \frac{K_j \cdot \delta s_j}{\sum K_i \cdot \delta z_i} \right) \cdot Q_T$ . Now a third assumption had to be made, concerning our choice of the  $\delta s_i$ , the stream layer thicknesses. It was assumed that within a given layer of mesh elements, between two adjacent sources, the sources "shared" the layer of elements equally. Specifically, each source's hydraulic zone of influence extended to the centerline of the adjacent layer of elements. In the exceptional case that a given layer of mesh elements was bounded on only one edge by a source, then that source's hydraulic zone of influence encompassed the entire width of the semi-bounded element layer. This is depicted schematically in figure 8. Each  $\delta s_i$  was the sum of the local  $\delta z_{t_i}$  and  $\delta z_{b_i}$ . It was assumed  $\delta z_{t_i}$  and  $\delta z_{b_{i-1}}$  were equal within each mesh layer  $\delta z_i$ . In other words  $\delta z_{t_i} = \delta z_{b_{i-1}} = \frac{\delta z_i}{2}$ . For which,  $Q_i = \left( \frac{K_i \cdot \delta z_{t_i} + K_{i+1} \cdot \delta z_{b_i}}{\sum K_i \cdot \delta z_i} \right) \cdot Q_T$

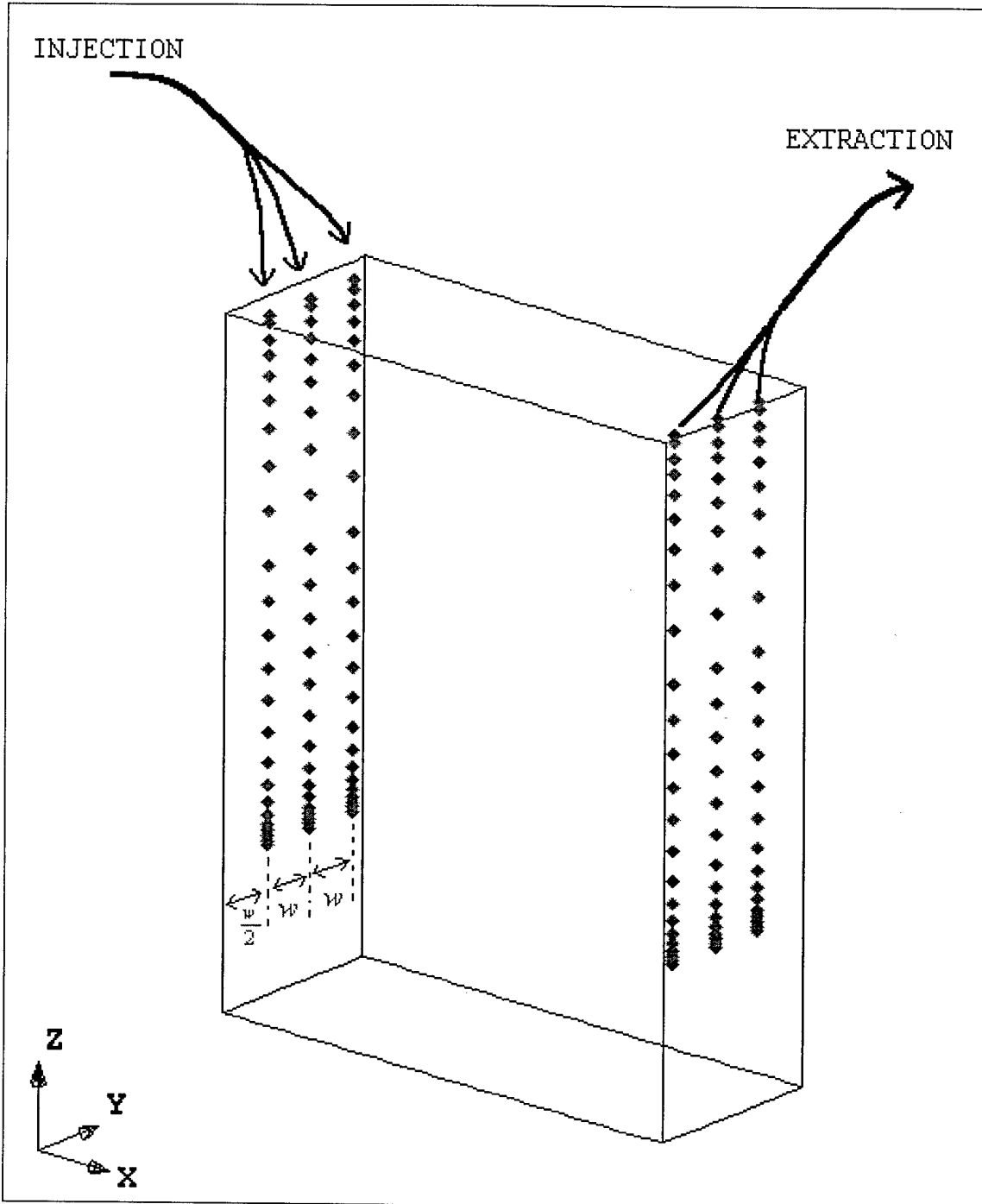


Figure 7. Well Discretization by Point Sources and Sinks

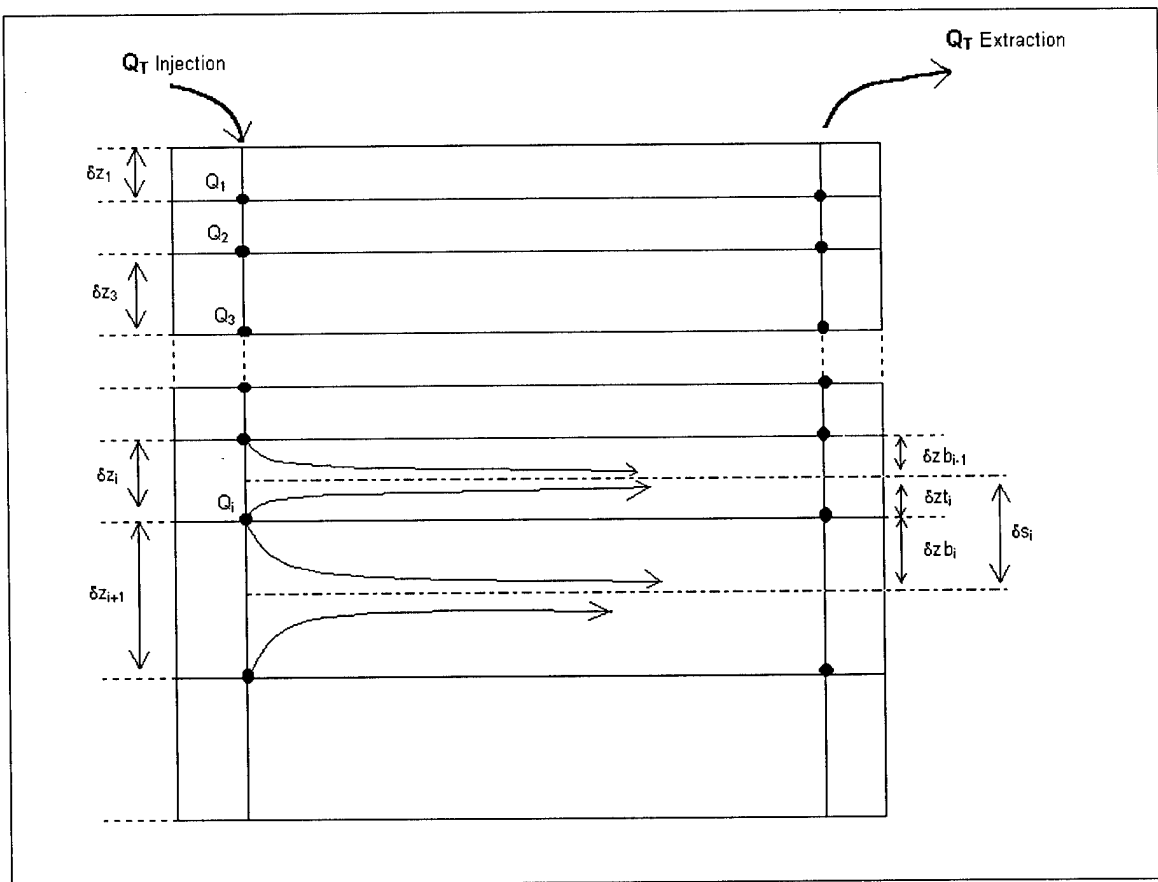


Figure 8. Source Placement and Streamsurface Geometry



### 3.2.e CURVES OF SOIL HYDRAULIC PROPERTIES

The FEMWATER model calls for the following three curves of soil hydraulic properties versus pressure head  $h$ :

1. Moisture content ( $\theta_w$ )
2. Water capacity ( $\frac{\partial \theta_w}{\partial h}$ )
3. Relative conductivity ( $K_r$ )

Since the test cell was taken to be saturated, these three properties are constant with  $h$  [11, pg 39] . However, according to Zakikhani [41] , it is prudent to include portions of the properties' curves for unsaturated regions of  $h$  since, during the transient course of computing a saturated solution, it is possible for the computed solution to dip into the unsaturated domain. Not properly representing this domain through the soil properties curves may lead to instability. Hence, computation of curves was done using the full Van Genuchten models [36] .

First, the so-called "effective moisture content",  $\theta_e$  must be defined – in which  $\alpha$ ,  $\beta$ , and  $\gamma = 1 - \frac{1}{\beta}$  are constant properties of the material in question:

$$\theta_e(h) = \begin{cases} [1 + (\alpha h)^\beta]^{-\gamma} & \text{if } h < 0 \\ 1 & \text{if } h \geq 0 \end{cases}$$

Then, with  $\theta_s$  and  $\theta_r$  (also material constants) defined as "saturation moisture content" and "residual moisture content" respectively, moisture content is defined as:

$$\theta_w = \theta_r + \theta_e(\theta_s - \theta_r)$$

Next,  $\frac{\partial \theta_e}{\partial h}(h)$  is given by

$$\frac{\partial \theta_e}{\partial h}(h) = \begin{cases} -[1 + (\alpha h)^\beta]^{(-\gamma-1)} \gamma (\alpha h)^\beta \frac{\beta}{h} & \text{if } h < 0 \\ 0 & \text{if } h \geq 0 \end{cases}$$

Then,

$$\frac{\partial \theta_w}{\partial h}(h) = \frac{\partial \theta_e}{\partial h}(h)(\theta_s - \theta_r)$$

And the Van Genuchten model for relative conductivity ( $K_r$ ) is given by:

$$K_r(h) = \sqrt{\theta_e(h)} \left[ 1 - \left( 1 - \theta_e(h)^{\frac{1}{\beta}} \right)^\gamma \right]$$

Using data provided in Van Genuchten's original paper [36] , as well as sample data provided in the FEMWATER manual [38] as a basis, values for the the parameters  $\alpha$ ,  $\beta$ ,  $\theta_s$ , and  $\theta_r$  were approximated. These are listed in Table 4 below.

Choosing sand for representative purposes, figures 9, 10, and 11 show  $\theta_e$ ,  $\frac{\partial \theta_e}{\partial h}$ , and  $K_r$  respectively versus pressure head  $h$ . Note that 1000 points were used for each curve to provide sufficient resolution in the vicinity of the inflections at  $h = 0$ .

Table 4. Van Genuchten Parameters for Soil Hydraulic Properties

	$\theta_s$	$\theta_r$	$\alpha (\frac{1}{m})$	$\beta$
SAND	0.43	0.045	14.5	2.68
SILTY CLAY LOAM	0.43	0.089	1	1.23
SILTY LOAM	0.45	0.067	2	1.41

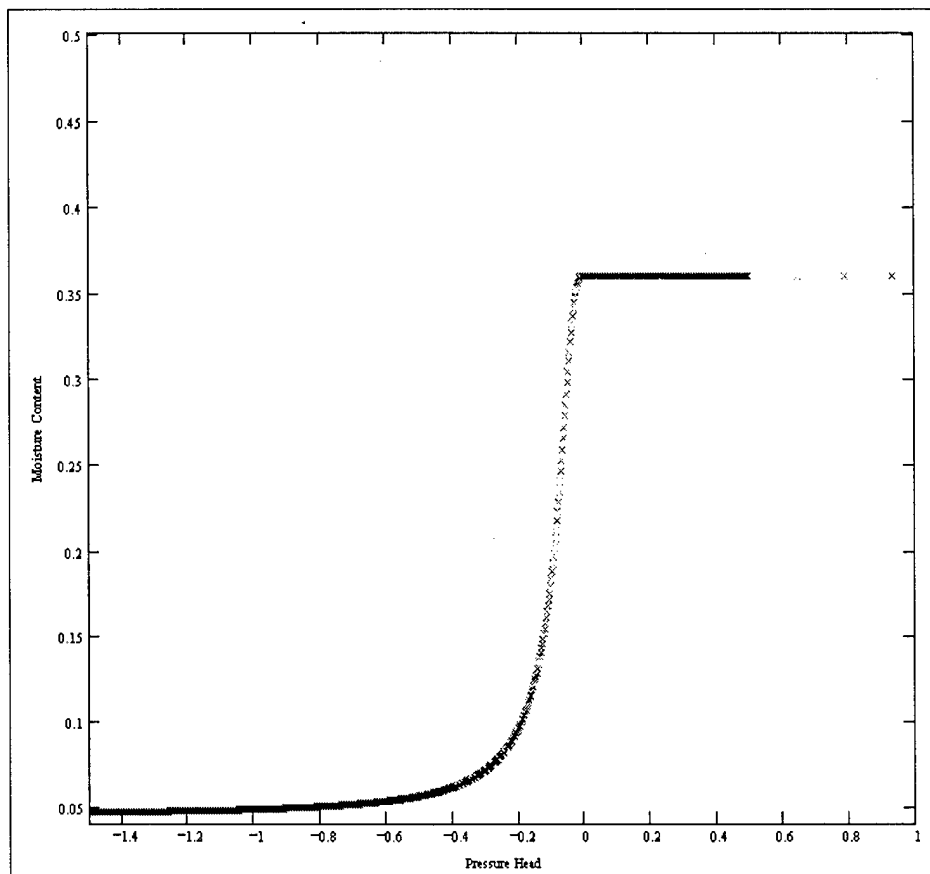


Figure 9. Moisture Content vs. Pressure Head (Sand)

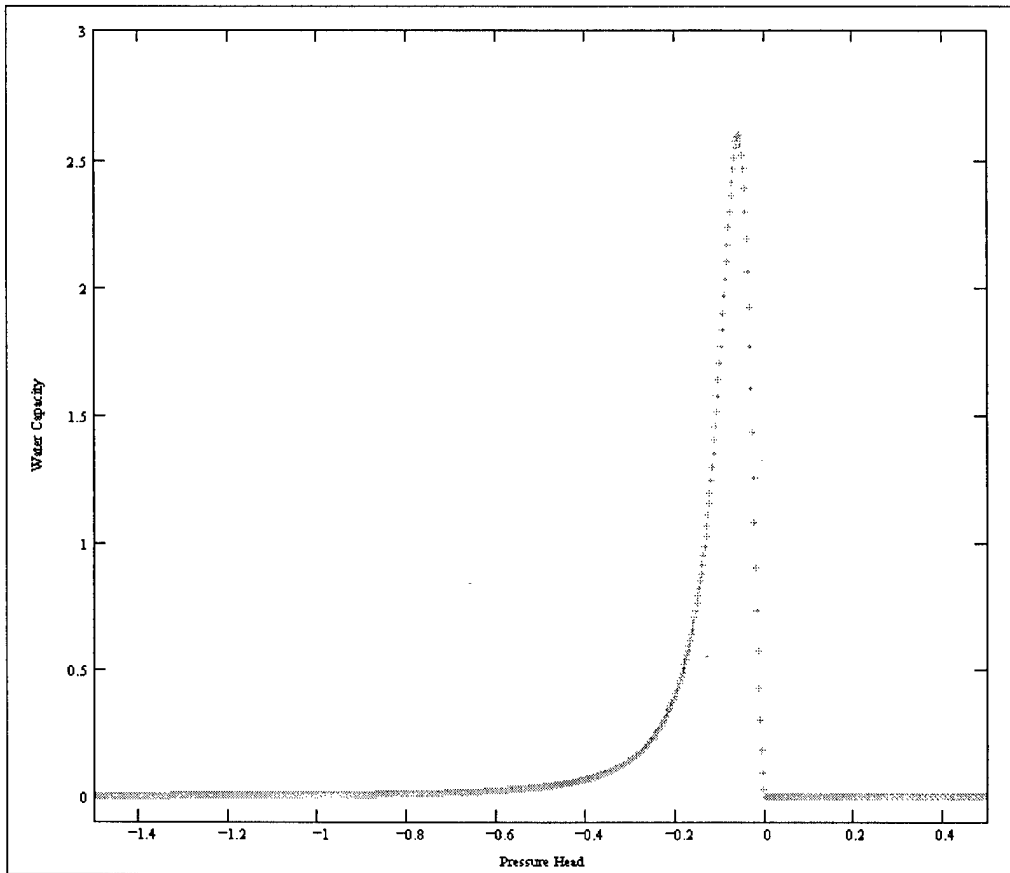


Figure 10. Water Capacity vs. Pressure Head (Sand)

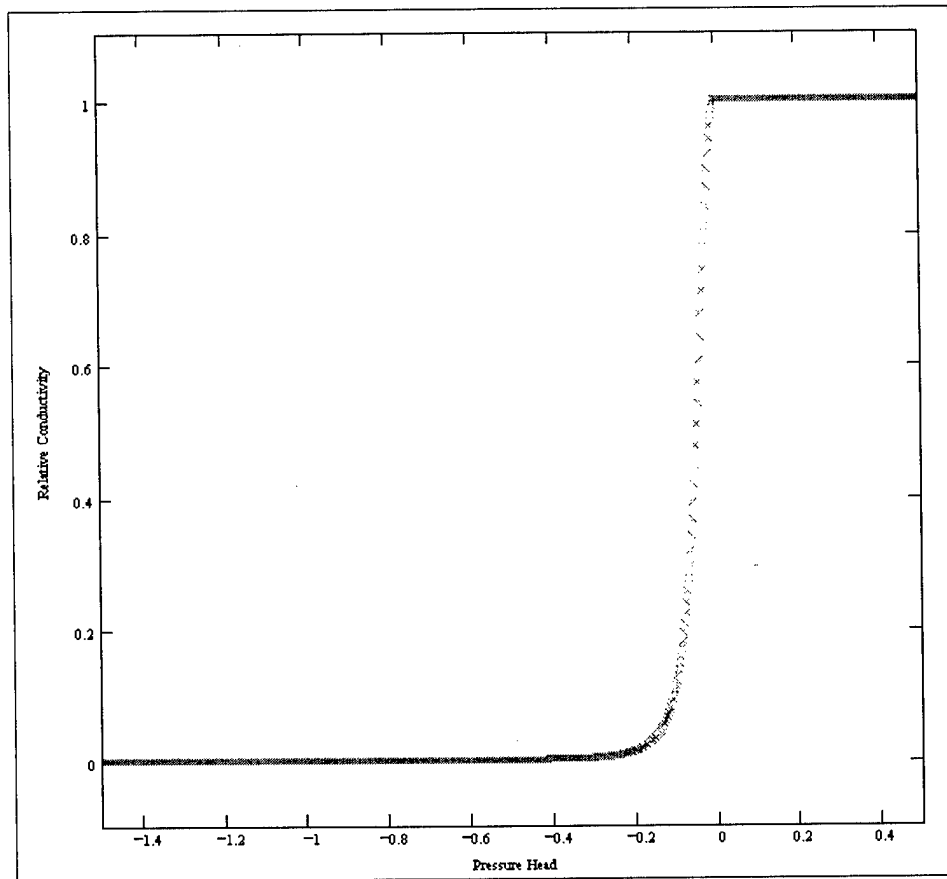


Figure 11. Relative Conductivity vs. Pressure Head (Sand)

## 4. NUMERICAL SIMULATIONS

In accordance with the research objectives stated in section 1.3; namely, to validate the numerical formulation and determine qualitative aspects of pump-and-treat remediation, the following simulations were run:

1. The flow solution showing the velocity field as vectors. In the subsequent computations, this computed velocity field formed the basis for all transport simulations. As explained in section 2.2 above, if the flow is steady-state, the velocity field enters into the transport equation as a spatially-variable coefficient. With the velocity field in hand, the transport equation can then be solved.
2. The transport solution resulting from the injection of a unit concentration of contaminant for 200 hours. This solution allowed a moment analysis cross-check.
3. Another transport solution for a 200 hour injection pulse, as above, but with retardation factor equal to one for all soil layers. This was to examine the effect of retardation on contaminant transport.
4. The transport solution resulting from the continuous pumping of the test cell with clean water, starting with a prescribed initial contaminant distribution. This was to spatially examine how the aquifer/aquitard composite was releasing or retaining contaminant.
5. The transport solution resulting from continuous pumping (as above) for 3600 hours, followed by pump stand-down for an additional 1900 hours, then resumption of pumping. This was to examine the effect of diffusive contaminant rebound from the aquitard sublayer.
6. The transport solution resulting from the continuous pumping of the test cell with clean water, starting with an initial contaminant distribution provided by the field experimenters [27]. This was to determine how well the FEMWATER simulation mimicked data from the Dover AFB remediation experiment.
7. The transport solution resulting from the continuous pumping of the test cell with clean water, starting with a prescribed initial contaminant distribution provided by Herman [21, pg 12]. This was to compare with another numerical simulation of the Dover AFB remediation experiment.

Sections 4.1 through 4.7 detail the seven simulations listed above.

## 4.1 COMPUTATION OF FLOW SOLUTION

A sample input file is given in appendix B.1. The computed velocity field is shown in figures 12, 13, and 14. For clarity, only every third computed velocity vector is shown in plot 12. Note that in figure 14 the large arrows depicting vector velocity in the immediate vicinity of the sink appear to be directed away from the sink. This is an anomaly of the plotting software. They should be oriented so that their heads converge, or "touch" at the sink. However, this would obscure detail in that area, hence their "backwards" orientation. There are several observations that can be made immediately:

1. The graphical disparity between flow admittance in the various aquifer and aquitard materials.
2. The fact that the fluid – albeit at different velocities – moves in parallel layers, supporting shear-generated mixing.
3. Figure 14 is a close up of the flow field in the vicinity of a sink node. It's remarkable (but not really surprising!) that the flow field is very three-dimensional in this area but very ordered and laminar near the center of the test cell (figure 13).

Finally, figure 15 shows the vertical distribution of longitudinal velocity at the center of the cell. Only every third computed velocity vector is shown in the plot. Once again, the division of flow between aquifer and aquitard layers is very evident.

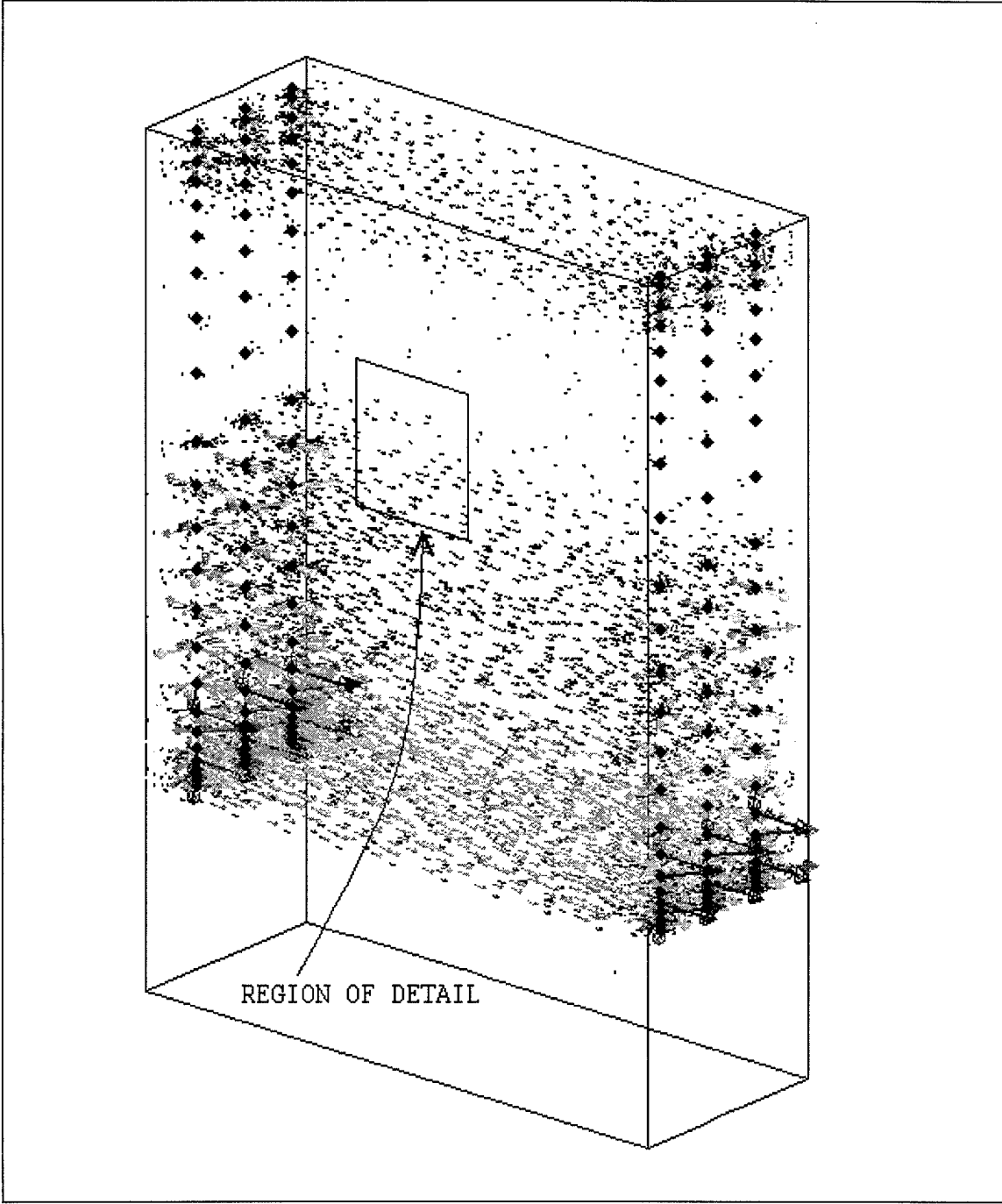


Figure 12. Velocity Vector Field



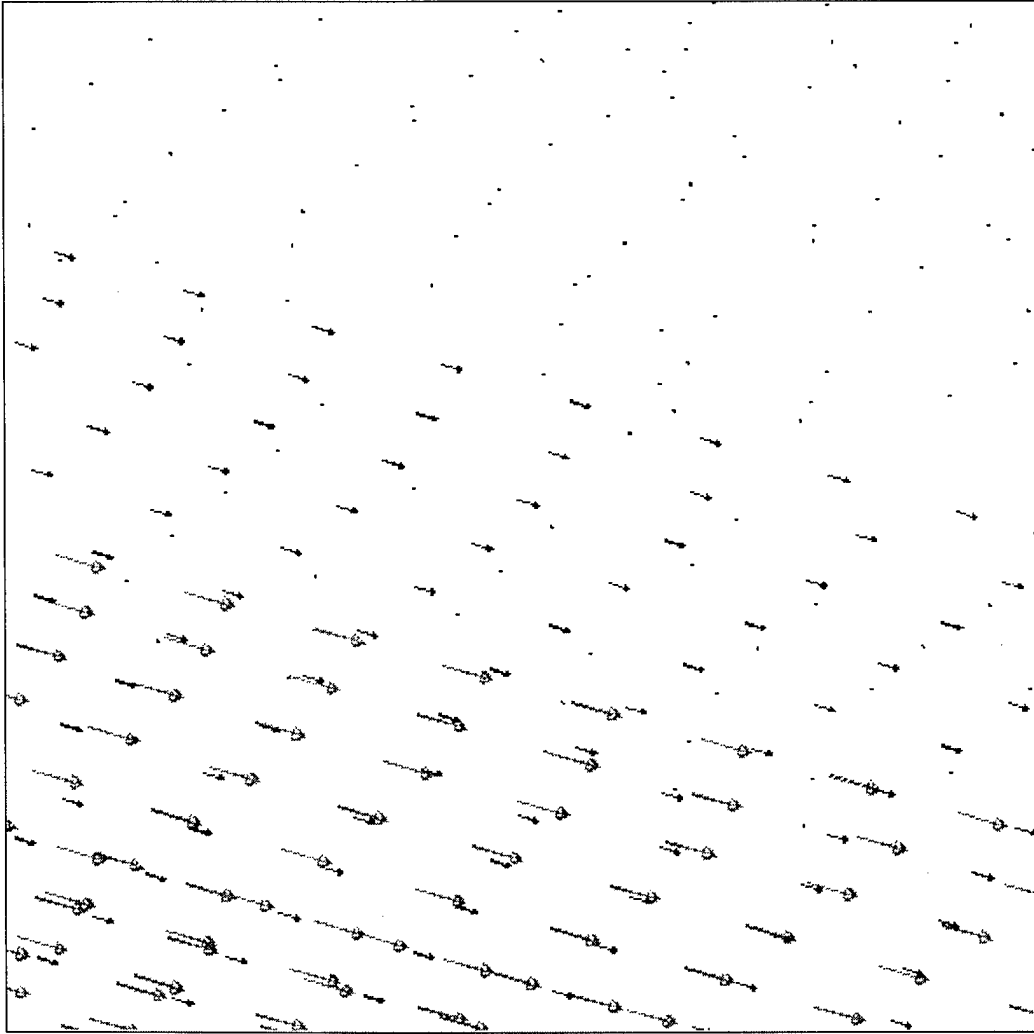


Figure 13. Velocity Vectors in the Region of Detail

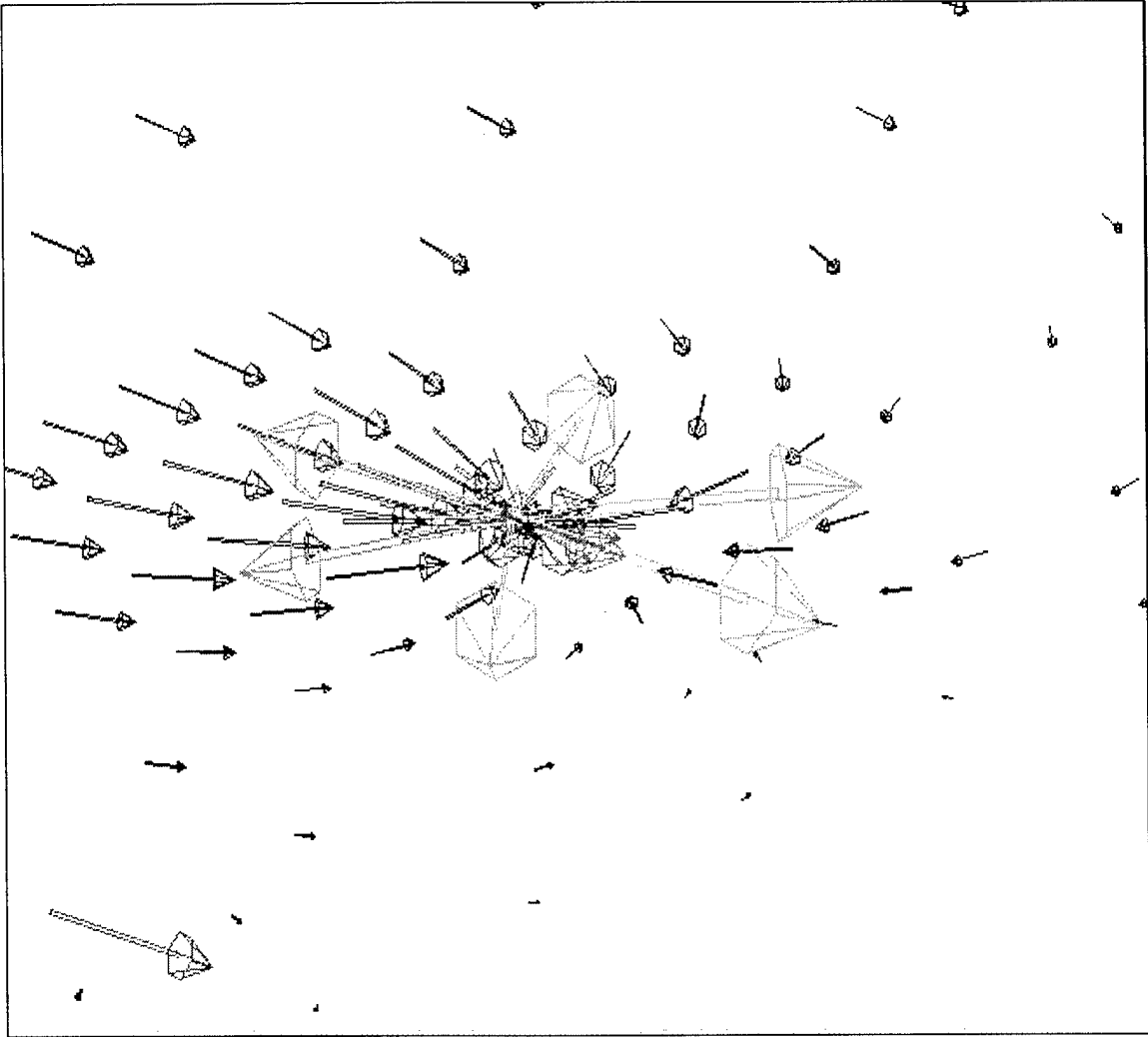


Figure 14. Velocity Vectors Near a Sink Node

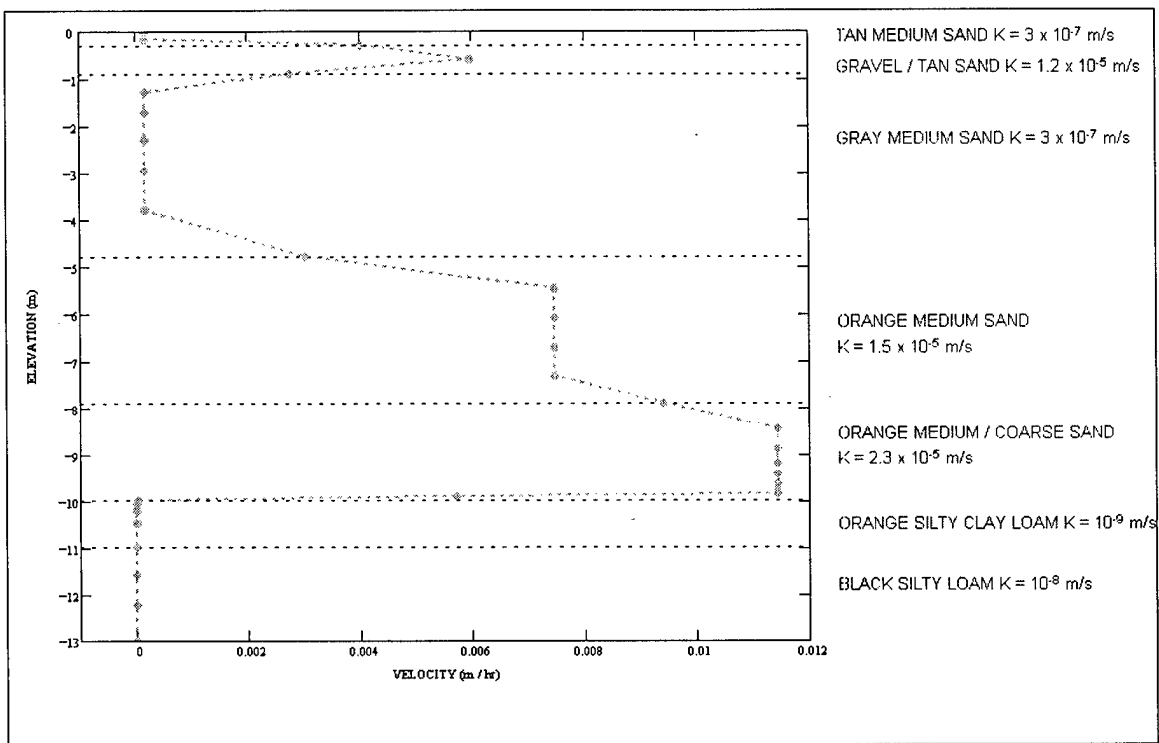


Figure 15. Vertical Distribution of Longitudinal Velocity (m / hr)

Normally, the validity of the flow solution would be ascertained by comparing the distribution of computed pressure head (from which the velocity field is derived) with the pressure head distribution measured in the field. However, the latter was unavailable at the time of writing. Nevertheless, the qualitative behaviour indicated in the observations above was consistent with expectations. A moment analysis (following section) of the results provided additional validation.

## 4.2 MOMENT ANALYSIS CROSS-CHECK

The cross-check was an order-of-magnitude comparison between two calculations of mean residence time of contaminant in transit between the injection wells and the extraction wells. The first ( $T_{res}$ ) is based solely on the physical characteristics of the test cell. The second ( $T'_{res}$ ) is based on a moment analysis of the computed curve of mass recovery rate versus time at the extraction well. The first calculation is as follows:

- 1 A mean velocity is calculated at the center of the cell over the depth of the cell:

$$V_{mean} = \frac{\sum_{i=1}^{N-1} \left( \frac{V_{i+1} + V_i}{2} \right) \cdot (h_{i+1} - h_i)}{h_N - h_1} = 0.003882 \text{ m/hr} \quad 9$$

where  $V_i$  and  $V_{i+1}$  are computed velocities.

- 2 A transport length,  $L$ , is given by the longitudinal distance between the line of injection wells and the line of extraction wells:

$$L = x_{extraction} - x_{injection} = 9.6654 - 0.3866 = 9.2788 \text{ m}$$

- 3 A composite retardation factor  $R_{com}$  is given by the expression:

$$R_{com} = \frac{\text{Capacity for solute in all zones}}{\text{Capacity for solute in mobile zones}}$$

$$R_{com} = \frac{\sum_{i=1}^N \text{porosity}_i \cdot \text{depth}_i \cdot R_{layer,i}}{\sum_{i=1}^5 \text{porosity}_i \cdot \text{depth}_i \cdot R_{layer,i}} = 12.2$$

where  $R_{layer,i}$  is the retardation coefficient associated with layer  $i$  – of thickness  $\text{depth}_i$ .

- 4 Finally, the mean residence time based on mean velocity  $V_{mean}$  and composite retardation factor  $R_{com}$  is

$$T_{res} = \frac{L}{V_{mean}} R_{com} = 29161 \text{ hours}$$

The second calculation,  $T'_{res}$ , is based on the moment analysis [14, pg 1575-1585] of the contaminant breakthrough curve at the extraction well. The idea is to compute, using the simple principle of moments, the "center of gravity" of the area under the curve of mass recovery rate versus time. In the present case the observation location is the line of extraction wells and  $T'_{res}$  is a measure of the mean residence time of contaminant in the test cell. The actual numerical simulation proceeded as follows: A unit concentration of contaminant was injected into the

test cell for a known length of time (200 hours). This was the test pulse. The introduction of contaminant was then ceased but the flushing cycle with clean water (at the original pumping rate) was maintained. Throughout this process, the mass collection rate at the extraction well was monitored. This is defined as the inner product of two vectors; namely, contaminant concentrations at the sink nodes and corresponding sink flow rates, i.e.  $\sum_{i=1}^{Nodes} C_i \cdot Q_i$ . The curves depicting injection and extraction mass rates respectively are shown schematically in figure 16 below. The rectangular, injection pulse is on the left. The bell-shaped "breakthrough" curve, describing extraction mass rate versus time, is on the right. To compute a mean residence time based on a moment analysis of the breakthrough curve at the extraction well, the following temporal moments were computed:

Zero Absolute Moment [ $M$ ]:

$$M_{0,t} = \int_0^{\infty} \left( \sum_{i=1}^{Nodes} C_i \cdot Q_i \right) dt$$

First Absolute Moment [ $M \cdot t$ ]:

$$M_{1,t} = \int_0^{\infty} \left( \sum_{i=1}^{Nodes} C_i \cdot Q_i \right) \cdot t dt$$

First Normalized Moment [ $t$ ]:

$$\mu'_{1,t} = \frac{M_{1,t}}{M_{0,t}}$$

Computed Mean Residence Time:

$$T'_{res} = \mu'_{1,t} - \frac{T_{pulse}}{2}$$

Where  $T_{pulse}$  is the duration of a rectangular tracer input pulse.  $T_{res}$  and  $T'_{res}$  must be compared to determine whether our computational model is self-consistent. Figure 17 shows the breakthrough curve at the extraction wells resulting from a  $T_{pulse} = 200$  hour injection pulse of unit concentration and  $0.192 \frac{m^3}{hr}$  injection rate. Note that the computation was performed for 7000 hrs after which an exponential tail (dotted portion of the curve) was fit to the

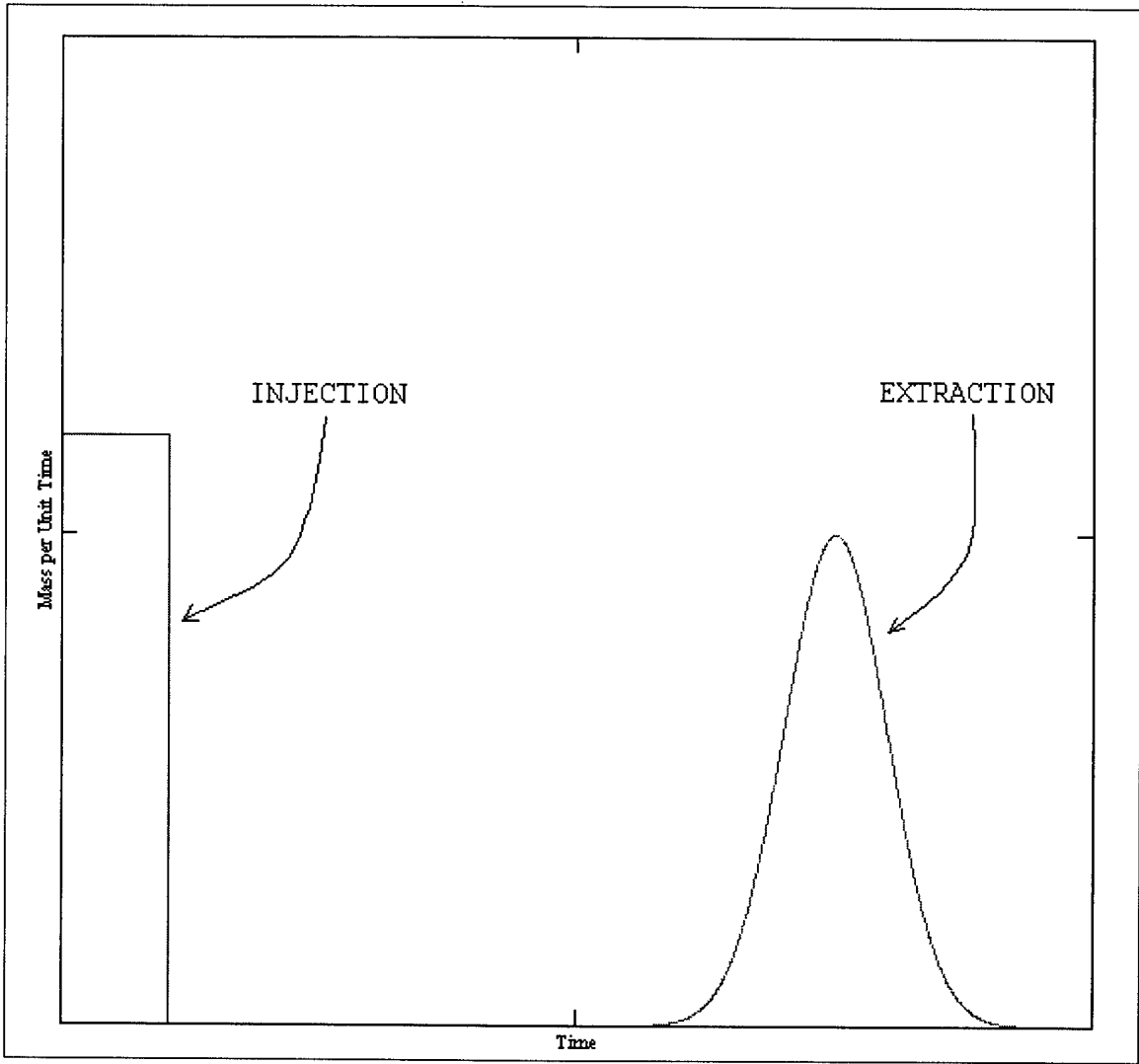


Figure 16. Schematic of Injection Pulse and Mass Recovery Curves

computed portion of the breakthrough curve as is commonly done [20, pg 4] . Essentially, the computed breakthrough curve is plotted on semi-Log coordinates. The trailing region of this curve (roughly the last 1000 hours) looks like a straight line in this coordinate frame. An exponential tail (which also looks like a straight line in these coordinates) can be matched directly. Figure 18 shows the same breakthrough curve with its parent rectangular injection pulse. Log-Log coordinates are necessary for clarity. The partial overlap in the injection and breakthrough profiles indicates that contaminant had begun to arrive at the extraction wells before the completion of the input pulse. The area under the breakthrough curve was calculated using the trapezoidal rule for the numerically-generated portion of the curve whereas the area under the exponential tail was computed analytically. The computed result of  $T'_{res} = 33834$  hours compares very favorably with the theoretical  $T_{res} = 29161$  hours.

Based on the favorable result of the moment-analysis cross-check, we can conclude that our numerical formulation constitutes a realistic model of the injection-extraction dynamics in the test cell under investigation.

In performing the moment analysis, cross-sectional contour profiles of injected contaminant in the test cell were generated as a by-product. These are shown, for various times, in figures 19 through 22. Colors represent aqueous contaminant concentration. Examining these contour plots provides valuable insight into the nature of the aquifer/aquitard system. The first figure (19) shows the contaminant plumes after the 200 hr injection pulse. Clearly, the contaminant has made significant inroads into the aquifer material but little progress in the aquitard layers. Moving particularly rapidly is the contaminant in the orange medium/coarse sand where the flow rate is highest (figure 15). At the end of the 200 hr contaminant injection pulse, the clean water flushing commences and in the subsequent plots we note the lateral dispersive spread of contaminant into the aquitard layers, even as the flushing acts to force contaminant in the



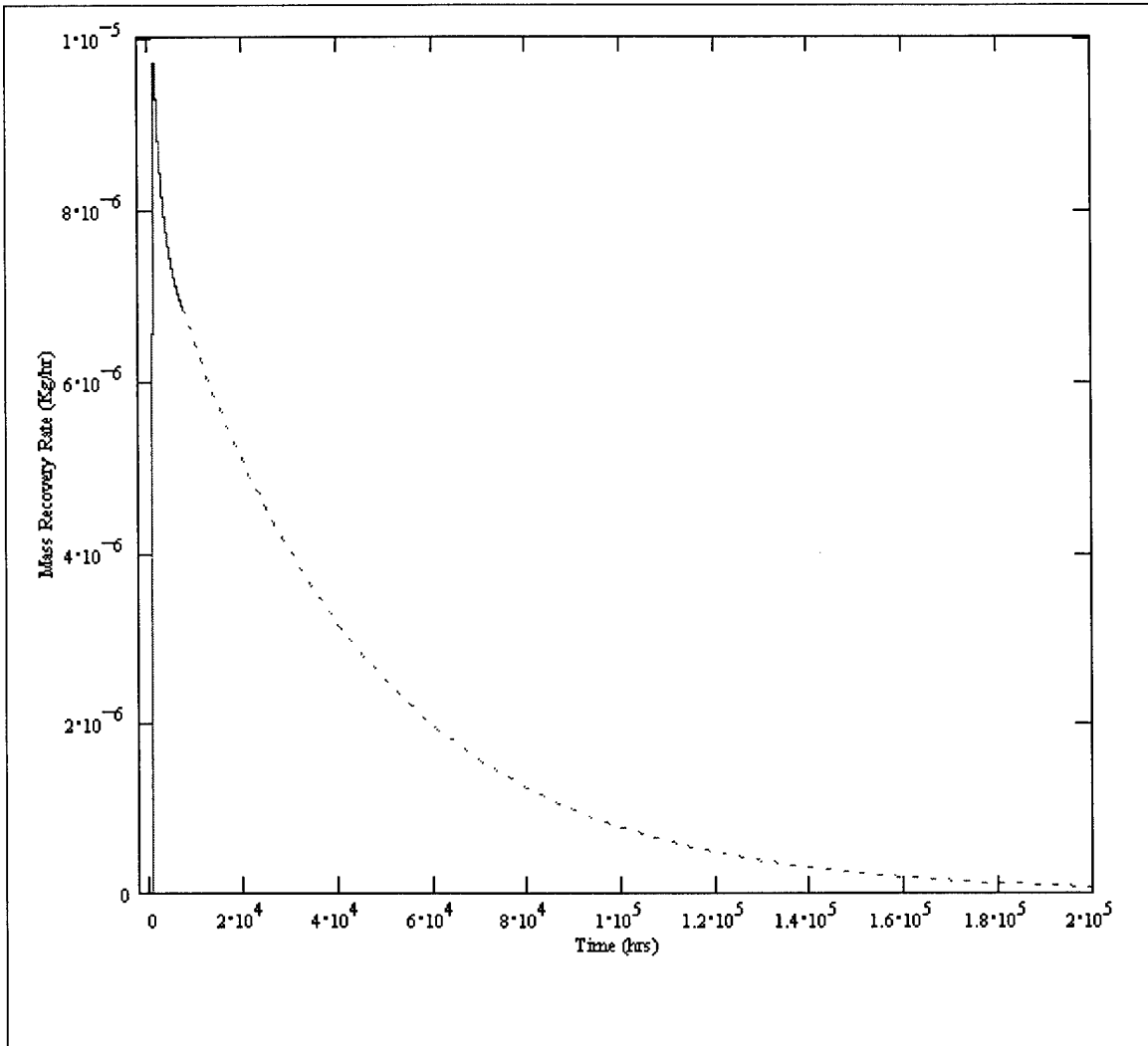


Figure 17. Mass Recovery Rate vs. Time for 200 hr Injection Pulse

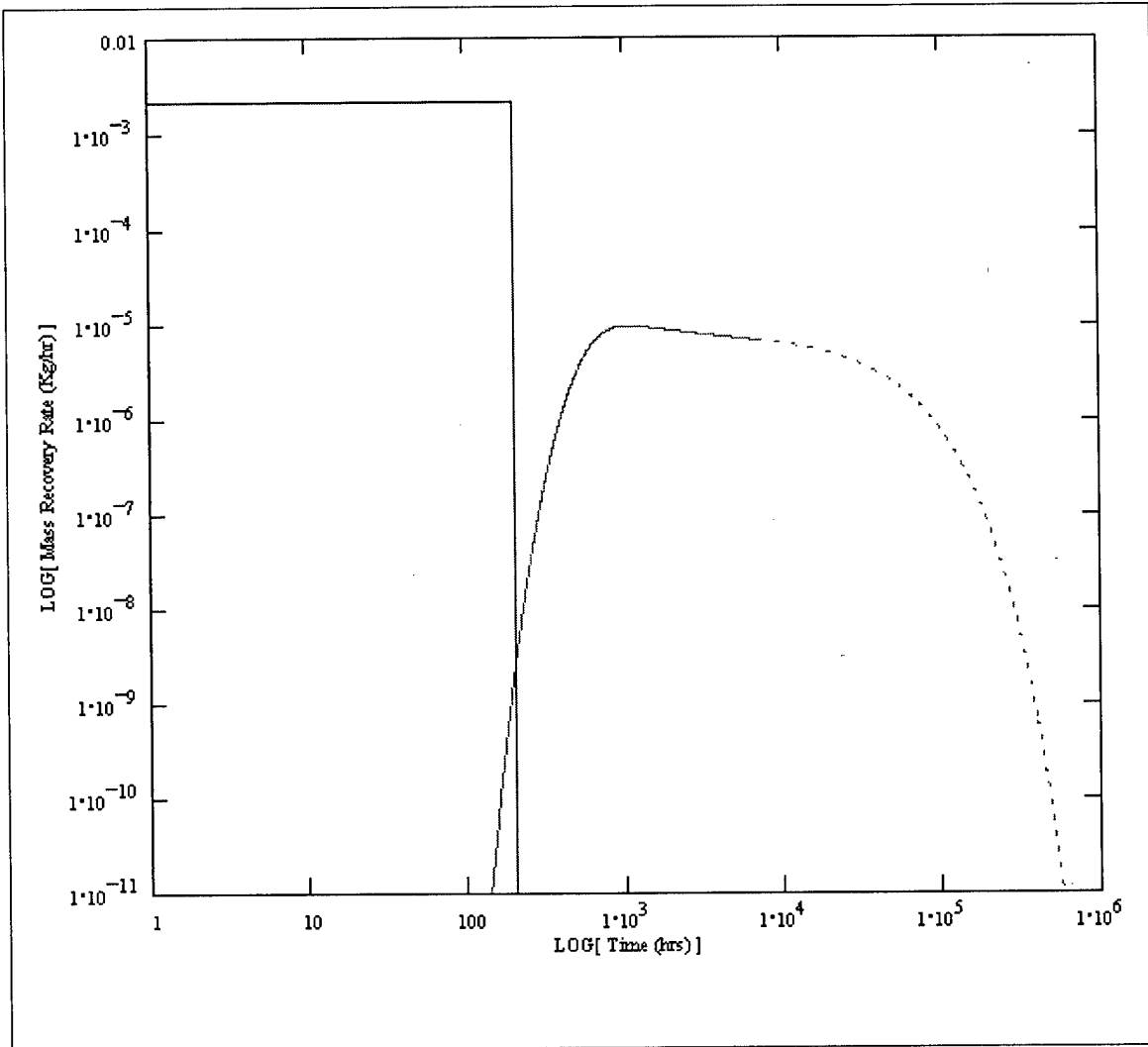


Figure 18. Injection Pulse and Extrapolated Extraction Breakthrough

aquifer layers towards the extraction wells. Recall that high hydraulic conductivity is unimportant in diffusion-dominated processes such as this lateral spreading into the aquitard material. Moreover, since it is not easy to purge aquitard layers of contaminant by clean water flushing, it follows that once contaminant has ensconced itself in these aquitard layers, it will be difficult to remove – hence the “diminishing returns” or tailing we see in the breakthrough curve (figure 17). Thus, the pulse injection simulation has provided graphical and computational evidence that the contaminated cell behaves dispersively under clean water flushing and resists efforts to purge it.

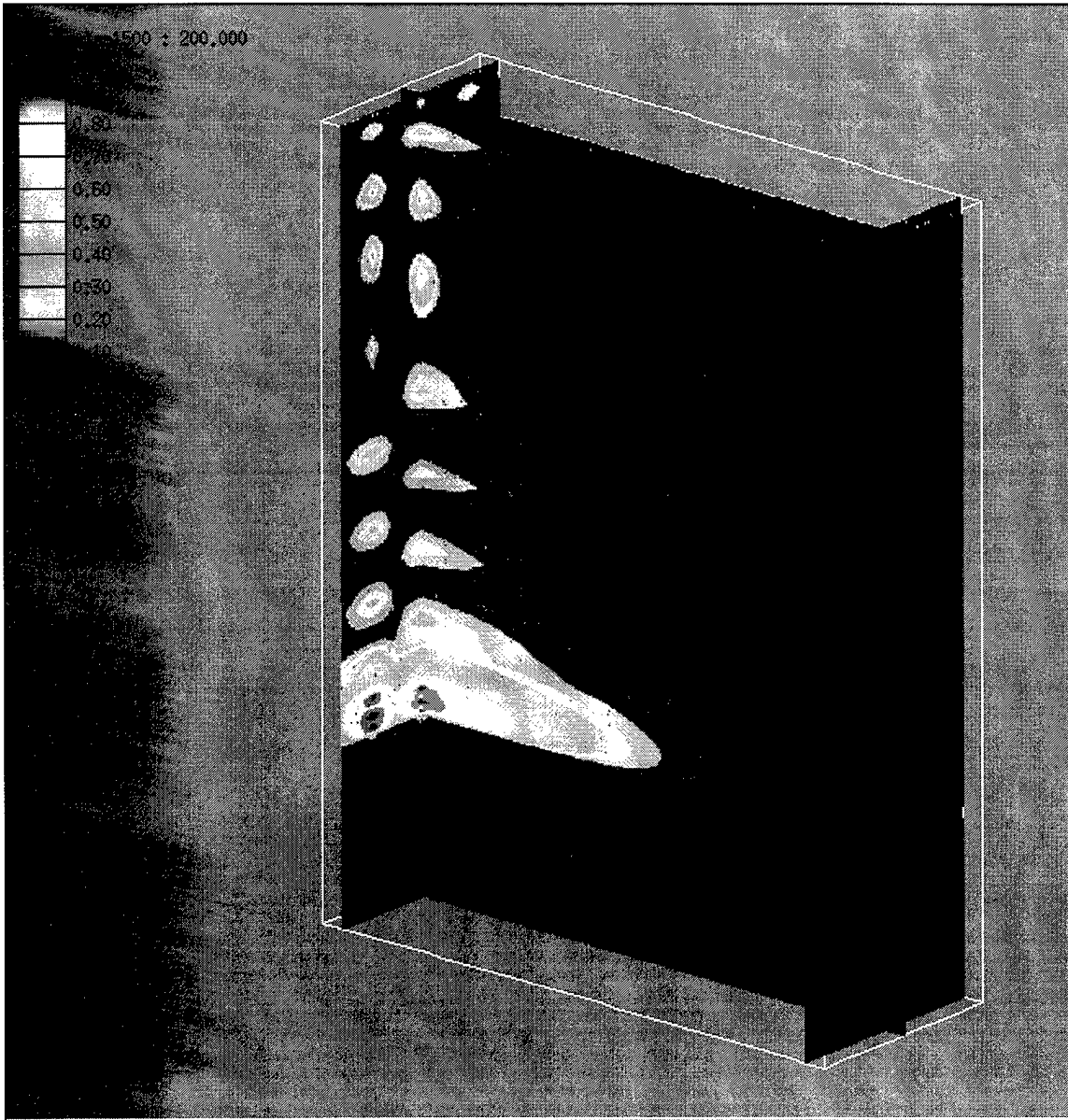


Figure 19. Contaminant Plumes After 200 hour Injection Pulse (Aqueous Concentration)

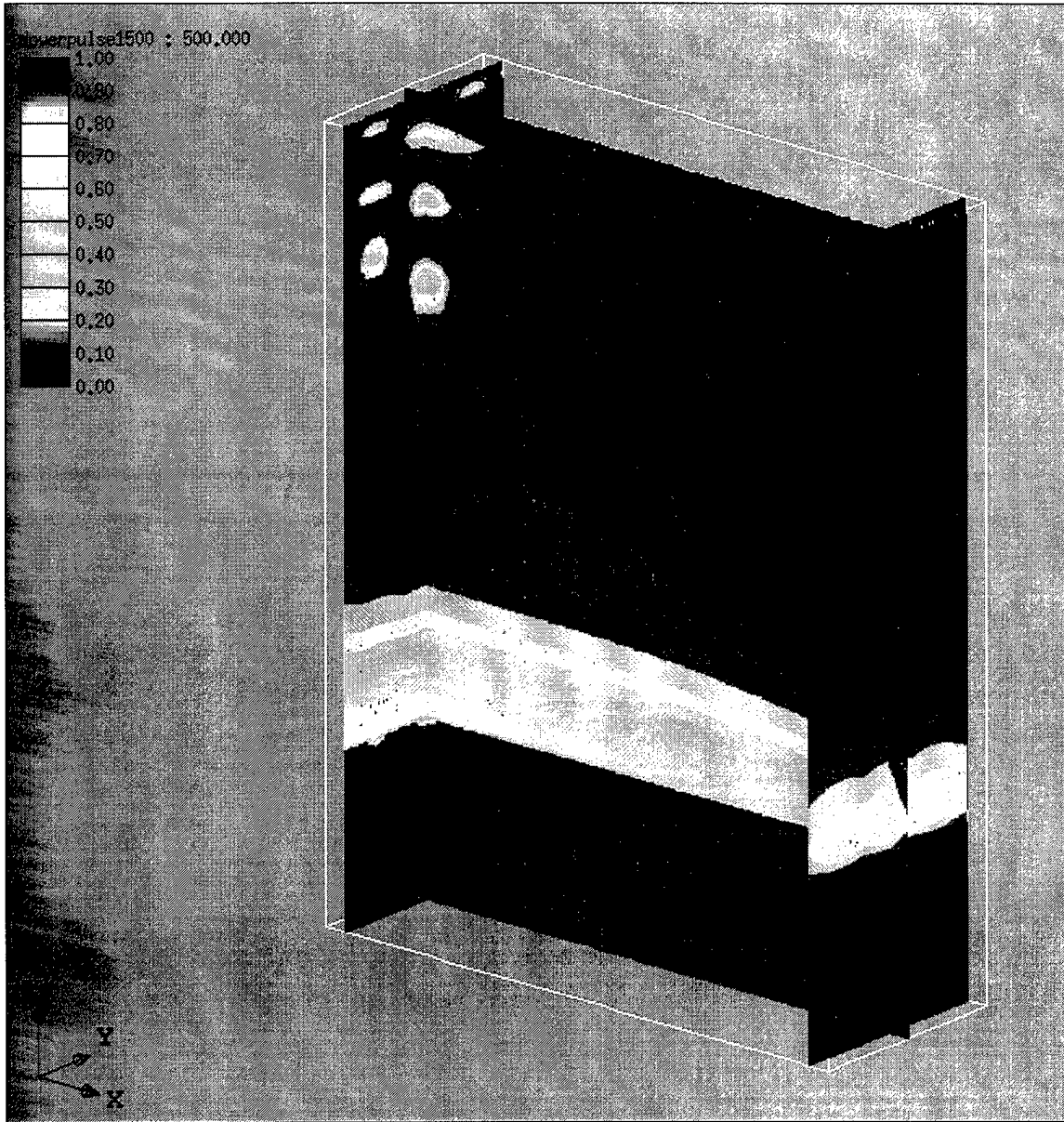


Figure 20. Contaminant Plumes at T=500 hrs, After 300 Hours of Clean Water Flushing

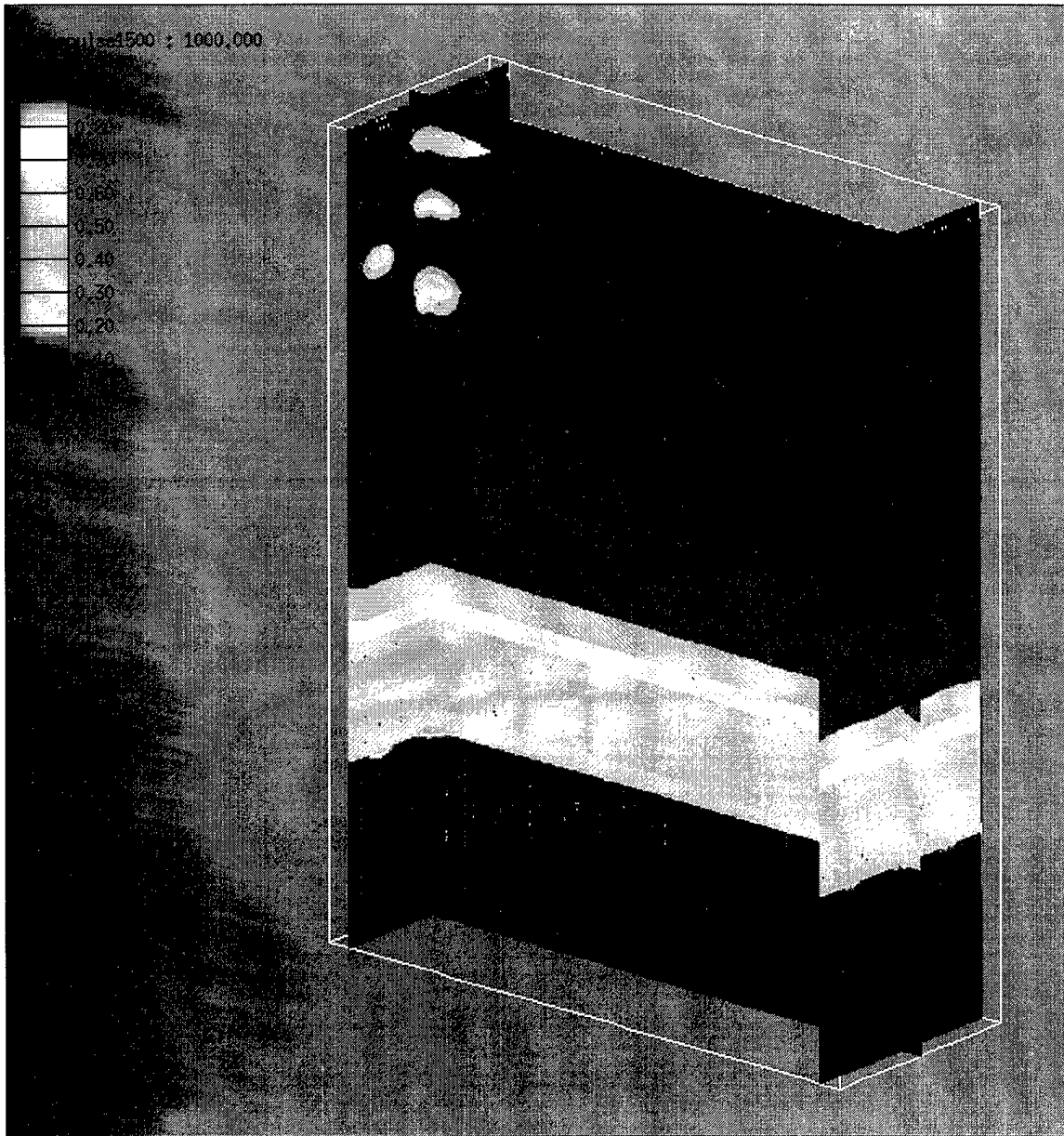


Figure 21. Contaminant Plumes at T=1000 hrs, After 800 Hours of Clean Water Flushing

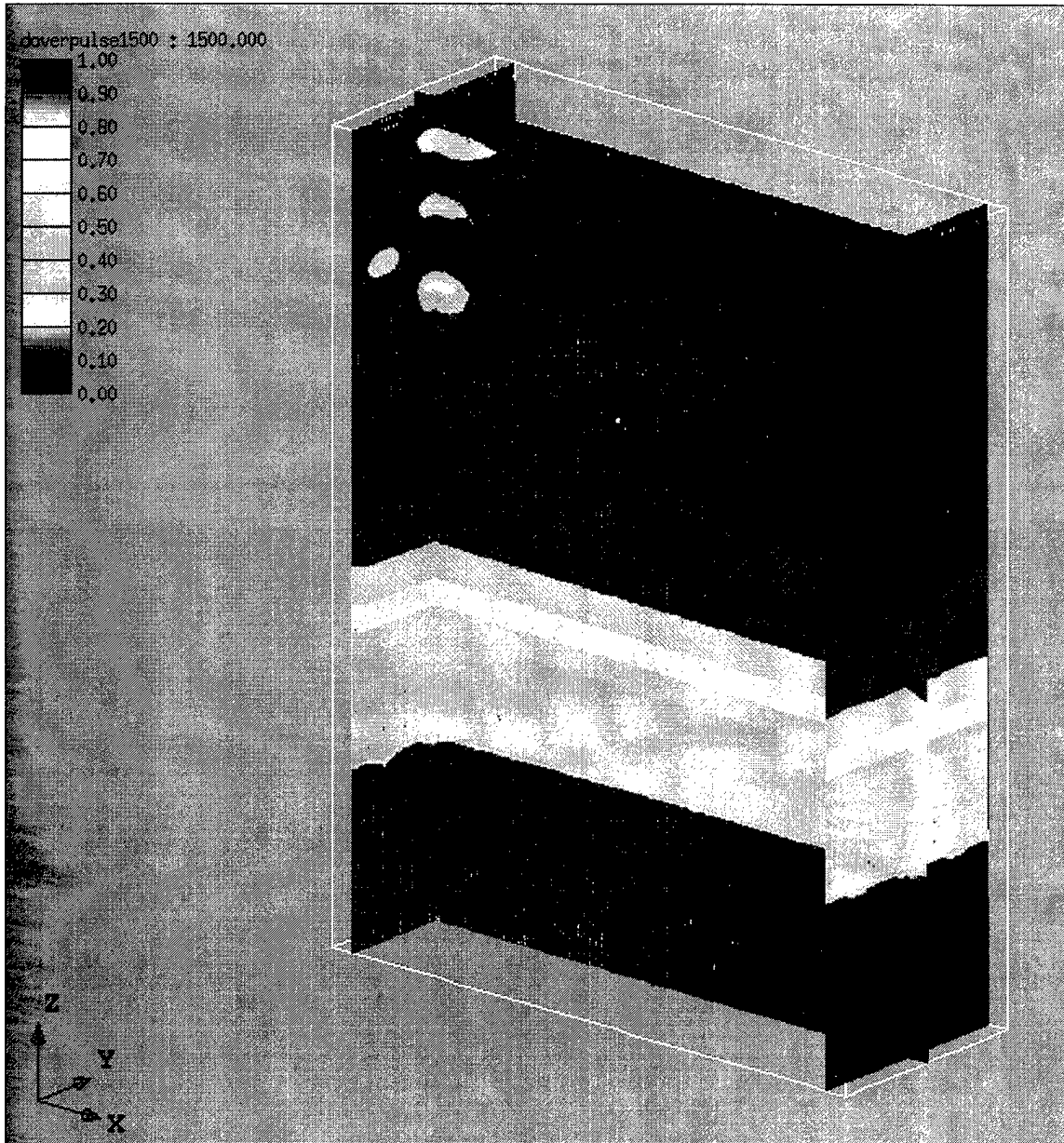


Figure 22. Contaminant Plumes at T=1500 hrs, After 1300 Hours of Clean Water Flushing

### 4.3 EFFECT OF RETARDATION FACTOR

Since the moment analysis simulation showed that the dispersive nature of the soil system in question played an important role in delaying contaminant flush-out, the question naturally arose as to the relative importance of the two delaying effects: dispersion and sorption. Recall that if the sorptive reaction behaves linearly and is at equilibrium, the solute will move at an average velocity equal to the average linear velocity of the ground water divided by the retardation factor. Therefore, retardation factor ( $R$ ) is key to describing the effect sorption has on the test cell's hydrodynamic characteristics. The retardation factor for a given soil type is defined as

$$R = 1 + \frac{\rho_B \cdot K_d}{\theta_W}$$

where  $\rho_B$  is the bulk density – the mass of the solids divided by the volume of the media.  $K_d$  is the distribution coefficient and  $\theta_W$  is the water capacity. The no-sorption ( $R = 1$ ) case forms a logical basis for comparison with the actual Dover simulation. The retardation factor can be forced to one by setting the distribution coefficient  $K_d$  in turn equal to zero. Thus, another transport solution was run for a 200 hour injection pulse, as in section 4.2 above, but with retardation factor equal to zero for all soil layers. This was to examine the effect sorption had on contaminant transport. Figures 23 and 24 show the effect retardation factor has on the mass recovery characteristics of the test cell. Namely, for  $R = 1$  the breakthrough curve peaks occurs 28% sooner and peaks 21% higher. This result was consistent with the expected behaviour for this case, and provided additional validation of the simulation.



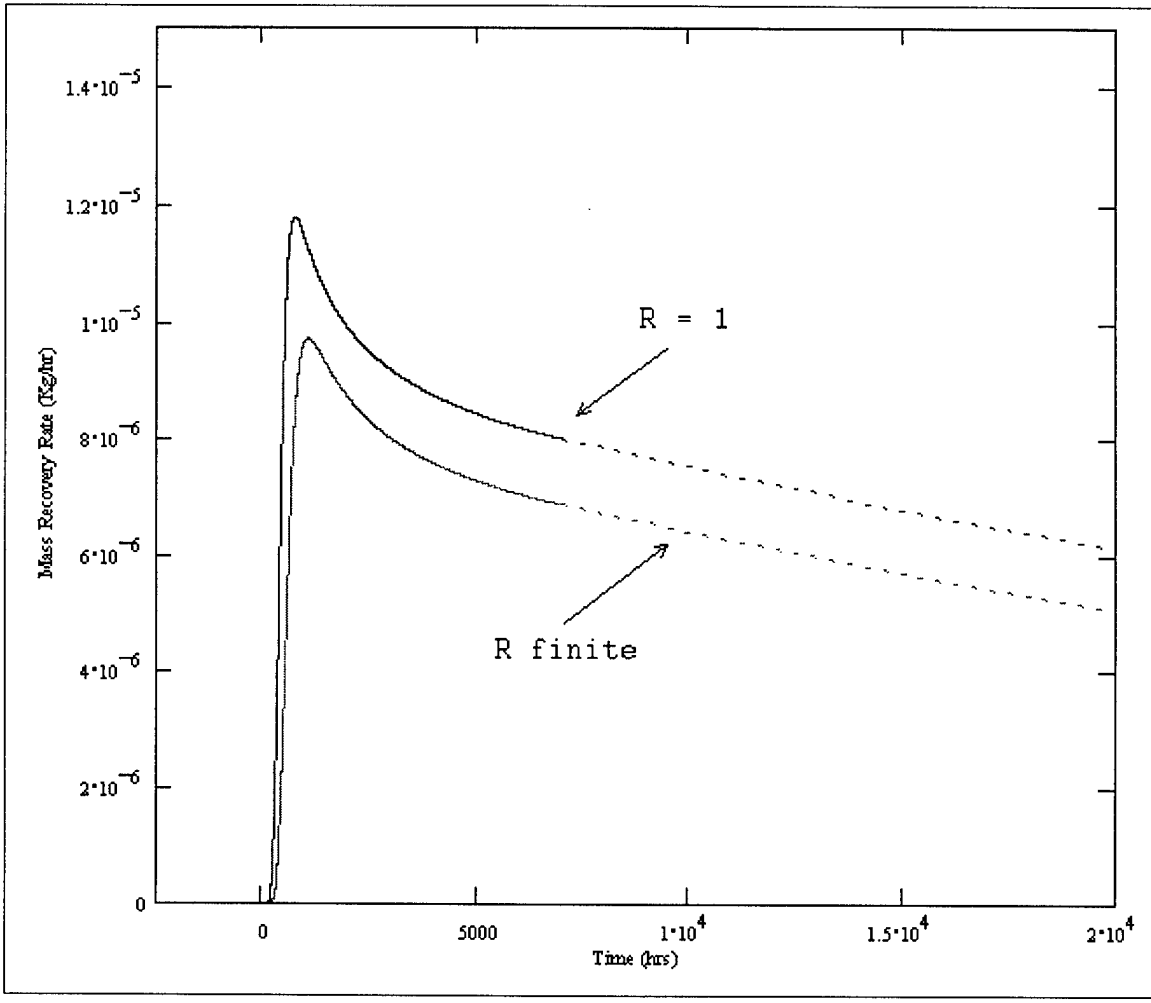


Figure 23. Breakthrough Curves Showing the Effect of Retardation Factor

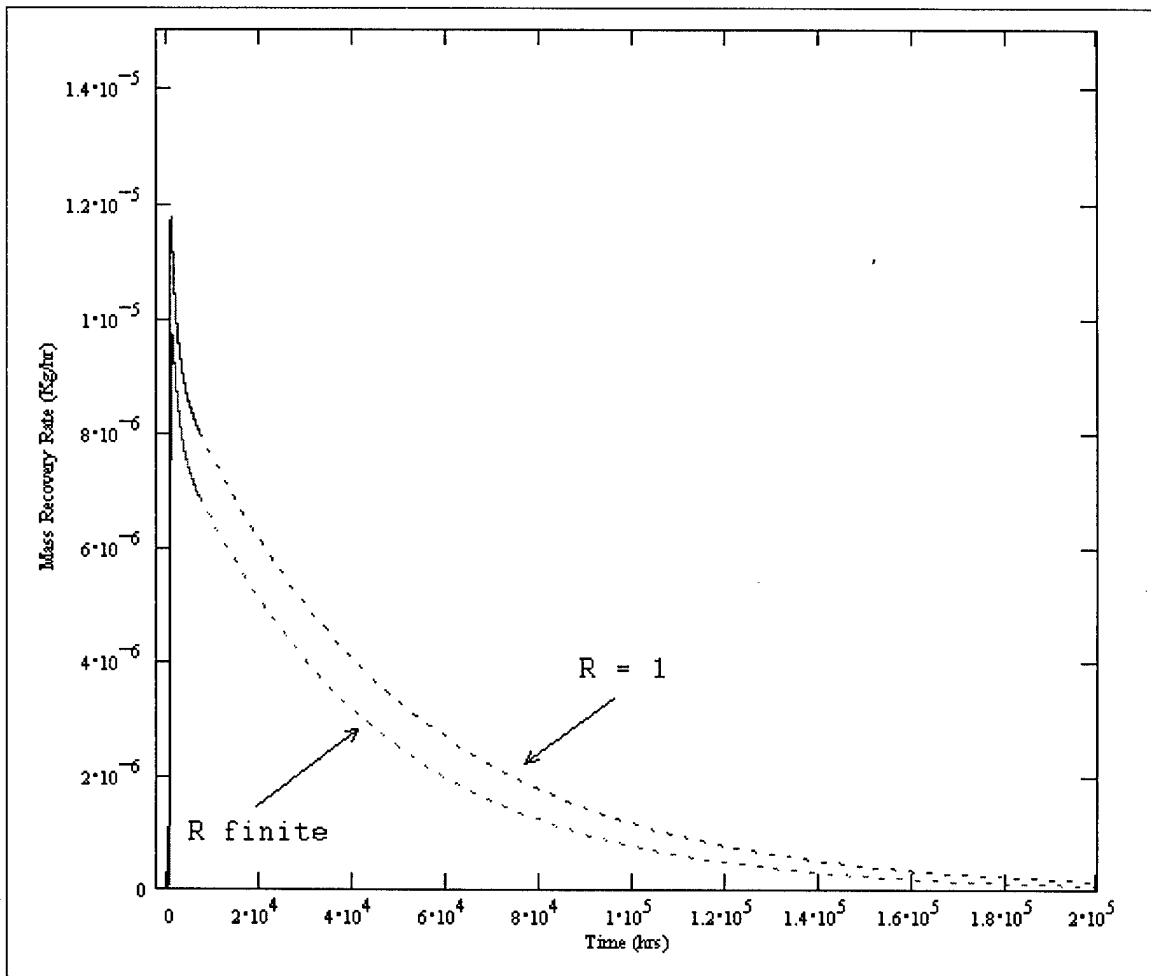


Figure 24. Breakthrough Curves Showing the Effect of Retardation Factor

#### 4.4 REMEDIATION BY CONTINUOUS PUMPING

A sample input file for the transport solution is given in appendix B.2. This simulation modeled contaminant purge when the initial contaminant distribution shown in figure 25 was subjected to clean water flushing. This initial contaminant distribution is shown in profile in figure 26. The four monitoring points (refer to table 4) are also shown in this plot. Figure 27 shows how the contaminant concentrations at the four monitoring points identified in table 4 and figure 3 vary with time. There are several features of this plot that stand out. First of all, there is an initial "lateral reconciliation" of contaminant in which the four curves converge rapidly. This indicates a smoothing of the peaks in the initial contaminant profile (figure 25) and this initial phase is over by  $T = 1500$  hours. Second comes the "transition" phase of the flush. Here, the ensemble slope of the reconciled curves shallows out, implying a decreasing contaminant extraction rate. In the third "mature" phase, the concentration at the former "peak" (monitor point #4) falls below that of the clay layer edge (monitor point #1) so that the clay layer now harbors a higher concentration of contaminant than the layers above it. This in turn suggests that the clay aquitard stubbornly retains contaminant then metes it out gradually – recontaminating the aquifer layer above and partially counteracting the convective purge occurring there. Figure 28 provides another view of these phenomena and implies that at high  $T$  (hours), there may be more of a redistribution of contaminant than a flush-out.

Turning our attention now to a time-ordered series of cross-sectional contour profiles, figures 29 through 36 show that the flushing action has the effect of removing contaminant from the cell, smoothing down the initial concentration peaks, and laterally dispersing contaminant into the upper (aquifer) layers of the cell. This is illustrated clearly in the line-plot figure 28. Note also that there is substantial qualitative difference between the situations depicted in the cross-sectionals for  $T = 0$  hours,  $T = 200$  hours, and  $T = 400$  hours, but very little qualitative dif-

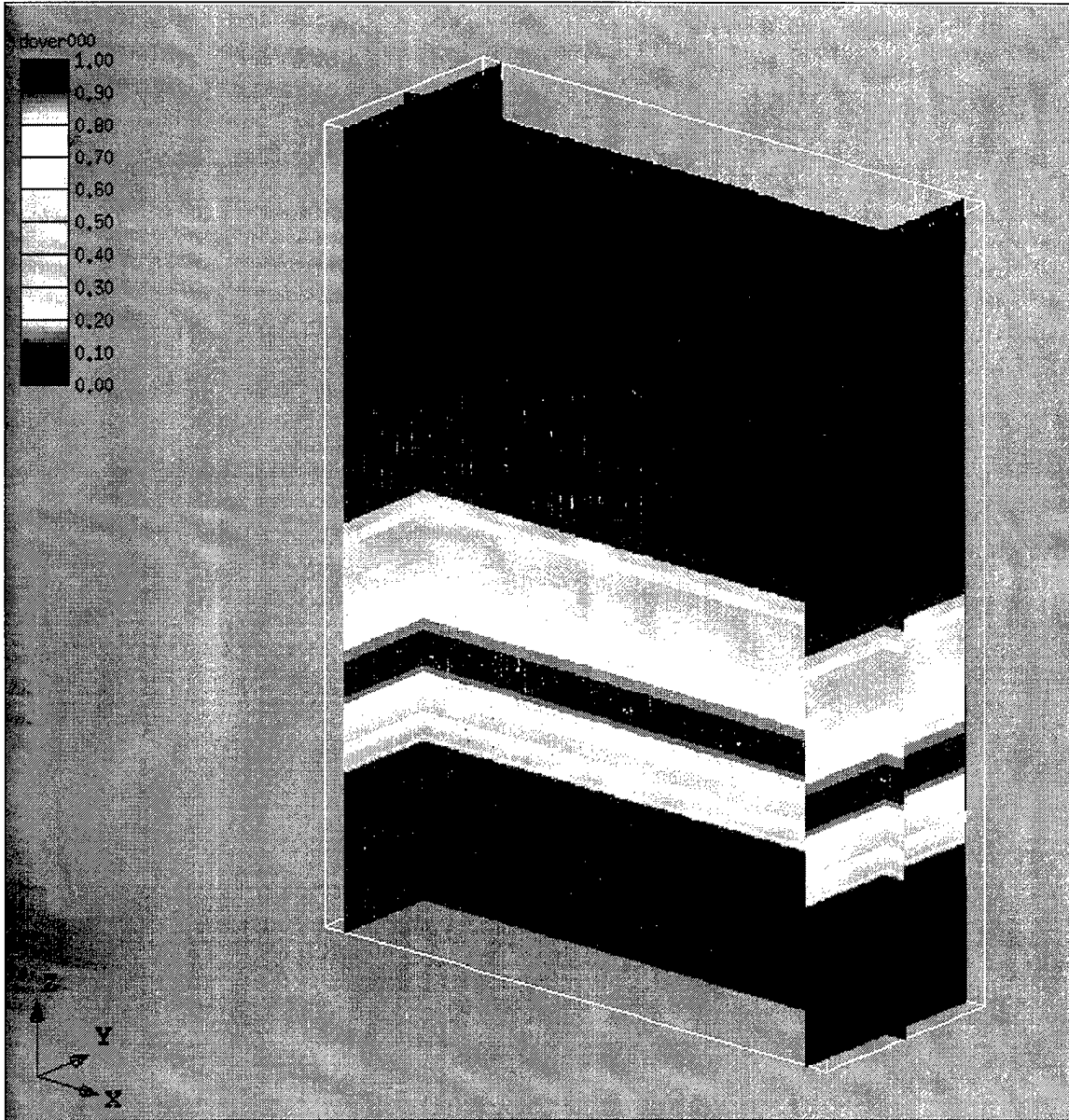


Figure 25. Initial Contaminant Profile  $T = 0$  hrs

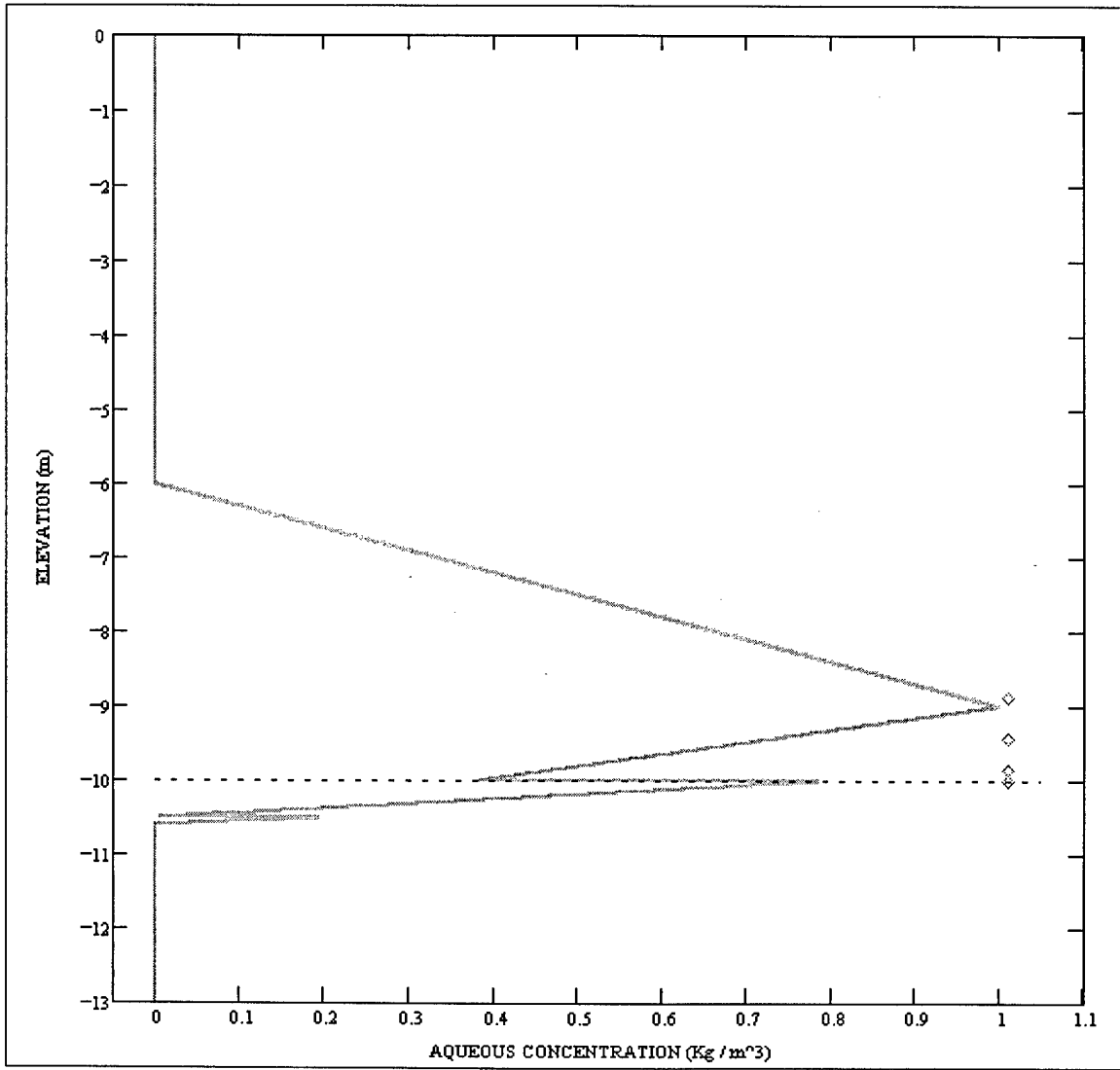


Figure 26. Inital Contaminant Profile and 4 Monitoring Points

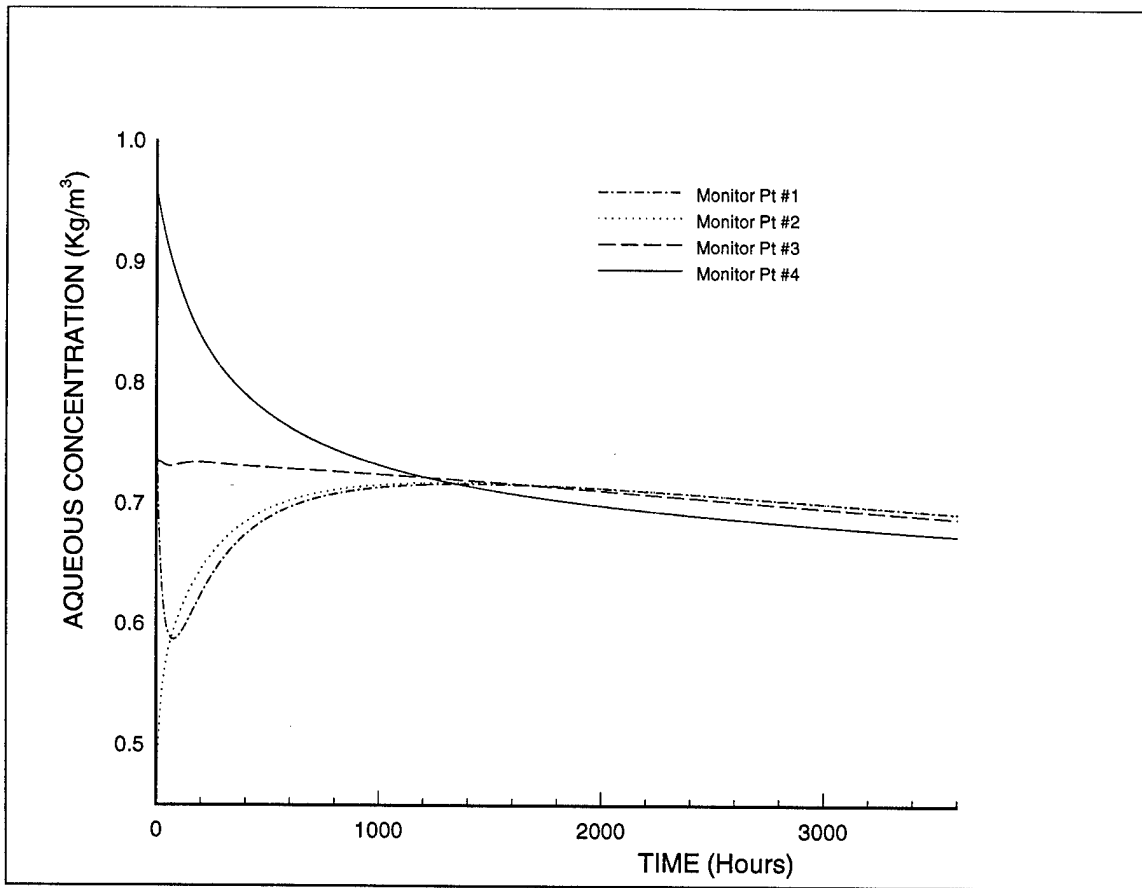


Figure 27. Contaminant Concentration vs Time (Hours) at the Four Monitoring Points

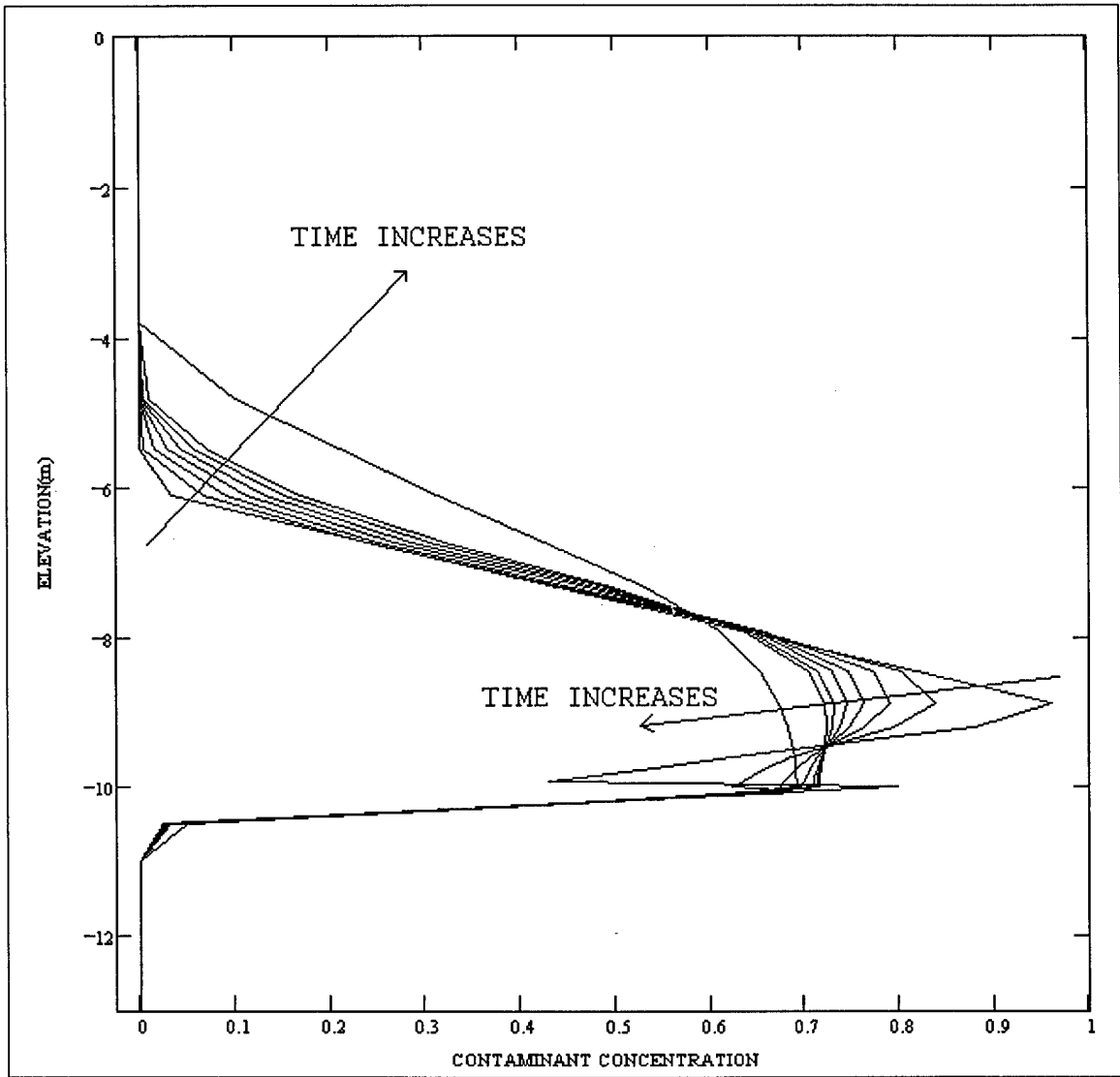


Figure 28. Time and Depth Variation of Contaminant Concentration at Center of Cell

ference between the profiles for  $T = 1200$  hours and  $T = 1400$  hours. This is commensurate with the "tailing" phenomenon shown in figure 27. On another level, there are several time scales in concert during the flushing dynamic. To name a few; a diffusive time scale inversely proportional to the fluid diffusivity  $D_m$ , a convective time scale associated with the mean longitudinal velocity through the cell, and a time scale based on the mixing shear velocity at the interface between the aquitard clay layer and its adjacent aquifer. These multiple time scales reflect the complicated nature of the physics. They also make the numerical simulation difficult (stiff) due to the range of time resolution required for various time steps. From an operational standpoint, the only real conclusion to be drawn is that in the presence of a contaminant-retaining aquitard, continuous pumping offers diminishing returns.



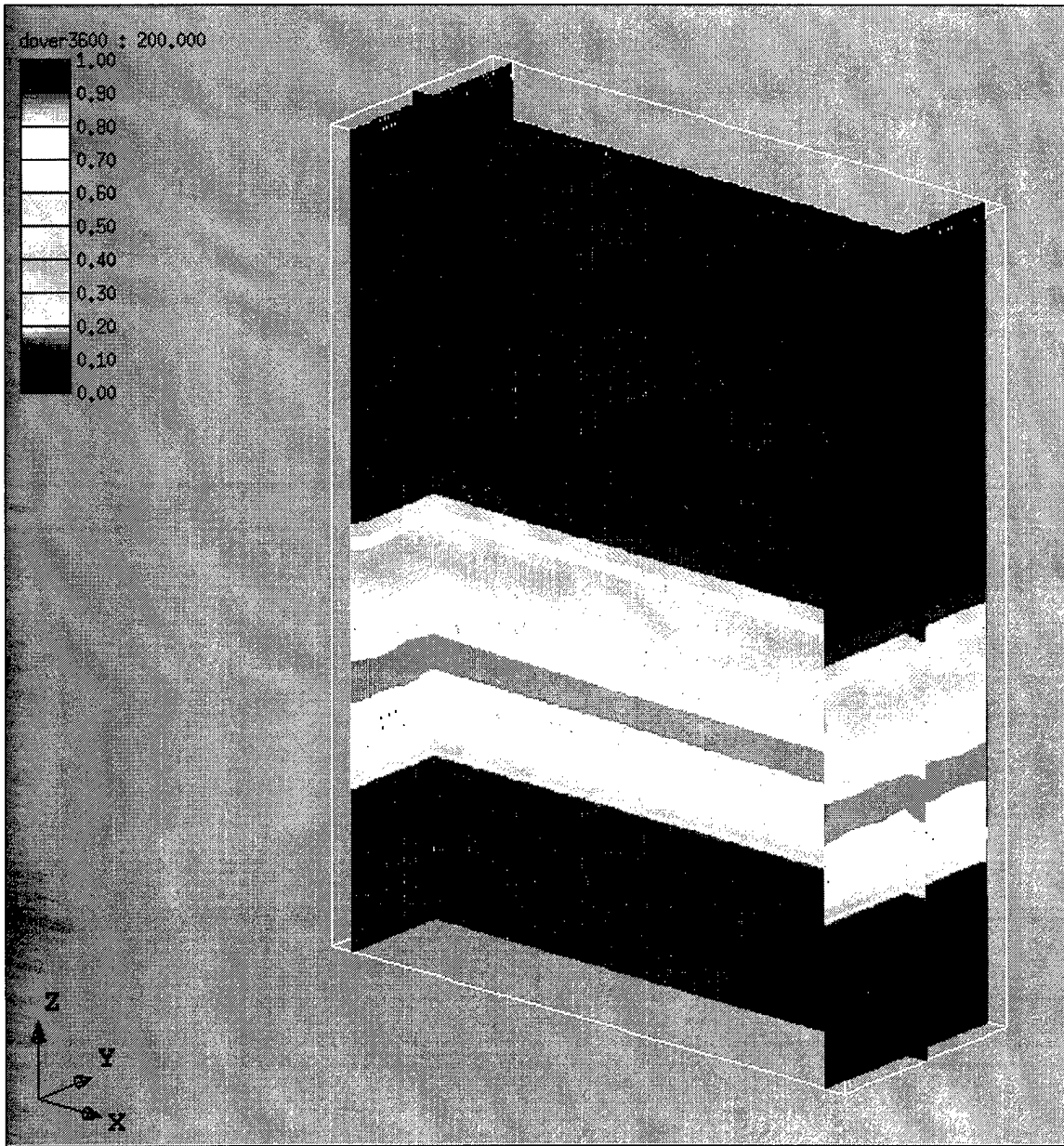


Figure 29. Contaminant Profile after 200 Hours of Clean-Water Flushing

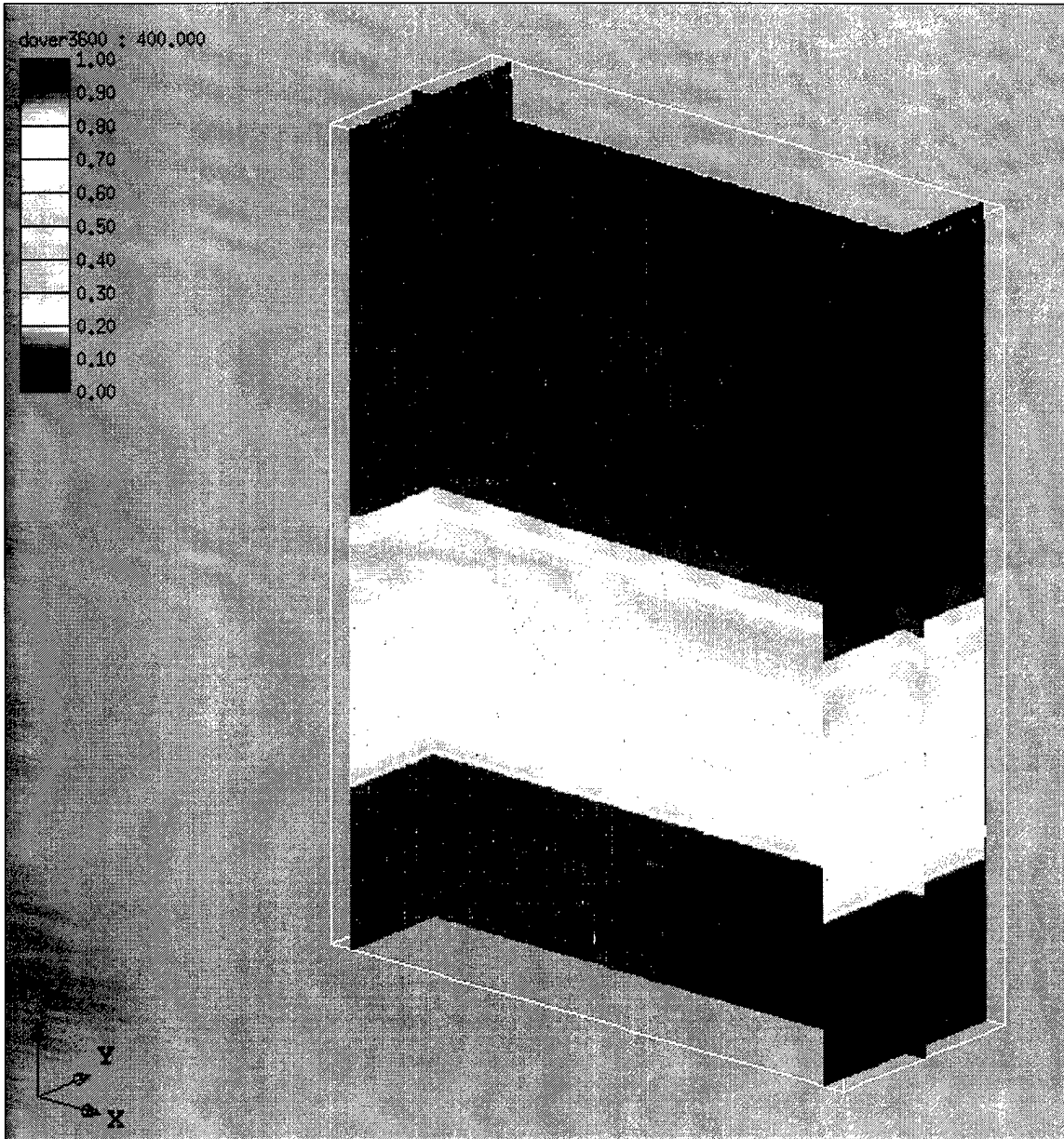


Figure 30. Contaminant Profile after 400 Hours of Clean-Water Flushing

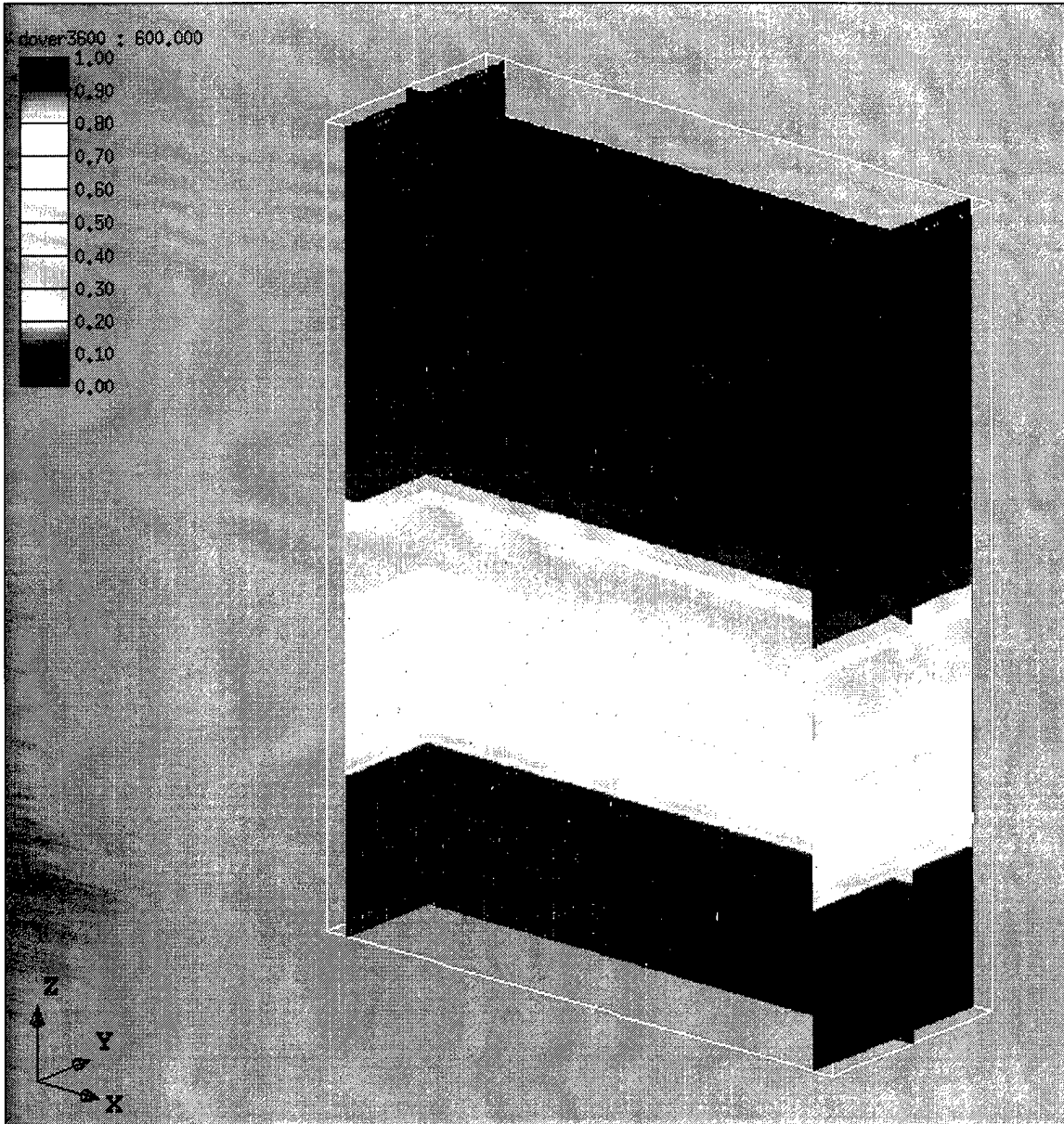


Figure 31. Contaminant Profile after 600 Hours of Clean-Water Flushing

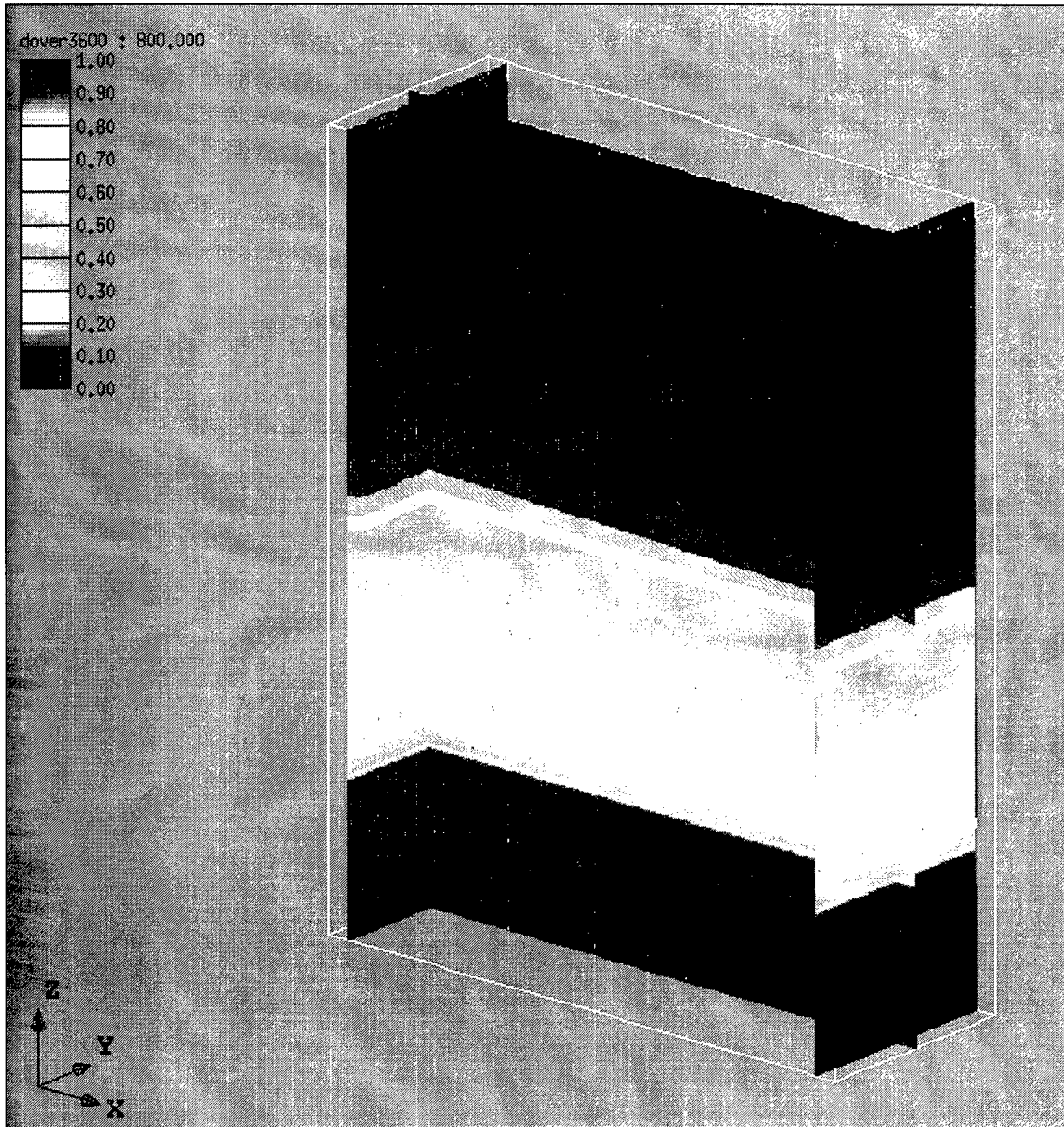


Figure 32. Contaminant Profile after 800 Hours of Clean-Water Flushing

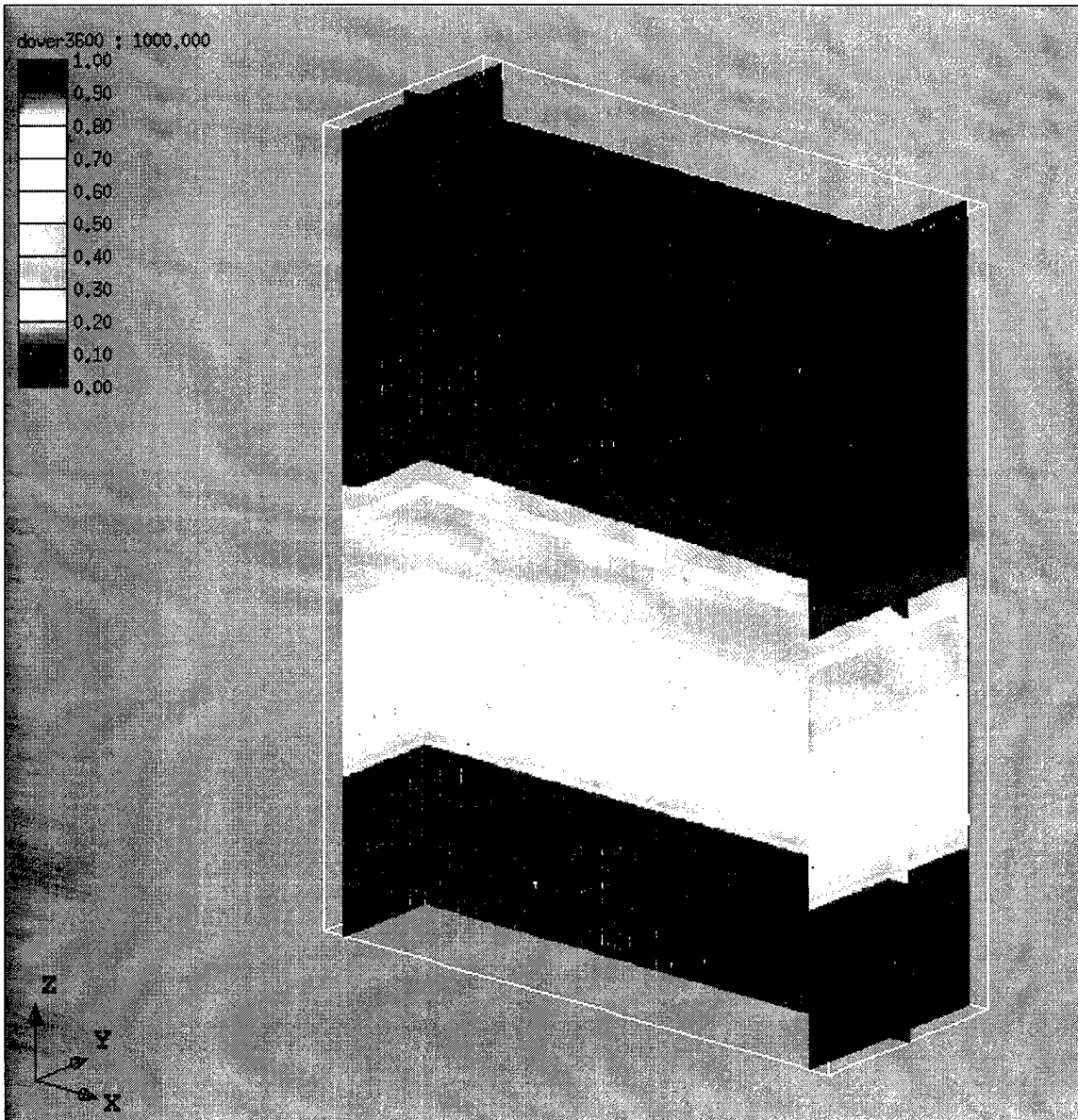


Figure 33. Contaminant Profile after 1000 Hours of Clean-Water Flushing

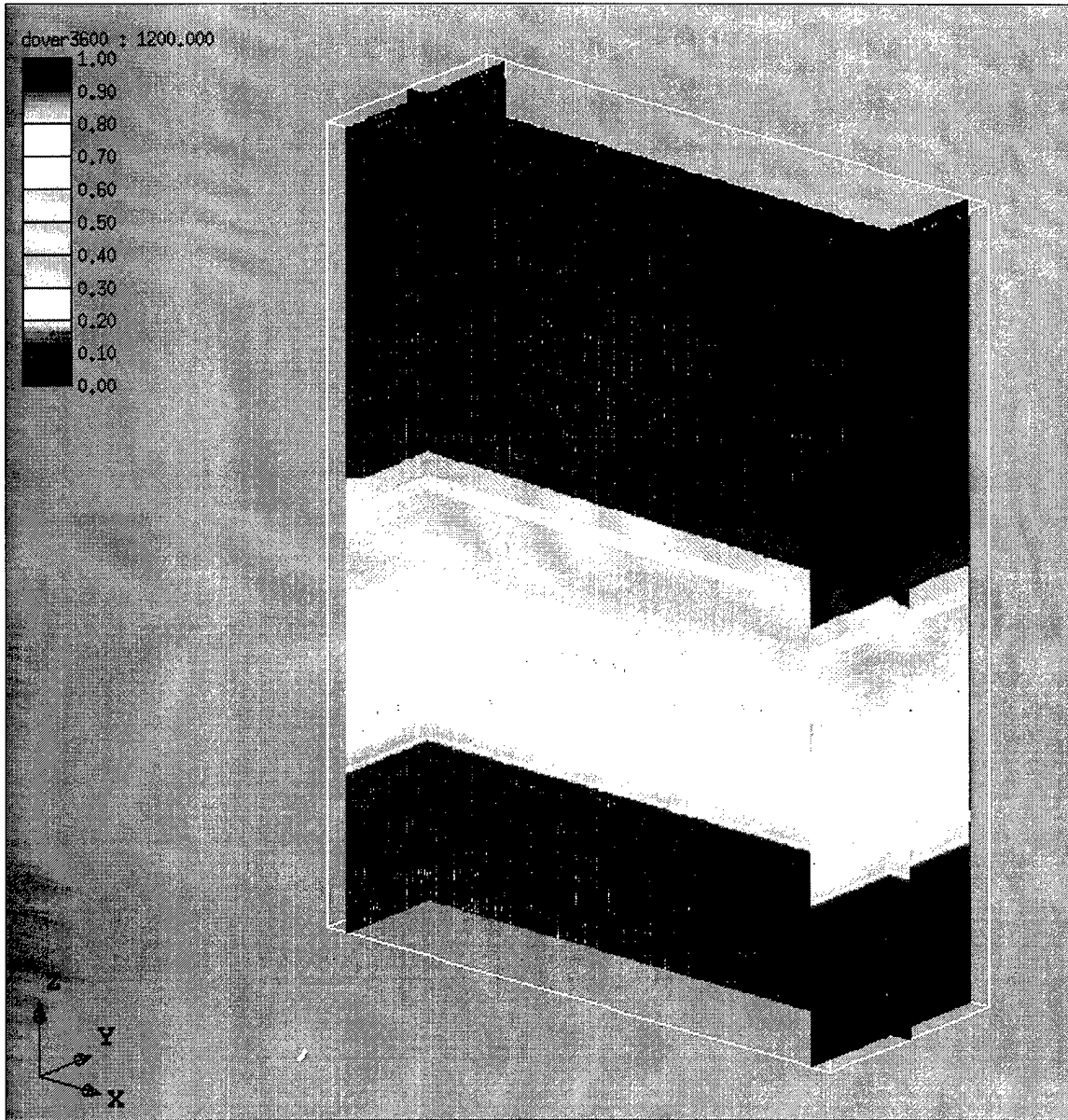


Figure 34. Contaminant Profile after 1200 Hours of Clean-Water Flushing

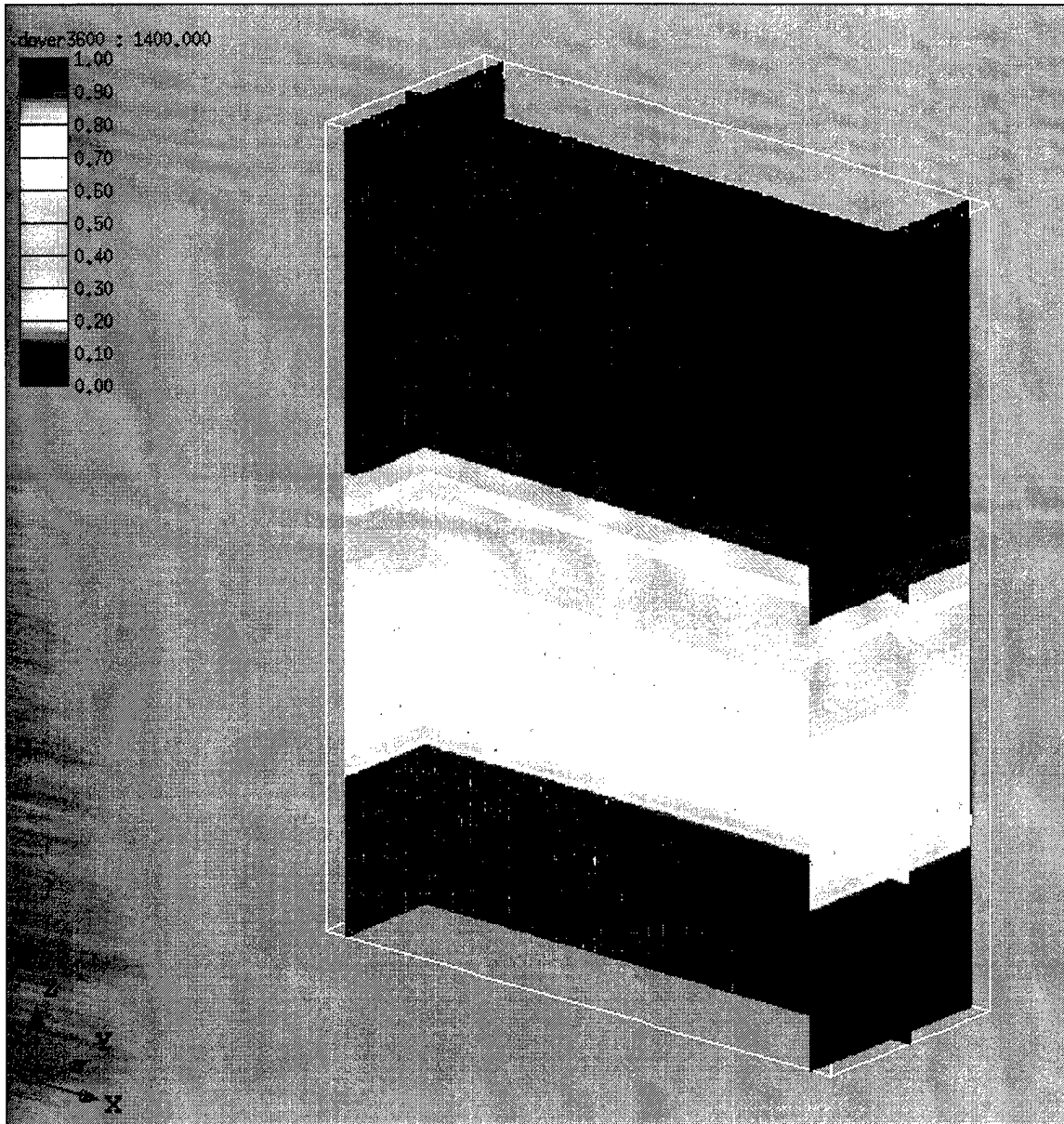


Figure 35. Contaminant Profile after 1400 Hours of Clean-Water Flushing

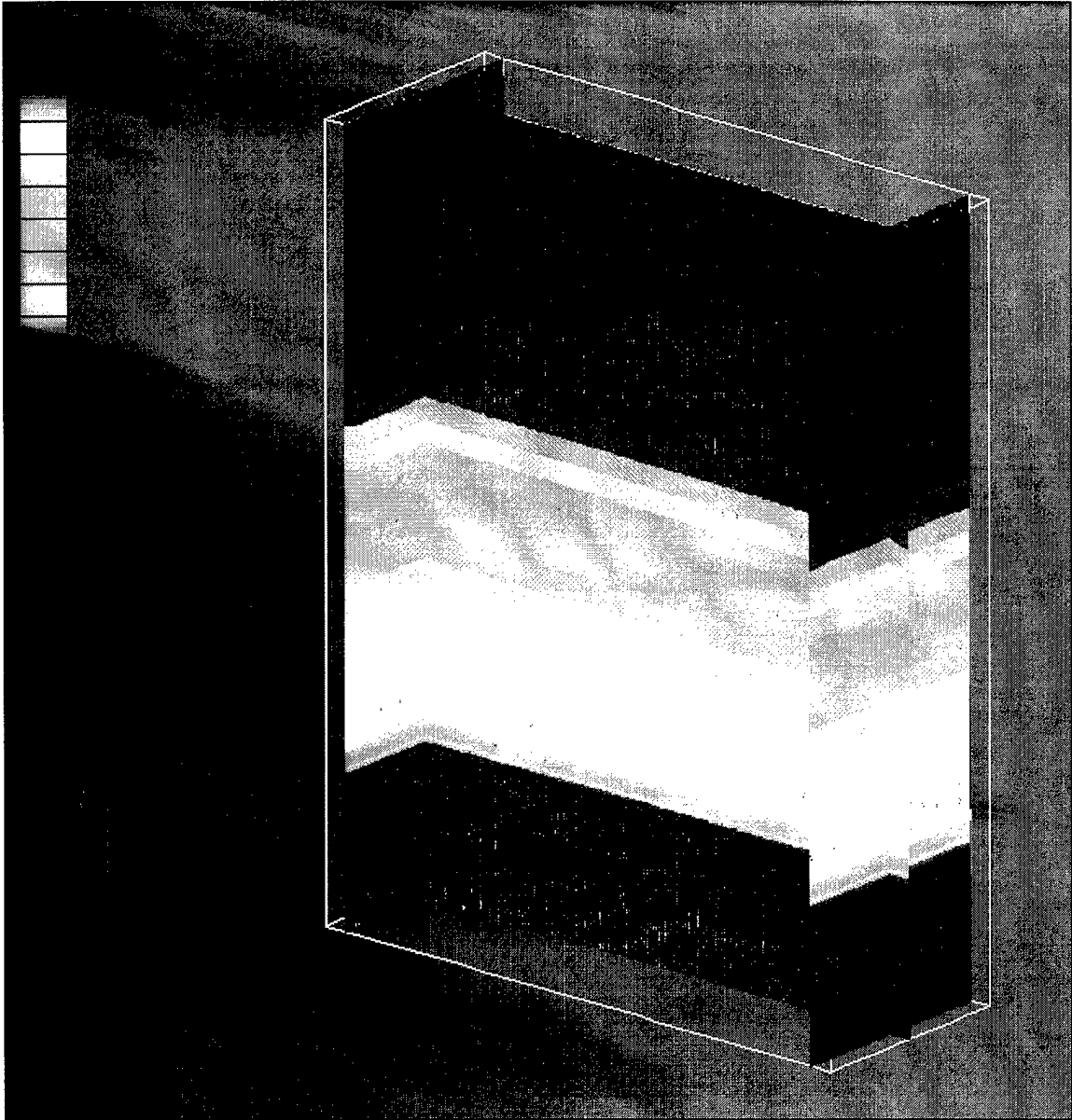


Figure 36. Contaminant Profile after 3600 Hours of Clean-Water Flushing



## 4.5 REBOUND

This case examined what happens when the injection pumps are switched off after the flushing operation has reached its "mature" stage. The question was whether the clay aquitard would continue to mete out contaminant diffusively in the absence of an injection-induced velocity field. However, examining figure 39, it is evident that the peak in the T=3600 hours contaminant concentration profile occurs between monitor points 1 & 2 and not within the clay layer. Beginning with a normal pump-down as before, the pumps were switched off at 3600 hours, allowing the plant to stand down for 1900 hours. The contaminant level at monitoring point #2 (just above the clay layer) was carefully observed. As depicted in figure 37, the contaminant begins to rise again before leveling out at approximately 5500 hours. This is rebound. However, figure 38 shows that even during pump stand-down, the contaminant level at the edge of the clay layer (monitoring point #1) continued to fall at almost the same rate as during pump-on. This is because MP1 is affected by a concentration gradient favoring local decrease. The reason why the concentrations registering at monitor points 1 & 2 diverge from each other is that the concentration gradients affecting these two points are in opposite directions. Moreover, the difference in slope magnitude between these two curves mirrors the difference in the two gradients affecting MP1 and MP2. Figure 39 shows that MP1 is at a much higher concentration than the point immediately beneath it in the clay layer whereas MP2 is at an only slightly lower concentration than the point adjacent to it. The important point is that mass transfer is by diffusion. Figure 37 shows that at pump-on at 5500 hours the slope of the concentration vs. time curve for monitoring point #2 literally plunges, with a slope much steeper than that for the portion previous to pump stand-down – corroborating the fact that a quantity of mass arose diffusively from below during stand-down, availing itself for subsequent purge under the convective action of pump-on. The steeper slope of the second pump-on cycle illustrates the increased mass

removal efficiency that the pulse pumping advocates suggest. Finally, note the rapid so-called "lateral reconciliation" between contaminant levels at monitoring points 1 and 2. This is due to the powerful shear-induced convective mixing which results from the steep velocity gradient between these two relatively close layers (see figure 15 and table 3).

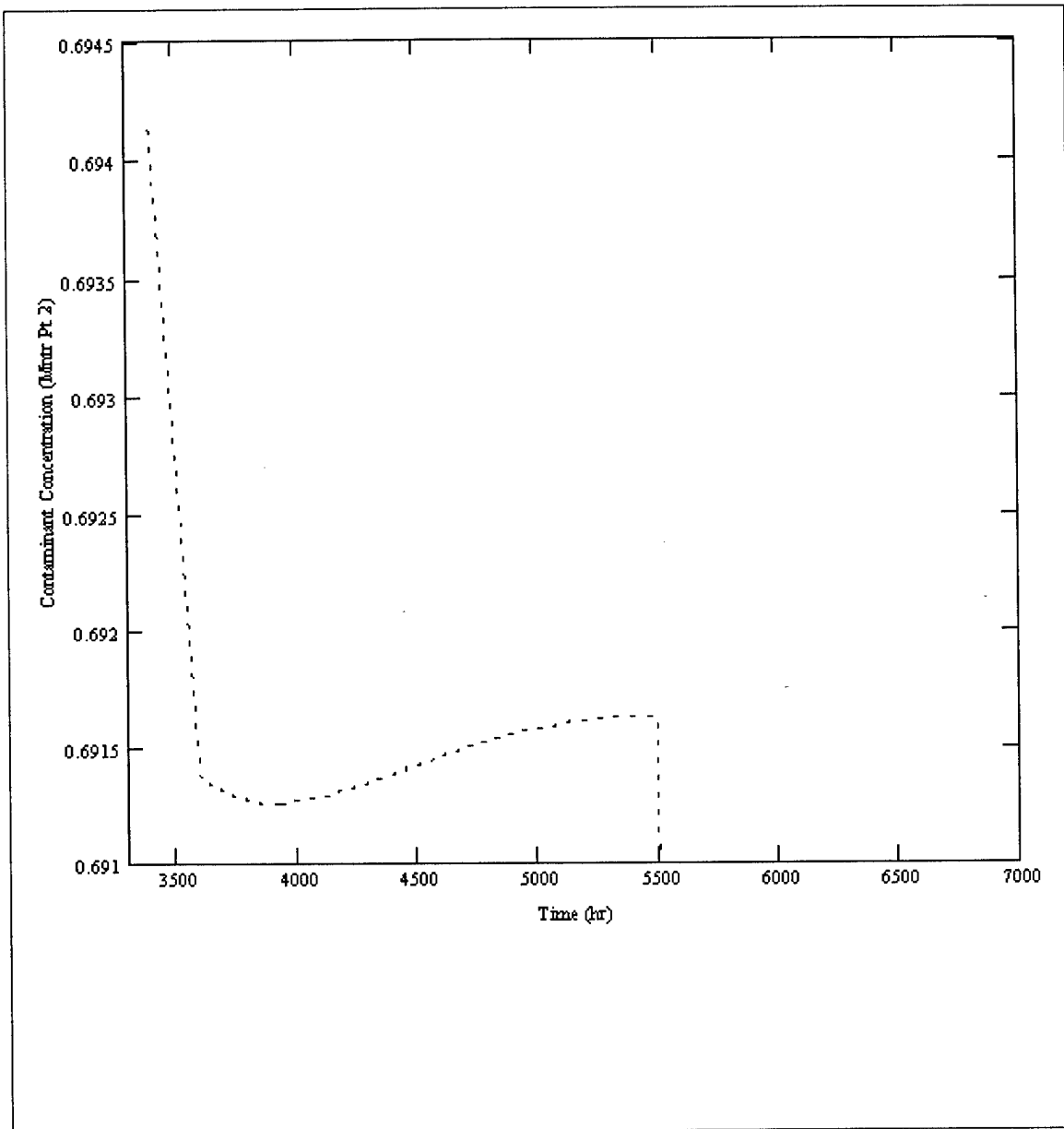


Figure 37. Contaminant Concentration at Monitor Point #2 Showing Rebound

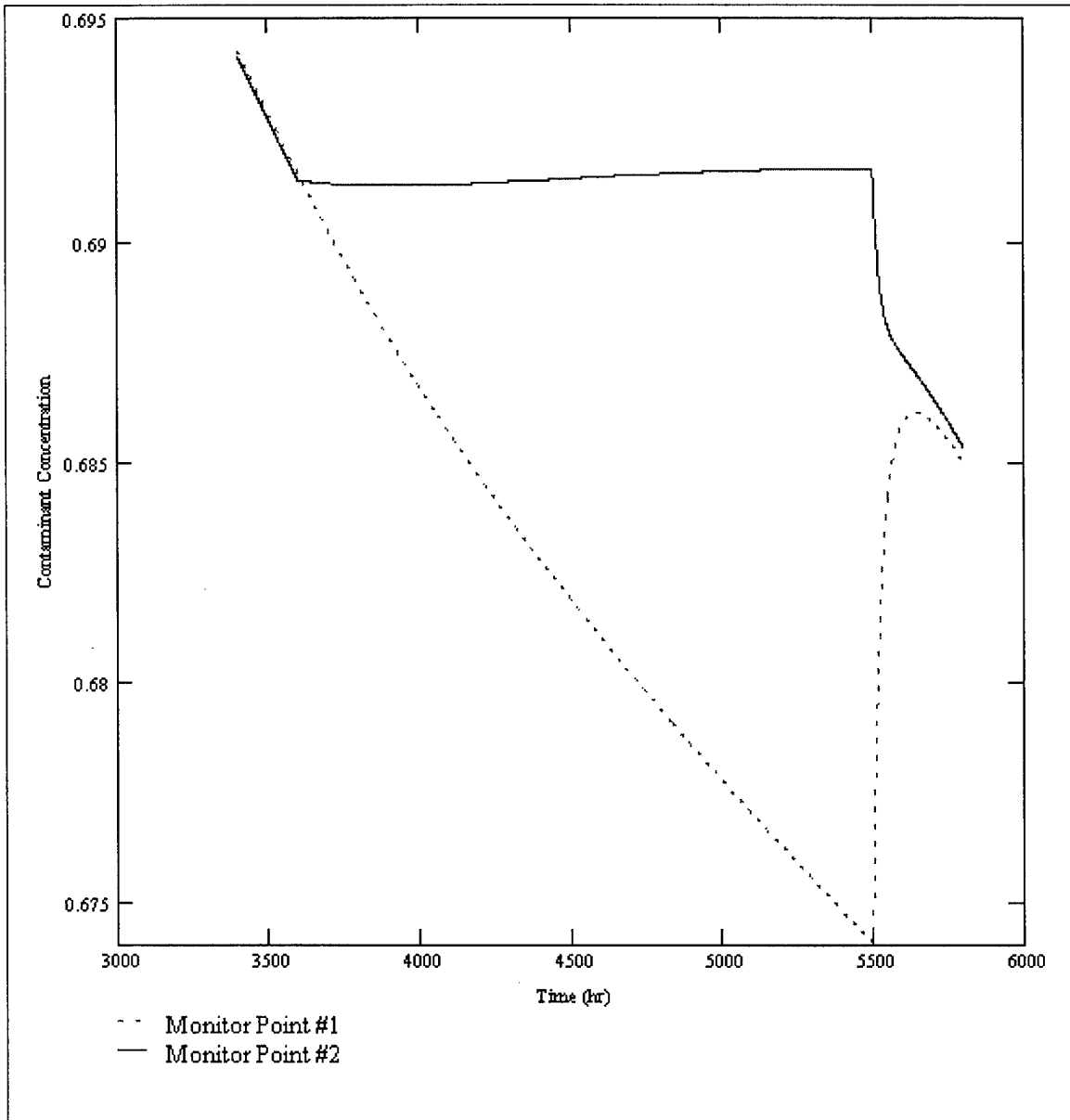


Figure 38. Contaminant Concentration at Monitor Points 1 and 2 Showing Resumption of Pumping After Rebound

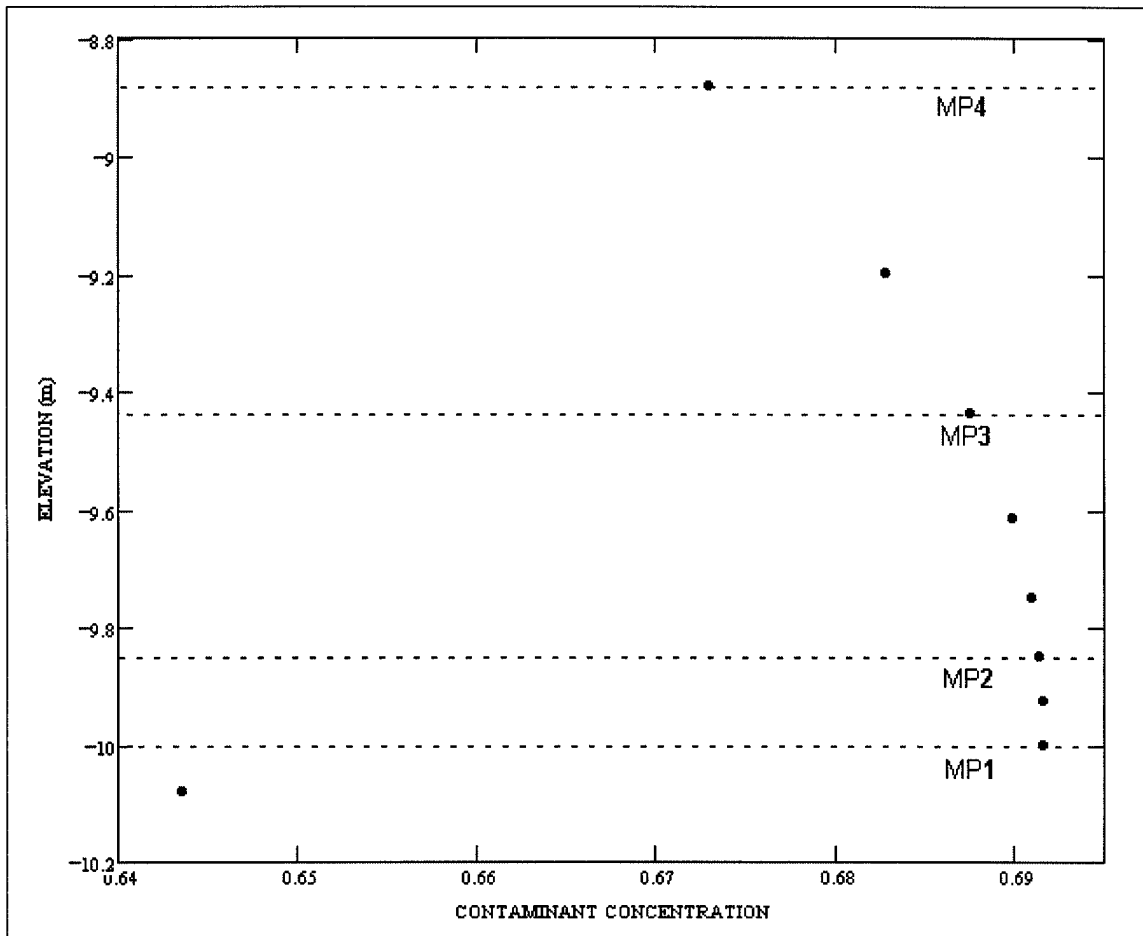


Figure 39. Contaminant Concentration in the Vicinity of the 4 Monitoring Points at T=3600 Hours

## 4.6 COMPARISON WITH FIELD EXPERIMENTAL DATA

Details of the experimental work conducted at Dover AFB are provided in [27]. Figure 40 below is the PCE portion of figure G-1 (Selected Elution Curves...) on page 188 of that work. The accompanying pump rate schedule does not appear in the report by Mackay, Ball et al [27] but was provided to this author by one of the collaborators, D.M. Mackay [26]. Figure 41 below shows the pump schedule at the field site. The reasons for the variance in the pump rate, according to the experimenters, included pump component wear-outs, clogged filters and valves, and a myriad of other unforeseeable circumstances that conspired against ideality. Note that the average pump rate over the entire 3700 hours shown is  $0.196 \frac{m^3}{hr}$  which is 2% higher than the  $0.192 \frac{m^3}{hr}$  assumed for the present numerical work. Also note that the experimenters recorded elution data points at different times than the pump strength data points so it was necessary to perform an interpolation between the latter to provide pump rate data corresponding temporally to the elution data. The inner product of elution and pump strength data provided the breakthrough curve shown in figure 42. Shown in the same figure is the breakthrough curve provided by FEMWATER. The breakthrough curve resulting from the numerical simulation is much flatter than the experimental result, undershooting at low hours and overshooting at high hours. The main reason for the discrepancy appears to be a FEMWATER tendency to be over-dispersive. Clearly, the breakthrough curve from the experiment shows plug-like elution of mass from the test cell. FEMWATER's solution on the other hand seems to be smeared, with dispersion playing a larger role than advection.

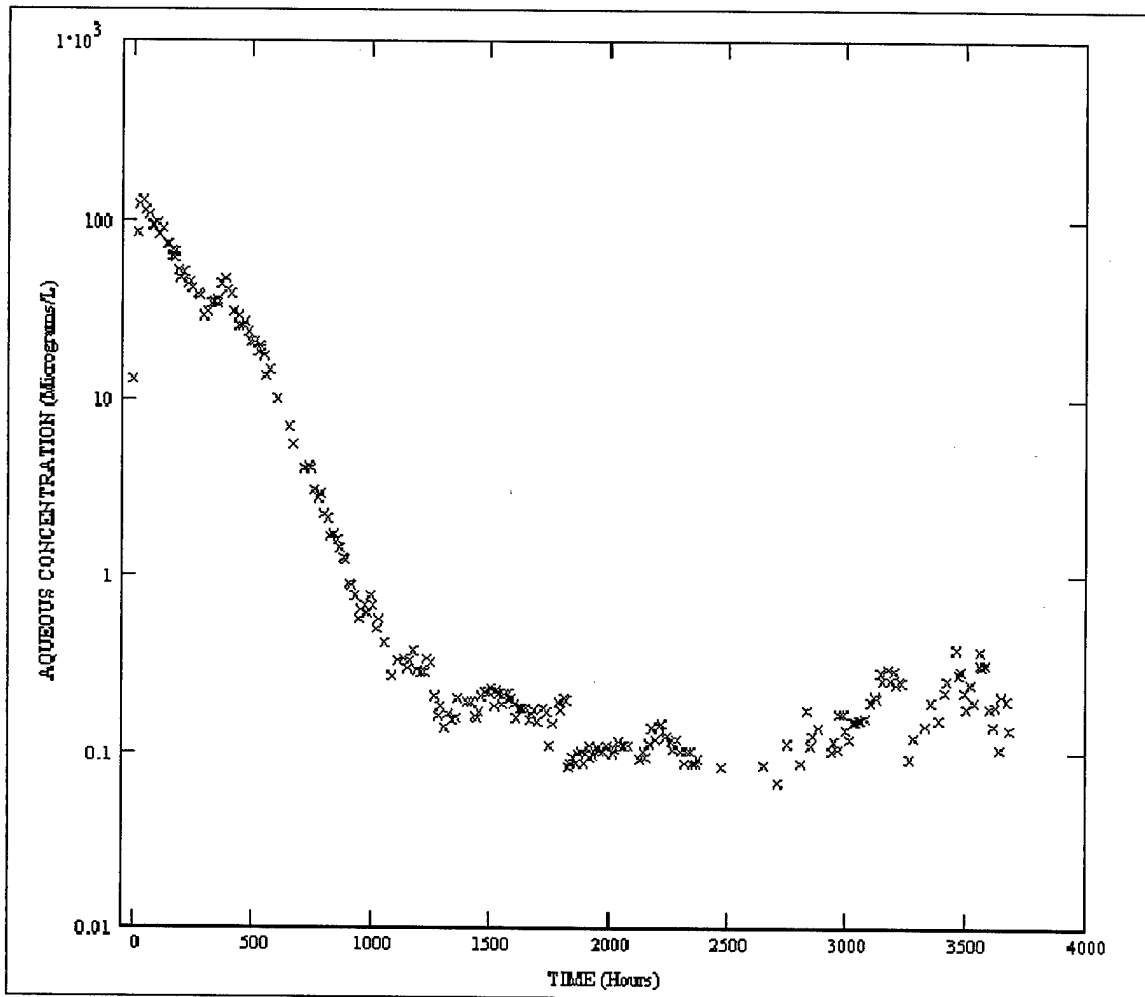


Figure 40. Elution Data for PCE (Fig G1 in [27])

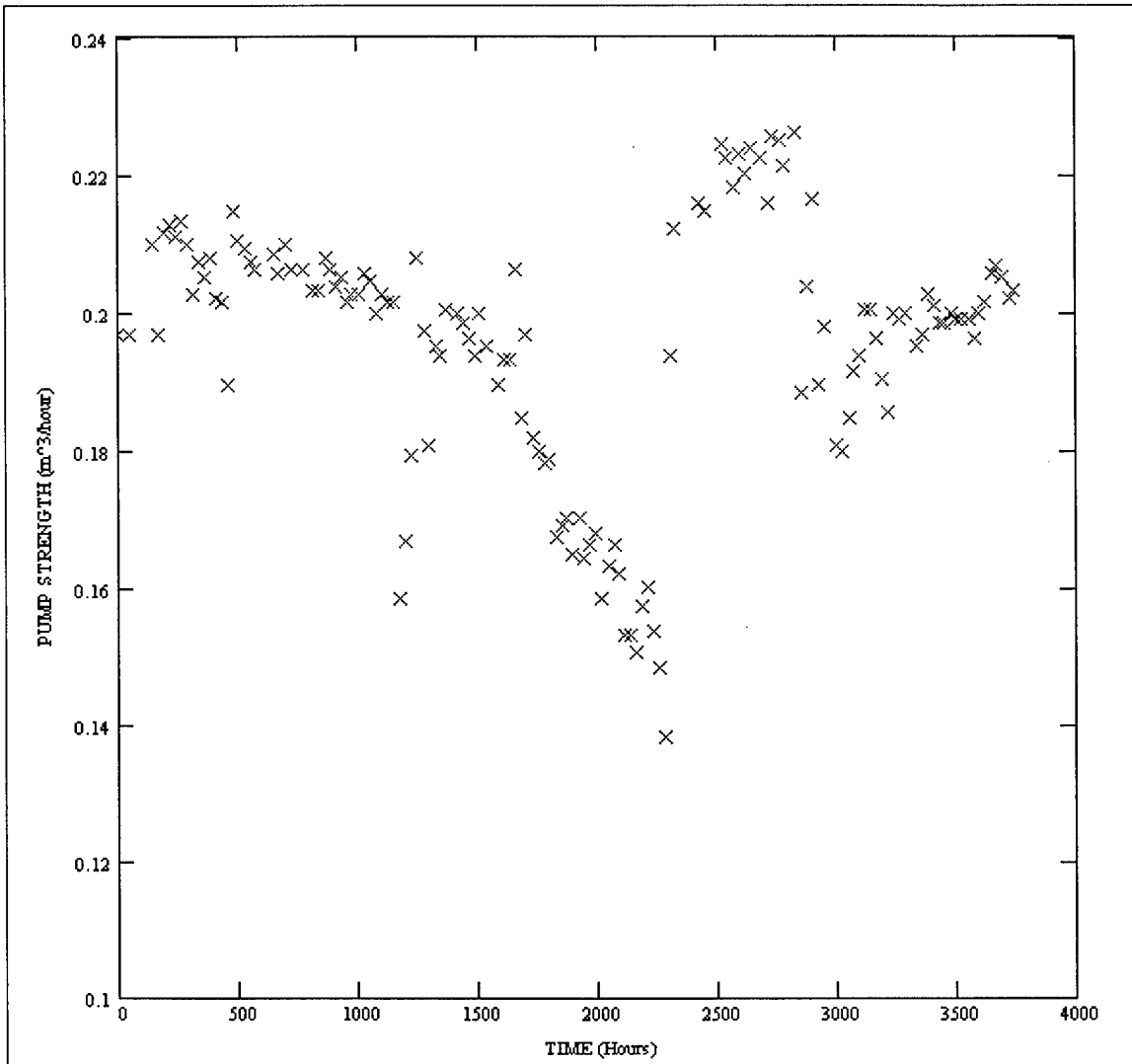


Figure 41. Pump Strength Schedule from Field Experiment



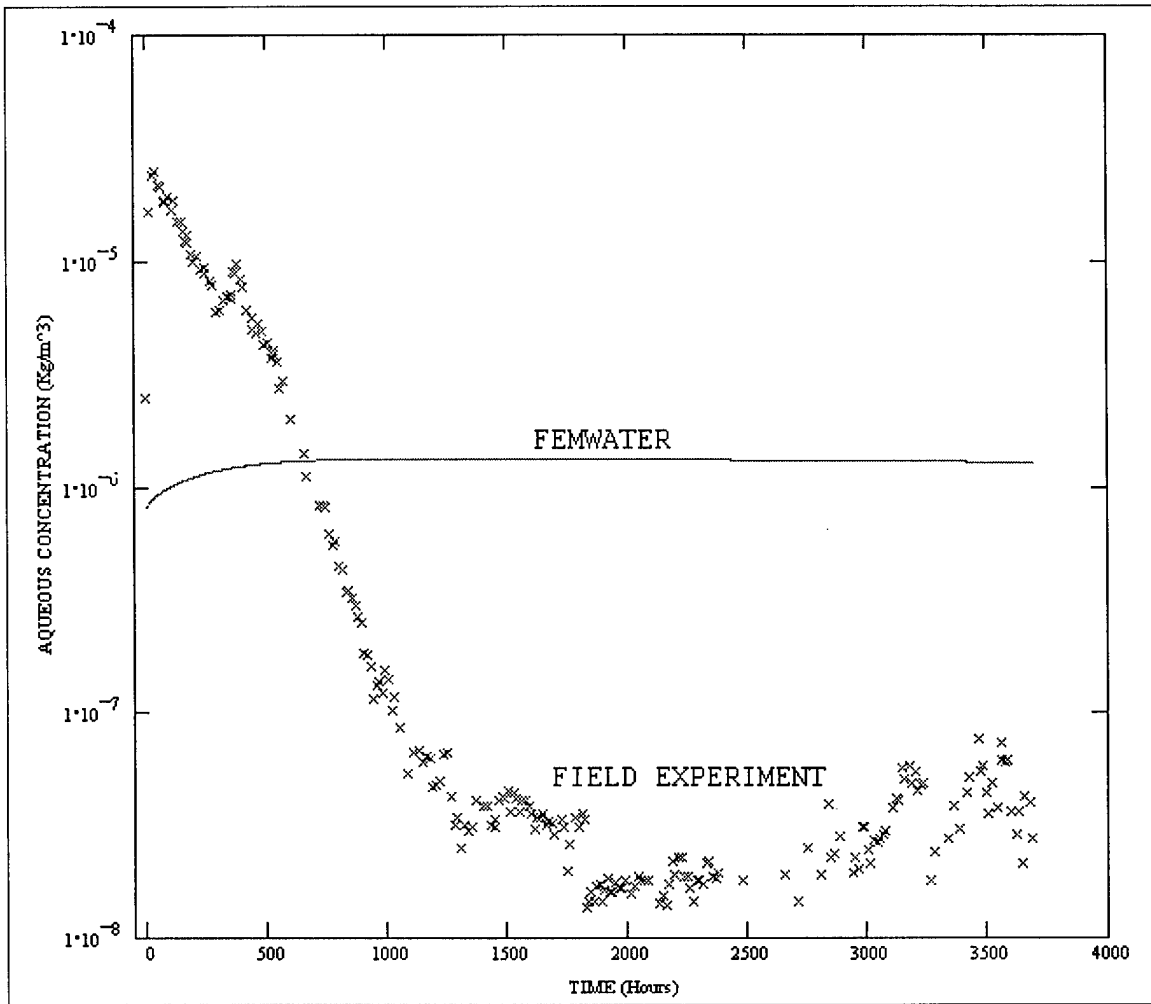


Figure 42. Breakthrough Curves for FEMWATER and Field Experiment

#### **4.7 COMPARISON WITH PREVIOUS NUMERICAL DATA**

Herman [21] conducted numerical simulations based on the aqueous concentration profile shown in figure 43. Figure 44 shows a comparison between Herman's and FEMWATER spatial concentration profiles at a point corresponding to "monitoring point #2" (table 3). Again, Herman's results show a plug-like elution dominated by advection whereas FEMWATER's solution contains smearing and mixing - hence the flatter breakthrough curve.

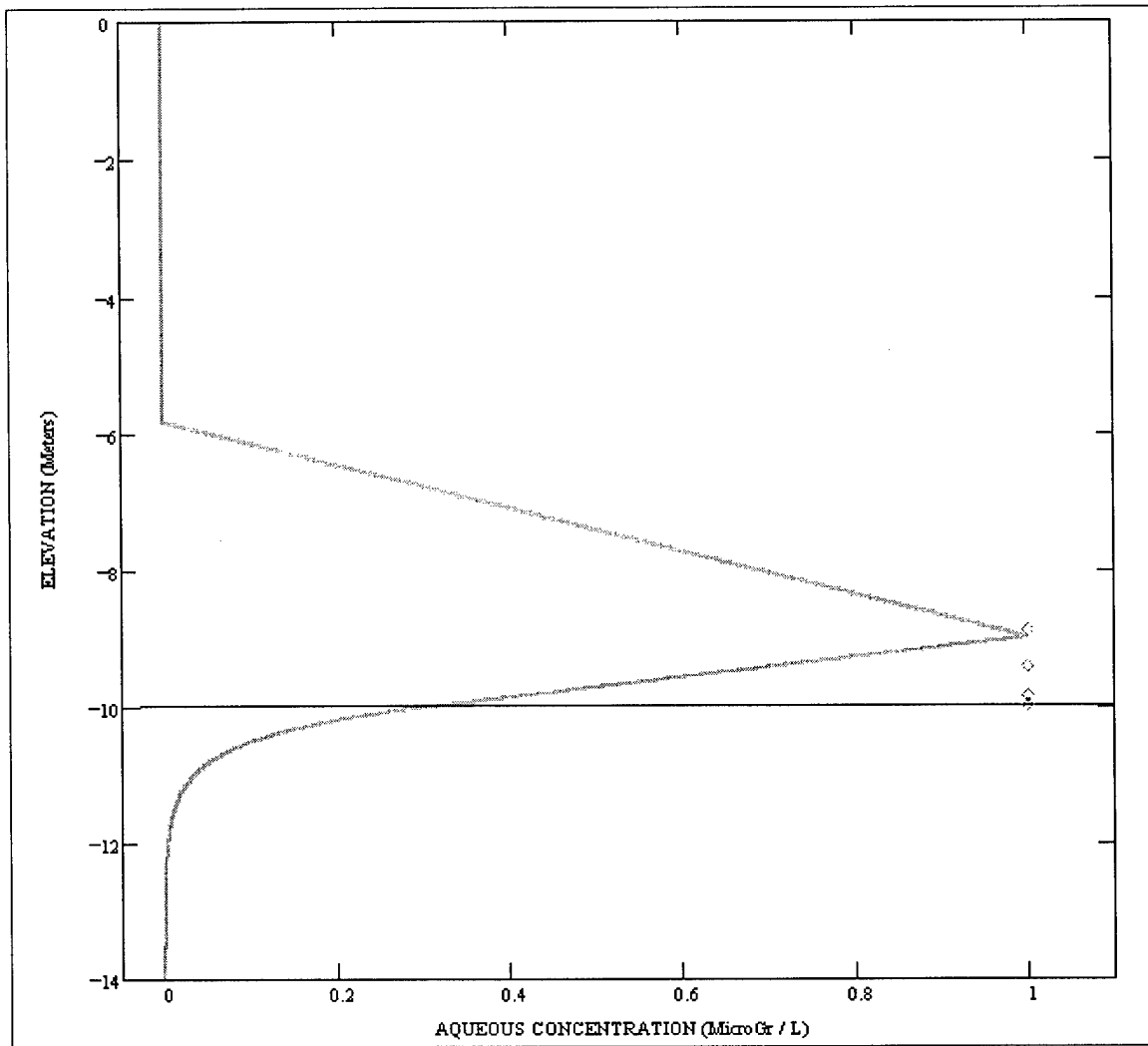


Figure 43. Initial Concentration Profile from Herman

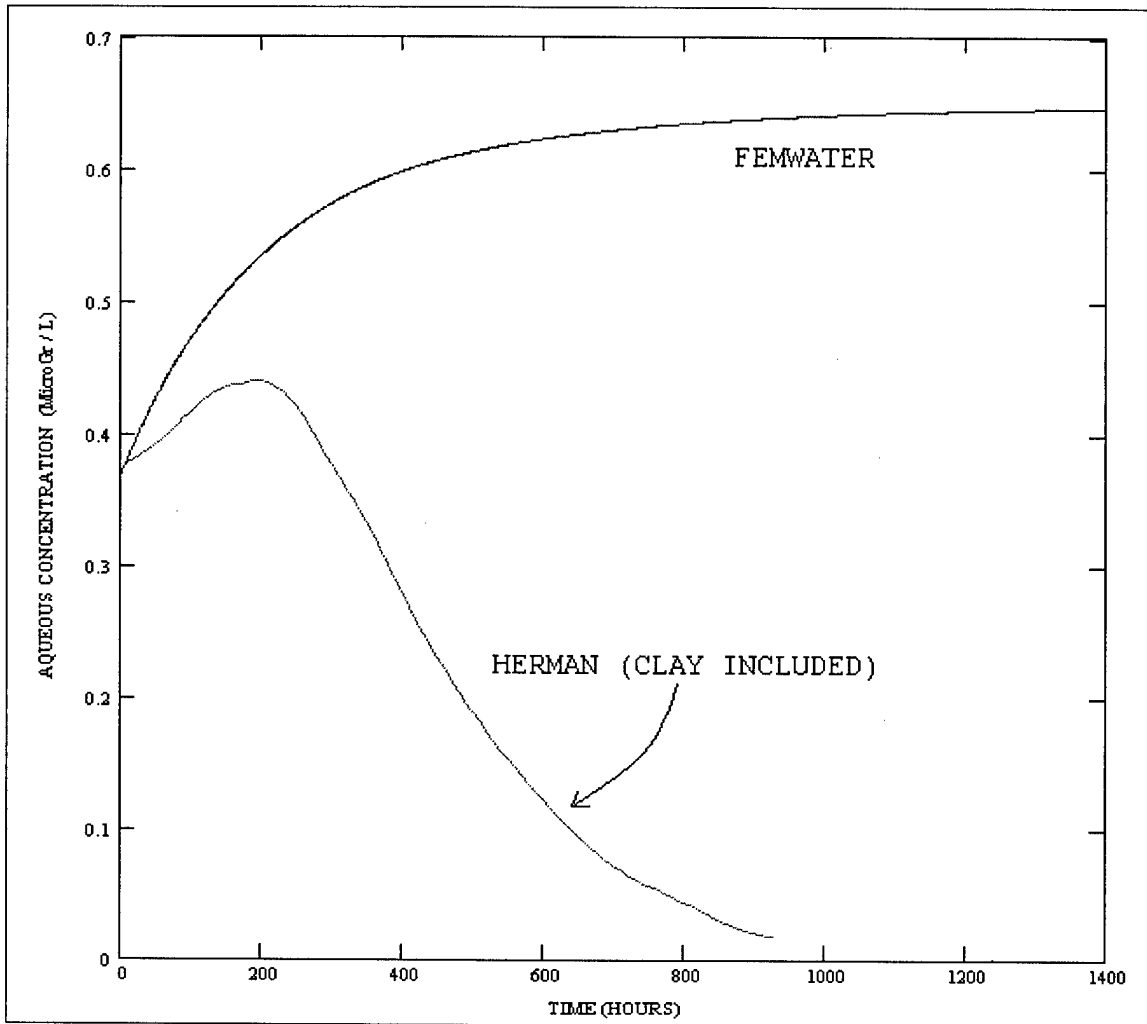


Figure 44. Comparison of Spatial Concentration Traces

## 4.8 GENERAL OBSERVATIONS ON FEMWATER PERFORMANCE

In the course of performing the calculations described in the previous sections, several trends were noticed:

1. The use of the full curves for soil hydraulic properties (section 3.2.e) appeared to be unnecessary: For the present calculations, the test cell was saturated and no benefit was derived by representing the curves in their unsaturated ranges. The computation converged to the unsaturated portion with the constant saturated value of each property extended into the unsaturated portion of  $h$ .
2. Though the FEMWATER manual claims that a convergence tolerance of  $10^{-3}$  should suffice for the flow calculation, the author found that decreasing this to  $10^{-6}$  affected the magnitude of the computed velocity  $|v|$  as listed in table 5 below. Clearly a 24% increase in mean  $|v|$  is not inconsequential, particularly in light of the fact that the velocity field plays such a key role in the transport equation. The rate of transport of contaminant is sensitive to the magnitude of the velocity. Among experienced researchers in the field, Zakikhani [41] recounts at least one instance in which tightening the convergence criterion on velocity made the difference (in the final transport solution) between poor agreement with experimental results and excellent agreement therewith.
3. Tightening the convergence criterion on transport calculations did not seem to make any difference in computed transport solutions so the manual-recommended value of  $10^{-3}$  was used throughout.

Table 5. Effects of Tightening Convergence Tolerance on Flow Solution

	Tole = $10^{-3}$	Tole = $10^{-6}$	Percent Increase
Min $ v $	$1.4 \times 10^{-7}$	$2.12 \times 10^{-7}$	51 %
Max $ v $	0.07308	0.07471	2 %
Mean $ v $	0.00392	0.00488	24 %
Std Dev $ v $	0.00672	0.00727	8 %

## **5. CONCLUSIONS & RECOMMENDATIONS FOR FURTHER STUDY**

### **5.1 CONCLUSIONS**

The author has succeeded in bringing the GMS/FEMWATER package on line. The Air Force now has a powerful tool for the analysis of ground-water hydrodynamics which is central to the environmental science. The following numbered statements summarize the conclusions drawn from the research conducted with this tool:

1. FEMWATER is capable of modeling tailing and rebound without an additional microscale model. Specifically, it is capable of representing diffusion processes when the soil reflects macroscopic structure without microscale parameters which are difficult to characterize.
2. FEMWATER appears to impose a lot of numerical dispersion. As a result, calculations of contaminant transport are dominated by smearing and mixing instead of advection.
3. FEMWATER has displayed an insensitivity to soil hydraulic properties when the plant is saturated.
4. FEMWATER has illustrated the effect of retardation factor on the sorptive retention of contaminant in the test cell: Retardation results in a temporally delayed peaking of the breakthrough curve and a lower peak.

While the FEMWATER results have been shown, through the moment analysis, to be self-consistent, the question of whether they adequately represent reality is still open.

### **5.2 RECOMMENDATIONS**

Future work should focus on:

1. Understanding the reasons behind FEMWATER's tendency to be over-dispersive.
2. More careful and detailed comparisons with actual field data. More effort must be made to model the soil strata as they really are, pursuant to better numerical simulations.
3. Effort to improve the well discretization model by doing away with the assumption that each source's hydraulic zone of influence extends to the centerline of the adjacent layer of elements.

## APPENDIX A UNIQUENESS IN THE ONE-DIMENSIONAL DIFFUSION EQUATION

Consider the problem:

$$\begin{aligned}\frac{\partial C}{\partial t} &= \frac{\partial^2 C}{\partial x^2} + F(x, t) \\ C(x, 0) &= f(x) \\ \frac{\partial C}{\partial x} &= 0 \text{ at } x = 0, x = L\end{aligned}$$

Suppose now that  $f(x) = 0$  then our problem becomes

$$\begin{aligned}\frac{\partial C}{\partial t} &= \frac{\partial^2 C}{\partial x^2} + F(x, t) \\ C(x, 0) &= 0 \\ \frac{\partial C}{\partial x} &= 0 \text{ at } x = 0, x = L\end{aligned}$$

For which we recognize that if  $F(x, t) = 0$ , then  $C = \text{constant}$  is a solution to the partial differential equation. The implications of this (see for example [8] ) are twofold:

1. A solution may exist for some problems and not for others
2. If a solution does exist it may not be unique; Another solution may exist within an additive constant

For uniqueness in the above instance, there must be a compatibility relation between the forcing function and the initial/boundary conditions.

## APPENDIX B SAMPLE FEMWATER INPUT FILES

The following FEMWATER input files are compatible with the version 1.1 of FEMWATER.

dated 1 August 1995

### B.1 INPUT FILE FOR FLOW SOLUTION

```
3DFEMWBC
T1 SMOOTHED GRID
T2 TARIQ HASHIM
T3 7MAR97
OP1 10
OP2 0 0 0 0 1 22
OP3 1.00000000e+00 1.00000000e+00 1.00000000e+00 1.00000000e+00
OP4 0 0 1
IP1 40 10 400 1.00000000e-06 1.00000000e-06
IP2 10 10 1.00000000e-03 1.00000000e-03
IP3 10 50 5.00000000e-01 5.00000000e-01
IP4 1.00000000e-03 1.00000000e-01
PT1 1 1 1 2
TC1 3.00000000e+02
TC2 0 1.20000000e+00
TC3 0
OC1 0 0 0 1
OC2 0 0
OC3 1 0 1
OC4 5 1 2 3 4 5
MP1 0
MP3 1.00000000e+03 4.68000000e+00 1.27000000e+08
MP4 1.00000000e+00 0.00000000e+00 0.00000000e+00 0.00000000e+00 1.00000000e+00 0.00000000e+00 0.00000000e+00
MP2 7 3.60000000e-05 3.60000000e-05 3.60000000e-05 0.00000000e+00 0.00000000e+00 0.00000000e+00
MP5 7 0.00000000e+00 1.30000000e+03 2.30000000e-01 2.30000000e-02 2.98000000e-06 6.00000000e-01 0.00000000e+00
1.00000000e+00
SP1 7 1 2 3
MP2 2 4.32000000e-02 4.32000000e-02 4.32000000e-02 0.00000000e+00 0.00000000e+00 0.00000000e+00
MP5 2 0.00000000e+00 1.70000000e+03 2.30000000e-01 2.30000000e-02 2.98000000e-06 6.00000000e-01 0.00000000e+00
1.00000000e+00
SP1 2 1 2 3
MP2 3 1.08000000e-03 1.08000000e-03 1.08000000e-03 0.00000000e+00 0.00000000e+00 0.00000000e+00
MP5 3 0.00000000e+00 1.70000000e+03 2.30000000e-01 2.30000000e-02 2.98000000e-06 6.00000000e-01 0.00000000e+00
1.00000000e+00
SP1 3 1 2 3
MP2 5 8.28000000e-02 8.28000000e-02 8.28000000e-02 0.00000000e+00 0.00000000e+00 0.00000000e+00
MP5 5 0.00000000e+00 1.70000000e+03 2.30000000e-01 2.30000000e-02 2.98000000e-06 6.00000000e-01 0.00000000e+00
```



1.000000e+00  
 SPI 5 1 2 3  
 MP2 4 5.4000000e-02 5.4000000e-02 5.4000000e-02 0.0000000e+00 0.0000000e+00 0.0000000e+00  
 MP5 4 0.000000e+00 1.700000e+03 2.300000e-01 2.300000e-02 2.980000e-06 6.000000e-01 0.000000e+00  
 1.000000e+00  
 SPI 4 1 2 3  
 MP2 6 3.6000000e-06 3.6000000e-06 3.6000000e-06 0.0000000e+00 0.0000000e+00 0.0000000e+00  
 MP5 6 0.000000e+00 1.300000e+03 2.300000e-01 2.300000e-02 2.980000e-06 6.000000e-01 0.000000e+00  
 1.000000e+00  
 SPI 6 1 2 3  
 MP2 8 1.0000000e-04 1.0000000e-04 1.0000000e-04 0.0000000e+00 0.0000000e+00 0.0000000e+00  
 MP5 8 0.000000e+00 1.500000e+03 2.300000e-01 2.300000e-02 2.980000e-06 6.000000e-01 0.000000e+00  
 1.000000e+00  
 SPI 8 1 2 3  
 MP2 1 1.0800000e-03 1.0800000e-03 1.0800000e-03 0.0000000e+00 0.0000000e+00 0.0000000e+00  
 MP5 1 0.000000e+00 1.700000e+03 2.300000e-01 2.300000e-02 2.980000e-06 6.000000e-01 0.000000e+00  
 1.000000e+00  
 SPI 1 1 2 3  
 XY1 1 3 0 0 0 0.0000000000000000e+00 moisture  
 -20.000 0.36000  
 0.000 0.36000  
 20.000 0.36000  
 XY1 2 3 0 0 0 0.0000000000000000e+00 conductivity  
 -20.000 1.00000  
 0.000 1.00000  
 20.000 1.00000  
 XY1 3 3 0 0 0 0.0000000000000000e+00 watercapacity  
 -20.000 0.00000  
 0.000 0.00000  
 20.000 0.00000  
 XY1 4 1 0 0 0 0.0000000000000000e+00 constant  
 0.000 1.14867000e-03  
 XY1 5 1 0 0 0 0.0000000000000000e+00 constant  
 0.000 1.00000000e+00  
 XY1 6 1 0 0 0 0.0000000000000000e+00 constant  
 0.000 -1.14867000e-03  
 XY1 7 1 0 0 0 0.0000000000000000e+00 constant  
 0.000 4.25430000e-05  
 XY1 8 1 0 0 0 0.0000000000000000e+00 constant  
 0.000 -4.25430000e-05  
 XY1 9 1 0 0 0 0.0000000000000000e+00 constant  
 0.000 1.16926100e-03  
 XY1 10 1 0 0 0 0.0000000000000000e+00 constant  
 0.000 -1.16926100e-03  
 XY1 11 1 0 0 0 0.0000000000000000e+00 constant  
 0.000 2.26897700e-03  
 XY1 12 1 0 0 0 0.0000000000000000e+00 constant

0.000 -2.26897700e-03  
XY1 13 1 0 0 0 0.0000000000000000e+00 constant  
0.000 7.74100000e-05  
XY1 14 1 0 0 0 0.0000000000000000e+00 constant  
0.000 -7.74100000e-05  
XY1 15 1 0 0 0 0.0000000000000000e+00 constant  
0.000 9.49090000e-05  
XY1 16 1 0 0 0 0.0000000000000000e+00 constant  
0.000 -9.49090000e-05  
XY1 17 1 0 0 0 0.0000000000000000e+00 constant  
0.000 1.16370000e-04  
XY1 18 1 0 0 0 0.0000000000000000e+00 constant  
0.000 -1.16370000e-04  
XY1 19 1 0 0 0 0.0000000000000000e+00 constant  
0.000 1.42681000e-04  
XY1 20 1 0 0 0 0.0000000000000000e+00 constant  
0.000 -1.42681000e-04  
XY1 21 1 0 0 0 0.0000000000000000e+00 constant  
0.000 1.74929000e-04  
XY1 22 1 0 0 0 0.0000000000000000e+00 constant  
0.000 -1.74929000e-04  
XY1 23 1 0 0 0 0.0000000000000000e+00 constant  
0.000 3.23226220e-03  
XY1 24 1 0 0 0 0.0000000000000000e+00 constant  
0.000 -3.23226200e-03  
XY1 25 1 0 0 0 0.0000000000000000e+00 constant  
0.000 6.16594500e-03  
XY1 26 1 0 0 0 0.0000000000000000e+00 constant  
0.000 -6.16594500e-03  
XY1 27 1 0 0 0 0.0000000000000000e+00 constant  
0.000 5.95701000e-03  
XY1 28 1 0 0 0 0.0000000000000000e+00 constant  
0.000 -5.95701000e-03  
XY1 29 1 0 0 0 0.0000000000000000e+00 constant  
0.000 5.75516500e-03  
XY1 30 1 0 0 0 0.0000000000000000e+00 constant  
0.000 -5.75516500e-03  
XY1 31 1 0 0 0 0.0000000000000000e+00 constant  
0.000 5.56088400e-03  
XY1 32 1 0 0 0 0.0000000000000000e+00 constant  
0.000 -5.56088400e-03  
XY1 33 1 0 0 0 0.0000000000000000e+00 constant  
0.000 6.78077400e-03  
XY1 34 1 0 0 0 0.0000000000000000e+00 constant  
0.000 -6.78077400e-03  
XY1 35 1 0 0 0 0.0000000000000000e+00 constant  
0.000 7.09446000e-03

XY1 36 1 0 0 0 0.000000000000000e+00 constant  
0.000 -7.09446000e-03  
XY1 37 1 0 0 0 0.000000000000000e+00 constant  
0.000 5.33751600e-03  
XY1 38 1 0 0 0 0.000000000000000e+00 constant  
0.000 -5.33751600e-03  
XY1 39 1 0 0 0 0.000000000000000e+00 constant  
0.000 4.01473400e-03  
XY1 40 1 0 0 0 0.000000000000000e+00 constant  
0.000 -4.01473400e-03  
XY1 41 1 0 0 0 0.000000000000000e+00 constant  
0.000 3.02101700e-03  
XY1 42 1 0 0 0 0.000000000000000e+00 constant  
0.000 -3.02101700e-03  
XY1 43 1 0 0 0 0.000000000000000e+00 constant  
0.000 2.27301100e-03  
XY1 44 1 0 0 0 0.000000000000000e+00 constant  
0.000 -2.27301100e-03  
XY1 45 1 0 0 0 0.000000000000000e+00 constant  
0.000 1.70983200e-03  
XY1 46 1 0 0 0 0.000000000000000e+00 constant  
0.000 -1.70983200e-03  
XY1 47 1 0 0 0 0.000000000000000e+00 constant  
0.000 1.28654100e-03  
XY1 48 1 0 0 0 0.000000000000000e+00 constant  
0.000 -1.28654100e-03  
XY1 49 1 0 0 0 0.000000000000000e+00 constant  
0.000 5.54708000e-04  
XY1 50 1 0 0 0 0.000000000000000e+00 constant  
0.000 -5.54708000e-04  
XY1 51 1 0 0 0 0.000000000000000e+00 constant  
0.000 2.03920000e-05  
XY1 52 1 0 0 0 0.000000000000000e+00 constant  
0.000 -2.03920000e-05  
PS1 32147 4  
PS2 32147 5  
PS1 32146 6  
PS1 32145 4  
PS2 32145 5  
PS1 32144 6  
PS1 32143 4  
PS2 32143 5  
PS1 32142 6  
PS1 31110 7  
PS2 31110 5  
PS1 31109 8  
PS1 31108 7

PS2 31108 5  
PS1 31107 8  
PS1 31106 7  
PS2 31106 5  
PS1 31105 8  
PS1 30073 9  
PS2 30073 5  
PS1 30072 10  
PS1 30071 9  
PS2 30071 5  
PS1 30070 10  
PS1 30069 9  
PS2 30069 5  
PS1 30068 10  
PS1 29036 11  
PS2 29036 5  
PS1 29035 12  
PS1 29034 11  
PS2 29034 5  
PS1 29033 12  
PS1 29032 11  
PS2 29032 5  
PS1 29031 12  
PS1 27999 13  
PS2 27999 5  
PS1 27998 14  
PS1 27997 13  
PS2 27997 5  
PS1 27996 14  
PS1 27995 13  
PS2 27995 5  
PS1 27994 14  
PS1 26962 15  
PS2 26962 5  
PS1 26961 16  
PS1 26960 15  
PS2 26960 5  
PS1 26959 16  
PS1 26958 15  
PS2 26958 5  
PS1 26957 16  
PS1 25925 17  
PS2 25925 5  
PS1 25924 18  
PS1 25923 17  
PS2 25923 5  
PS1 25922 18

PS1 25921 17  
PS2 25921 5  
PS1 25920 18  
PS1 24888 19  
PS2 24888 5  
PS1 24887 20  
PS1 24886 19  
PS2 24886 5  
PS1 24885 20  
PS1 24884 19  
PS2 24884 5  
PS1 24883 20  
PS1 23851 21  
PS2 23851 5  
PS1 23850 22  
PS1 23849 21  
PS2 23849 5  
PS1 23848 22  
PS1 23847 21  
PS2 23847 5  
PS1 23846 22  
PS1 22814 23  
PS2 22814 5  
PS1 22813 24  
PS1 22812 23  
PS2 22812 5  
PS1 22811 24  
PS1 22810 23  
PS2 22810 5  
PS1 22809 24  
PS1 21777 25  
PS2 21777 5  
PS1 21776 26  
PS1 21775 25  
PS2 21775 5  
PS1 21774 26  
PS1 21773 25  
PS2 21773 5  
PS1 21772 26  
PS1 20740 27  
PS2 20740 5  
PS1 20739 28  
PS1 20738 27  
PS2 20738 5  
PS1 20737 28  
PS1 20736 27  
PS2 20736 5

PS1 20735 28  
PS1 19703 29  
PS2 19703 5  
PS1 19702 30  
PS1 19701 29  
PS2 19701 5  
PS1 19700 30  
PS1 19699 29  
PS2 19699 5  
PS1 19698 30  
PS1 18666 31  
PS2 18666 5  
PS1 18665 32  
PS1 18664 31  
PS2 18664 5  
PS1 18663 32  
PS1 18662 31  
PS2 18662 5  
PS1 18661 32  
PS1 17629 33  
PS2 17629 5  
PS1 17628 34  
PS1 17627 33  
PS2 17627 5  
PS1 17626 34  
PS1 17625 33  
PS2 17625 5  
PS1 17624 34  
PS1 16592 35  
PS2 16592 5  
PS1 16591 36  
PS1 16590 35  
PS2 16590 5  
PS1 16589 36  
PS1 16588 35  
PS2 16588 5  
PS1 16587 36  
PS1 15555 37  
PS2 15555 5  
PS1 15554 38  
PS1 15553 37  
PS2 15553 5  
PS1 15552 38  
PS1 15551 37  
PS2 15551 5  
PS1 15550 38  
PS1 14518 39

PS2 14518 5  
PS1 14517 40  
PS1 14516 39  
PS2 14516 5  
PS1 14515 40  
PS1 14514 39  
PS2 14514 5  
PS1 14513 40  
PS1 13481 41  
PS2 13481 5  
PS1 13480 42  
PS1 13479 41  
PS2 13479 5  
PS1 13478 42  
PS1 13477 41  
PS2 13477 5  
PS1 13476 42  
PS1 12444 43  
PS2 12444 5  
PS1 12443 44  
PS1 12442 43  
PS2 12442 5  
PS1 12441 44  
PS1 12440 43  
PS2 12440 5  
PS1 12439 44  
PS1 11407 45  
PS2 11407 5  
PS1 11406 46  
PS1 11405 45  
PS2 11405 5  
PS1 11404 46  
PS1 11403 45  
PS2 11403 5  
PS1 11402 46  
PS1 10370 47  
PS2 10370 5  
PS1 10369 48  
PS1 10368 47  
PS2 10368 5  
PS1 10367 48  
PS1 10366 47  
PS2 10366 5  
PS1 10365 48  
PS1 2074 49  
PS2 2074 5  
PS1 2073 50

PS1 2072 49  
PS2 2072 5  
PS1 2071 50  
PS1 2070 49  
PS2 2070 5  
PS1 2069 50  
PS1 1037 51  
PS2 1037 5  
PS1 1036 52  
PS1 1035 51  
PS2 1035 5  
PS1 1034 52  
PS1 1033 51  
PS2 1033 5  
PS1 1032 52  
ICH 0 1.00000000e+01  
ICC 0 1.00000000e+01  
ICS 0  
ICT 0.00000000e+00  
ICF 0 0 0  
END



## B.2 INPUT FILE FOR TRANSPORT SOLUTION

3DFEMWBC  
T1 SMOOTHED GRID  
T2 TARIQ HASHIM  
T3 7MAR97  
OP1 1  
OP2 1 1 0 0 1 22  
OP3 1.00000000e+00 1.00000000e+00 1.00000000e+00 1.00000000e+00  
OP4 0 0 1  
IP1 40 10 400 1.00000000e-06 1.00000000e-06  
IP2 10 10 1.00000000e-03 1.00000000e-03  
IP3 10 50 5.00000000e-01 5.00000000e-01  
IP4 1.00000000e-03 1.00000000e-01  
PT1 1 1 1 2  
TC1 1400.0  
TC2 0 1.00000000e+00  
TC3 0  
OC1 0 0 0 1  
OC2 0 0  
OC3 1 0 200.0  
OC4 5 1 2 3 4 5  
MP1 0  
MP3 1.00000000e+03 4.68000000e+00 1.27000000e+08  
MP4 1.00000000e+00 0.00000000e+00 0.00000000e+00 0.00000000e+00 1.00000000e+00 0.00000000e+00 0.00000000e+00  
0.00000000e+00  
MP2 7 3.60000000e-05 3.60000000e-05 3.60000000e-05 0.00000000e+00 0.00000000e+00 0.00000000e+00  
MP5 7 0.00000000e+00 1.30000000e+03 2.30000000e-01 2.30000000e-02 2.98000000e-06 6.00000000e-01 0.00000000e+00  
1.00000000e+00  
SP1 7 1 2 3  
MP2 2 4.32000000e-02 4.32000000e-02 4.32000000e-02 0.00000000e+00 0.00000000e+00 0.00000000e+00  
MP5 2 0.00000000e+00 1.70000000e+03 2.30000000e-01 2.30000000e-02 2.98000000e-06 6.00000000e-01 0.00000000e+00  
1.00000000e+00  
SP1 2 1 2 3  
MP2 3 1.08000000e-03 1.08000000e-03 1.08000000e-03 0.00000000e+00 0.00000000e+00 0.00000000e+00  
MP5 3 0.00000000e+00 1.70000000e+03 2.30000000e-01 2.30000000e-02 2.98000000e-06 6.00000000e-01 0.00000000e+00  
1.00000000e+00  
SP1 3 1 2 3  
MP2 5 8.28000000e-02 8.28000000e-02 8.28000000e-02 0.00000000e+00 0.00000000e+00 0.00000000e+00  
MP5 5 0.00000000e+00 1.70000000e+03 2.30000000e-01 2.30000000e-02 2.98000000e-06 6.00000000e-01 0.00000000e+00  
1.00000000e+00  
SP1 5 1 2 3  
MP2 4 5.40000000e-02 5.40000000e-02 5.40000000e-02 0.00000000e+00 0.00000000e+00 0.00000000e+00  
MP5 4 0.00000000e+00 1.70000000e+03 2.30000000e-01 2.30000000e-02 2.98000000e-06 6.00000000e-01 0.00000000e+00  
1.00000000e+00  
SP1 4 1 2 3  
MP2 6 3.60000000e-06 3.60000000e-06 3.60000000e-06 0.00000000e+00 0.00000000e+00 0.00000000e+00

MP5 6 0.000000e+00 1.300000e+03 2.300000e-01 2.300000e-02 2.980000e-06 6.000000e-01 0.000000e+00  
 1.000000e+00  
 SP1 6 1 2 3  
 MP2 8 1.000000e-04 1.000000e-04 1.000000e-04 0.000000e+00 0.000000e+00 0.000000e+00  
 MP5 8 0.000000e+00 1.500000e+03 2.300000e-01 2.300000e-02 2.980000e-06 6.000000e-01 0.000000e+00  
 1.000000e+00  
 SP1 8 1 2 3  
 MP2 1 1.080000e-03 1.080000e-03 1.080000e-03 0.000000e+00 0.000000e+00 0.000000e+00  
 MP5 1 0.000000e+00 1.700000e+03 2.300000e-01 2.300000e-02 2.980000e-06 6.000000e-01 0.000000e+00  
 1.000000e+00  
 SP1 1 1 2 3  
 XY1 1 3 0 0 0 0.0000000000000000e+00 moisture  
 -20.000 0.36000  
 0.000 0.36000  
 20.000 0.36000  
 XY1 2 3 0 0 0 0.0000000000000000e+00 conductivity  
 -20.000 1.00000  
 0.000 1.00000  
 20.000 1.00000  
 XY1 3 3 0 0 0 0.0000000000000000e+00 watercapacity  
 -20.000 0.00000  
 0.000 0.00000  
 20.000 0.00000  
 XY1 4 1 0 0 0 0.0000000000000000e+00 constant  
 0.000 1.14867000e-03  
 XY1 5 1 0 0 0 0.0000000000000000e+00 constant  
 0.000 1.00000000e+00  
 XY1 6 1 0 0 0 0.0000000000000000e+00 constant  
 0.000 -1.14867000e-03  
 XY1 7 1 0 0 0 0.0000000000000000e+00 constant  
 0.000 4.25430000e-05  
 XY1 8 1 0 0 0 0.0000000000000000e+00 constant  
 0.000 -4.25430000e-05  
 XY1 9 1 0 0 0 0.0000000000000000e+00 constant  
 0.000 1.16926100e-03  
 XY1 10 1 0 0 0 0.0000000000000000e+00 constant  
 0.000 -1.16926100e-03  
 XY1 11 1 0 0 0 0.0000000000000000e+00 constant  
 0.000 2.26897700e-03  
 XY1 12 1 0 0 0 0.0000000000000000e+00 constant  
 0.000 -2.26897700e-03  
 XY1 13 1 0 0 0 0.0000000000000000e+00 constant  
 0.000 7.74100000e-05  
 XY1 14 1 0 0 0 0.0000000000000000e+00 constant  
 0.000 -7.74100000e-05  
 XY1 15 1 0 0 0 0.0000000000000000e+00 constant  
 0.000 9.49090000e-05

XY1 16 1 0 0 0 0.000000000000000e+00 constant  
0.000 -9.49090000e-05  
XY1 17 1 0 0 0 0.000000000000000e+00 constant  
0.000 1.16370000e-04  
XY1 18 1 0 0 0 0.000000000000000e+00 constant  
0.000 -1.16370000e-04  
XY1 19 1 0 0 0 0.000000000000000e+00 constant  
0.000 1.42681000e-04  
XY1 20 1 0 0 0 0.000000000000000e+00 constant  
0.000 -1.42681000e-04  
XY1 21 1 0 0 0 0.000000000000000e+00 constant  
0.000 1.74929000e-04  
XY1 22 1 0 0 0 0.000000000000000e+00 constant  
0.000 -1.74929000e-04  
XY1 23 1 0 0 0 0.000000000000000e+00 constant  
0.000 3.23226220e-03  
XY1 24 1 0 0 0 0.000000000000000e+00 constant  
0.000 -3.23226200e-03  
XY1 25 1 0 0 0 0.000000000000000e+00 constant  
0.000 6.16594500e-03  
XY1 26 1 0 0 0 0.000000000000000e+00 constant  
0.000 -6.16594500e-03  
XY1 27 1 0 0 0 0.000000000000000e+00 constant  
0.000 5.95701000e-03  
XY1 28 1 0 0 0 0.000000000000000e+00 constant  
0.000 -5.95701000e-03  
XY1 29 1 0 0 0 0.000000000000000e+00 constant  
0.000 5.75516500e-03  
XY1 30 1 0 0 0 0.000000000000000e+00 constant  
0.000 -5.75516500e-03  
XY1 31 1 0 0 0 0.000000000000000e+00 constant  
0.000 5.56088400e-03  
XY1 32 1 0 0 0 0.000000000000000e+00 constant  
0.000 -5.56088400e-03  
XY1 33 1 0 0 0 0.000000000000000e+00 constant  
0.000 6.78077400e-03  
XY1 34 1 0 0 0 0.000000000000000e+00 constant  
0.000 -6.78077400e-03  
XY1 35 1 0 0 0 0.000000000000000e+00 constant  
0.000 7.09446000e-03  
XY1 36 1 0 0 0 0.000000000000000e+00 constant  
0.000 -7.09446000e-03  
XY1 37 1 0 0 0 0.000000000000000e+00 constant  
0.000 5.33751600e-03  
XY1 38 1 0 0 0 0.000000000000000e+00 constant  
0.000 -5.33751600e-03  
XY1 39 1 0 0 0 0.000000000000000e+00 constant

0.000 4.01473400e-03  
XY1 40 1 0 0 0 0.000000000000000e+00 constant  
0.000 -4.01473400e-03  
XY1 41 1 0 0 0 0.000000000000000e+00 constant  
0.000 3.02101700e-03  
XY1 42 1 0 0 0 0.000000000000000e+00 constant  
0.000 -3.02101700e-03  
XY1 43 1 0 0 0 0.000000000000000e+00 constant  
0.000 2.27301100e-03  
XY1 44 1 0 0 0 0.000000000000000e+00 constant  
0.000 -2.27301100e-03  
XY1 45 1 0 0 0 0.000000000000000e+00 constant  
0.000 1.70983200e-03  
XY1 46 1 0 0 0 0.000000000000000e+00 constant  
0.000 -1.70983200e-03  
XY1 47 1 0 0 0 0.000000000000000e+00 constant  
0.000 1.28654100e-03  
XY1 48 1 0 0 0 0.000000000000000e+00 constant  
0.000 -1.28654100e-03  
XY1 49 1 0 0 0 0.000000000000000e+00 constant  
0.000 5.54708000e-04  
XY1 50 1 0 0 0 0.000000000000000e+00 constant  
0.000 -5.54708000e-04  
XY1 51 1 0 0 0 0.000000000000000e+00 constant  
0.000 2.03920000e-05  
XY1 52 1 0 0 0 0.000000000000000e+00 constant  
0.000 -2.03920000e-05  
PS1 32147 4  
PS2 32147 5  
PS1 32146 6  
PS1 32145 4  
PS2 32145 5  
PS1 32144 6  
PS1 32143 4  
PS2 32143 5  
PS1 32142 6  
PS1 31110 7  
PS2 31110 5  
PS1 31109 8  
PS1 31108 7  
PS2 31108 5  
PS1 31107 8  
PS1 31106 7  
PS2 31106 5  
PS1 31105 8  
PS1 30073 9  
PS2 30073 5

PS1 30072 10  
PS1 30071 9  
PS2 30071 5  
PS1 30070 10  
PS1 30069 9  
PS2 30069 5  
PS1 30068 10  
PS1 29036 11  
PS2 29036 5  
PS1 29035 12  
PS1 29034 11  
PS2 29034 5  
PS1 29033 12  
PS1 29032 11  
PS2 29032 5  
PS1 29031 12  
PS1 27999 13  
PS2 27999 5  
PS1 27998 14  
PS1 27997 13  
PS2 27997 5  
PS1 27996 14  
PS1 27995 13  
PS2 27995 5  
PS1 27994 14  
PS1 26962 15  
PS2 26962 5  
PS1 26961 16  
PS1 26960 15  
PS2 26960 5  
PS1 26959 16  
PS1 26958 15  
PS2 26958 5  
PS1 26957 16  
PS1 25925 17  
PS2 25925 5  
PS1 25924 18  
PS1 25923 17  
PS2 25923 5  
PS1 25922 18  
PS1 25921 17  
PS2 25921 5  
PS1 25920 18  
PS1 24888 19  
PS2 24888 5  
PS1 24887 20  
PS1 24886 19

PS2 24886 5  
PS1 24885 20  
PS1 24884 19  
PS2 24884 5  
PS1 24883 20  
PS1 23851 21  
PS2 23851 5  
PS1 23850 22  
PS1 23849 21  
PS2 23849 5  
PS1 23848 22  
PS1 23847 21  
PS2 23847 5  
PS1 23846 22  
PS1 22814 23  
PS2 22814 5  
PS1 22813 24  
PS1 22812 23  
PS2 22812 5  
PS1 22811 24  
PS1 22810 23  
PS2 22810 5  
PS1 22809 24  
PS1 21777 25  
PS2 21777 5  
PS1 21776 26  
PS1 21775 25  
PS2 21775 5  
PS1 21774 26  
PS1 21773 25  
PS2 21773 5  
PS1 21772 26  
PS1 20740 27  
PS2 20740 5  
PS1 20739 28  
PS1 20738 27  
PS2 20738 5  
PS1 20737 28  
PS1 20736 27  
PS2 20736 5  
PS1 20735 28  
PS1 19703 29  
PS2 19703 5  
PS1 19702 30  
PS1 19701 29  
PS2 19701 5  
PS1 19700 30

PS1 19699 29  
PS2 19699 5  
PS1 19698 30  
PS1 18666 31  
PS2 18666 5  
PS1 18665 32  
PS1 18664 31  
PS2 18664 5  
PS1 18663 32  
PS1 18662 31  
PS2 18662 5  
PS1 18661 32  
PS1 17629 33  
PS2 17629 5  
PS1 17628 34  
PS1 17627 33  
PS2 17627 5  
PS1 17626 34  
PS1 17625 33  
PS2 17625 5  
PS1 17624 34  
PS1 16592 35  
PS2 16592 5  
PS1 16591 36  
PS1 16590 35  
PS2 16590 5  
PS1 16589 36  
PS1 16588 35  
PS2 16588 5  
PS1 16587 36  
PS1 15555 37  
PS2 15555 5  
PS1 15554 38  
PS1 15553 37  
PS2 15553 5  
PS1 15552 38  
PS1 15551 37  
PS2 15551 5  
PS1 15550 38  
PS1 14518 39  
PS2 14518 5  
PS1 14517 40  
PS1 14516 39  
PS2 14516 5  
PS1 14515 40  
PS1 14514 39  
PS2 14514 5

PS1 14513 40  
PS1 13481 41  
PS2 13481 5  
PS1 13480 42  
PS1 13479 41  
PS2 13479 5  
PS1 13478 42  
PS1 13477 41  
PS2 13477 5  
PS1 13476 42  
PS1 12444 43  
PS2 12444 5  
PS1 12443 44  
PS1 12442 43  
PS2 12442 5  
PS1 12441 44  
PS1 12440 43  
PS2 12440 5  
PS1 12439 44  
PS1 11407 45  
PS2 11407 5  
PS1 11406 46  
PS1 11405 45  
PS2 11405 5  
PS1 11404 46  
PS1 11403 45  
PS2 11403 5  
PS1 11402 46  
PS1 10370 47  
PS2 10370 5  
PS1 10369 48  
PS1 10368 47  
PS2 10368 5  
PS1 10367 48  
PS1 10366 47  
PS2 10366 5  
PS1 10365 48  
PS1 2074 49  
PS2 2074 5  
PS1 2073 50  
PS1 2072 49  
PS2 2072 5  
PS1 2071 50  
PS1 2070 49  
PS2 2070 5  
PS1 2069 50  
PS1 1037 51



PS2 1037 5  
PS1 1036 52  
PS1 1035 51  
PS2 1035 5  
PS1 1034 52  
PS1 1033 51  
PS2 1033 5  
PS1 1032 52  
ICH 0 1.00000000e+01  
ICC 0 0.00000000e+00  
ICS 0  
ICT 0.00000000e+00  
ICF 0 1 0  
END

## *Bibliography*

- [1] Adams, Thomas A. and Robert C. Virmontes. *Analytical Modeling of Aquifer Decontamination by Pulsed Pumping when Contaminant Transport is Affected by Rate-Limited Sorption and Desorption*. MS thesis, School of Engineering, Air Force Institute of Technology, Wright-Patterson AFB, OH, 1993. AFIT/GEE/ENG/93-S1.
- [2] Bear, Jacob. *Hydraulics of Groundwater* (1979 Edition). McGraw-Hill, 1979.
- [3] Brogan, Scott D. *Aquifer Remediation in the Presence of Rate-Limited Sorption*. MS thesis, Stanford University, Stanford, CA, 1991. ON0117200062836.
- [4] Brogan, Scott D. *Aquifer Remediation in the Presence of Rate-Limited Sorption*. MS thesis, Stanford University, Stanford, CA, 1991. ON0117200062836.
- [5] Brusseau, Mark L. "The Impact of Pore Water Velocity," *Journal of Contaminant Hydrology*, 9, 353–368, April, 1992.
- [6] Brusseau, Mark L. and P.S.C. Rao. "Sorption Non-Ideality During Organic Contaminant Transport in Porous Media," *CRC Critical Reviews in Environmental Control*, 19, 33–99, January, 1989.
- [7] Caspers, Jeffrey L. *Modeling of Ground Water Aquifer Remediation by Pulsed Pumping when Contaminant Transport is Affected by Physical, Non-Equilibrium Sorption and Desorption*. MS thesis, School of Engineering, Air Force Institute of Technology, Wright-Patterson AFB, OH, 1994. AFIT/GEE/ENC/94S-O1.
- [8] Colton, David. *PARTIAL DIFFERENTIAL EQUATIONS, AN INTRODUCTION*. The Random House.
- [9] Engineering Computer Graphics Laboratory, Brigham Young University, Provo, Utah. *Groundwater Modeling System Reference Manual* (Version 1.1 Edition), 1995.
- [10] EPA. *The Toxic-Release Inventory: A National Perspective*. Technical Report EPA 560/4-89/005, Washington: GPO: The Environmental Protection Agency (EPA), 1989b.
- [11] Freeze, R. Allan and John A. Cherry. *Groundwater* (1979 Edition). Prentice-Hall, 1979.
- [12] Goltz, Mark N. "Contaminant Transport Modeling," *The Military Engineer*, 83, 24–25, May-June, 1991b.
- [13] Goltz, Mark N. and Paul V. Roberts. "Three-Dimensional Solutions for Solute Transport in an Infinite Medium with Mobile and Immobile Zones," *Water Resources Research*, 22, 1139–1148, July, 1986c.
- [14] Goltz, Mark N. and Paul V. Roberts. "Using the Method of Moments to Analyze Three-Dimensional Diffusion-Limited Solute Transport from Temporal and Spatial Perspectives," *Water Resources Research*, 23, 8, 1575–1585 1987.
- [15] Gorelick, Steven M., R. Allan Freeze David Donahue and Joseph F. Keeley. *Ground Water Contamination: Optimal Capture and Containment*. Boca Raton, FL: Lewis Publishers, 1993.
- [16] Grove, D.B. and K.G. Stollenwerk. "Chemical Reactions Simulated by Ground Water Quality Models," *Water Resources Bulletin*, 23, 601–615 August, 1987.

- [17] Haggerty, Roy. *Design of Multiple Contaminant Remediation in the Presence of Rate Limitations*. MS thesis, Stanford University, Stanford, CA, 1992. ON0117200108233.
- [18] Haley J.L., B. Hanson, C. Enfield and J. Glass. "Evaluating the Effectiveness of Ground Water Extraction Systems," *Ground Water Monitoring Review*, 11, 119–124 Winter, 1991.
- [19] Hall, Clinton and Jeffrey A. Johnson. "Limiting Factors in Ground Water Remediation," *Journal of Hazardous Materials*, 32 215–223 December, 1992.
- [20] Helms, A.D., K. Hatfield M.D. Annable P.S.C. Rao W.D. Graham and A.L. Wood. "Application of Moment Estimation Techniques to Partitioning Tracer Data for Characterization of Residual NAPL Distribution," *Journal of Contaminant Hydrology* 1997. UNPUBLISHED.
- [21] Herman, Jason T. *Macroscale Diffusion-Limited Sorption Modeling – A Preliminary Modeling Exercise for a Dover AFB Site*. MS thesis, School of Engineering, Air Force Institute of Technology, Wright-Patterson AFB, OH, 1995. AFIT/GEE/ENC/95D-4.
- [22] Huso, Rand C. *Numerical Modeling of Contaminant Transport with Rate-Limited Sorption/Desorption Aquifer*. MS thesis, School of Engineering, Air Force Institute of Technology, Wright-Patterson AFB, OH, 1989. AD-A215-429.
- [23] Jensen, Lawrence J. "Safe Drinking Water Act." *Environmental Law Handbook* Rockville, MD: Government Institutes, Inc., 1993.
- [24] Mackay, D.M., D.L. Freyburg P.B. Roberts and J.A. Cherry. "A Natural Gradient Experiment on Solute Transport in a Sand Aquifer, 1, Approach and Preliminary Evaluation," *Water Resources Research*, 22 2047–2058 December, 1986.
- [25] Mackay, D.M. and J.A. Cherry. "Ground Water Contamination: Pump-and-Treat Remediation," *Environmental Science and Technology*, 23 630–636 June, 1989.
- [26] Mackay, Douglas M. Department of Earth Sciences at the University of Waterloo. Private Communication, September 1998.
- [27] Mackay, Douglas M, William P. Ball et al. *Field and Laboratory Studies of Pulsed Pumping for Cleanup of Contaminated Aquifers*. Technical Report, Department of Earth Sciences, University of Waterloo, July 1997.
- [28] Miller, Cass T. and Alan J. Rabideau. "Development of Split-Operator, Petrov-Galerkin Methods to Simulate Transport and Diffusion Problems," *Water Resources Research*, 29 2227–2240 July, 1993.
- [29] Olsen, Roger L. and Michael C. Kavanaugh. "Can Groundwater Restoration be Achieved," *Water Environment Technology*, 5 42–47 March, 1993.
- [30] Powers, S.E., C.O. Loureiro L.M. Abriola and W.J. Weber Jr. "Theoretical Study of the Significance of Non-Equilibrium Dissolution of Non-Aqueous Phase Liquids in Sub-Surface Systems," *Water Resources Research*, 27 463–477 April, 1991.
- [31] Rabideau, Alan J. and Cass T. Miller. "Two-Dimensional Modeling of Aquifer Remediation Influenced by Sorption Non-Equilibrium and Hydraulic Conductivity Heterogeneity," *Water Resources Research*, 30 1457–1470 May, 1994.

- [32] Szecsody, James Edward. *Sorption Kinetics of Hydrophobic Organic Compounds onto Organic Modified Surfaces*. PhD dissertation, University of Arizona, Tucson, AZ, 1988. ON8909278.
- [33] Travis, C.C. and C.B. Doty. "Can Contaminated Aquifers at Superfund Sites be Remediated?," *Environmental Science and Technology*, 24 1464–1466 1990.
- [34] Valocchi, A.J. "Validity of the Local Equilibrium Assumption for Modeling Sorbing Solute Transport through Homogeneous Soils," *Water Resources Research*, 21 808–821 June, 1985.
- [35] Valocchi, A.J. "Effect of Radial Flow on Deviations from Local Equilibrium During Sorbing Solute Transport through Homogeneous Soils," *Water Resources Research*, 22 1693–1701 December, 1986.
- [36] Van Genuchten, M.T. "A Closed-Form Equation for Predicting the Hydraulic Conductivity of Unsaturated Soils," *Journal of the Soil Science Society of America*, 44 892–898 1980.
- [37] Voss, Clifford I. *A Finite-Element Simulation Model for Saturated-Unsaturated Fluid Density Dependent Ground Water Flow with Energy Transport of Chemically Reactive Single-Species Solute Transport*. Technical Report 84-4369, Washington: USGS, 1984.
- [38] Waterways Experiment Station, Vicksburg, MS. *FEMWATER User's Manual* (Draft Edition), February 1996. WES Technical Report HL-96.
- [39] Weber Jr., W.J., P.M. McGinley and L.E. Katz. "Sorption Phenomena in Subsurface Systems," *Water Resources Research*, 25 499–528 May, 1991.
- [40] Yu, Charley. "A General Solute Transport Model and its Applications in Contaminant Migration Analyses." *Proceedings of the National Well Water Association Conference on Practical Application of Ground Water Models*. 353–372. Worthington, OH: Water Well Journal Publishing Company, 1985.
- [41] Zakikhani, Mansour: US Army Corps of Engineers Waterways Experiment Station Private Communication, 1997.